Increasing the biomass estimation accuracy of a single fish school using a cylindrical multi-beam fishery sonar

Sindre Vatnehol

Dissertation for the degree of philosophiae doctor (PhD)

at the University of Bergen

2016

Dissertation date: 2. September 2016

Year: 2016

Title: Increasing the biomass estimation accuracy of a single fish school using a cylindrical multi-beam fishery sonar

Author: Sindre Nordlund Vatnehol

Print: AiT Bjerch AS / University of Bergen

Scientific environment

The work presented was mainly conducted in the Institute of Marine Research in Norway (IMR), either in the office located in within the group Marine Ecosystem Acoustics or onboard the Research Vessel G. O. Sars. Two weeks were spent onboard the fishing vessel Eros on the sandeel survey, and two weeks on the fishing vessel Vendla on the spring-spawning herring survey. Six months were spent in the North Western Fishery Science Centre, NOAA in Seattle, USA, supervised by Dr. Dezhang Chu.

The PhD was funded by the Research council of Norway through the project CRISP (Grant No.: 203477). The visit to Seattle was funded internally by IMR.

Acknowledgements

Professor Egil Ona is thanked for the supervision and the great inspiration during the PhD studies, and Dr. Gavin Macaulay is thanked for sharing his extensive knowledge. Also other members of the Marine Ecosystem Acoustic group at IMR are thanked for their advice, discussions and for providing an enjoyable working environment.

Dezhang Chu is thanked for hosting and supervision during the stay in Seattle.

Asgeir Steinsland is thanked for all technical support while working onboard the R/V G. O. Sars.

Ole Bernt Gammelsæter and others at Simrad are thanked for valuable and detailed information on the sonar.

Skippers and crew on F/V Eros, F/V Artus and F/V Kings Bay are thanked for access to the SX90 or SU90 data during calibration trials. Skippers and crew on R/V G. O. Sars are also thanked for their assistance during data acquisition.

David Maclennan is thanked for reviewing most of the presented work.

My family is thanked for their constant support, and my wife Frida, our daughter Hjørdis and our son Eimund are always thanked for the support, patience and for distracting me from my work when I needed a break.

Abstract

Purse-seining is regarded as one of the most effective methods for capturing migrating pelagic schools (Ben-Yami, 1994; Watson et al., 2006), where the school is encircled and entrapped by the net, pumped aboard into the cargo hold, then delivered to the coast for processing. For avoiding increased mortality during slipping of unwanted catch (Lockwood et al., 1983; Huse & Vold, 2010; Tenningen et al., 2012), the fishermen need reliable information on the school's total biomass, density and species before shooting the purse-seine. Migrating pelagic fish schools, such as the Atlantic mackerel (*Scomber scombrus*) and the Norwegian spring spawning herring (*Clupea harengus L.*), often swim near the sea surface. Therefore, the vertical echosounder may perform poorly if much of the population is within this near-surface blind zone, or if the fish move to avoid the vessel (Misund, 1993b; Ona et al., 2007b; Hjellvik et al., 2008; Totland et al., 2009). Then, calibrated, horizontally-observing tools are needed if this portion of the population is to be quantified.

Schooling fish can be detected and observed remotely using multi-beam sonars, such as the Kongsberg Maritime Simrad SX90 (Simrad, 2007) or the Furuno FSV-30 used in Nishimori et al. (2009). In standard operation, the sonar transmits a conical acoustic beam through the entire water volume around the fishing vessel (Brehmer et al., 2006). During reception, 64 acoustical beams are formed through array processing techniques applied to the transducer element outputs (Blomberg et al., 2012). Calibration of the accessible beams is a necessity if an accurate quantitative measures are required (Aglen, 1994). A precise calibration rig was designed to move the target with adequate control to map a single beam in detail (Paper 1). The initial rig was unsatisfactory as its size and weight limited its capacity to calibrate multiple sonar beams. A second rig was therefore designed for swifter movement of the target through multiple beams from each rig-mounting location. Within-beam target-tracking algorithms were then a prerequisite. The theory behind realizations of both a Split-Beam algorithm and an Interpolated Neighbouring Beam algorithm was described for the cylindrical transducer array with 256 circular

elements (Paper 2) where the Split-Beam algorithm facilitated target positioning with precision between ±0.2 and ±0.25º. In a practical field calibration, the reference target was steered to the centre of each accessible beam, or to cross the beam horizontally and vertically, guided by the Split-Beam positioning (Paper 3). Multiple calibration trials have shown accuracy around ±0.5 dB is to be expected in what is regarded as a typical field calibration environment. Still, this accuracy was found to be susceptible to rapid but small variations of both the salinity and temperature of the stratified water, where a 0.8 dB drop of the measured sphere target strength has been seen. A further improvement of the calibration accuracy does not, however, contribute any significance reduction of the total uncertainty when finally computing the school's biomass.

The volume of a single school is estimated by evaluating its three measured extensions, the length, width and height. The two across-beams extensions, width and height, were seen to be overestimated due to the border effects created by the finite beam width, an effect also reported for echosounders (Diner, 2001). In paper 4, this effect was investigated on several simulated schools of known sizes, where two across-beam smearing effects were identified as the Long Range Smearing and Short Range Smearing effects. Correction of both effects increased the accuracy, giving precisions for the volume estimate between 6.6-8.7 % for the width and 8.5-10.5% for the height. The mean estimated volume of a real school of herring was reduced by 55% by correcting for the smearing effects.

When converting the received acoustic energy into a quantitative biomass measure, the backscattered is divided by a mean backscattering cross-section representative of the species and individual-fish size. For horizontal acoustic transmissions, finding a representative backscattering cross-section is complicated since the cross-section is not only dependent on the distribution of the pitch and roll angles (Nakken & Olsen, 1977), the depth (Ona, 2003) or length of fish (Foote, 1980b), but also the yaw angle (Cutter & Demer, 2007). Circumnavigating the school is proposed as a means of increasing the accuracy of the volume density, where only school data from favourable incidence angles are used, for example close to the

broadside of the school. If both low-frequency and a high-frequency fishery sonar are available, a comparison of the frequency response may give an indication of the actual angle of incidence. Such Dual-Frequency analysis may contribute to a more accurate volume density in situations where a full circumnavigation is not possible.

This synthesis represents only part of the total work conducted in one of the working package in the CRISP project, intended to provide the skipper accurate and reliable information on the school biomass during the last stages of an inspection.

List of publications

Vatnehol, S., Totland, A. and Ona, E.: "*Two mechanical rigs for field calibration of multi-beam fishery sonars*", Methods in Oceanography (2016), http://dx.doi.org/10.1016/j.mio.2016.02.011 (Published)

Vatnehol, S. and Ona, E.: "*Evaluation of target position algorithms for multi-beam fishery sonars*". Submitted to Journal of the Acoustical Society of America

Macaulay, G.J., Vatnehol, S. and Ona, E.: "*Practical calibration of ship-mounted fisheries sonars*". Planned for submission to Journal of the Acoustical Society of America.

Vatnehol, S., Hector Peña and Ona, E.: "*Estimating the true volume of fish schools from observation with multi-beam fishery sonars*". Planned for submission to ICES Journal of Marine Science

Contents

Introduction

Pelagic Fishery

The fishing industry is one of the major industries in Norway. In 2014, 280,000 ton mackerel (*Scomber Scombrus*), 410,000 ton herring (*Clupea Herengus*), 400,000 ton blue whiting (*Micromesistius poutassou*) and 76,000 ton capelin (*Mallotus villosus*) were caught by Norwegian-registered fishing vessels, and then delivered to the Norwegian coast for processing. These three species represent the largest proportion of all pelagic catches (Figure 1).

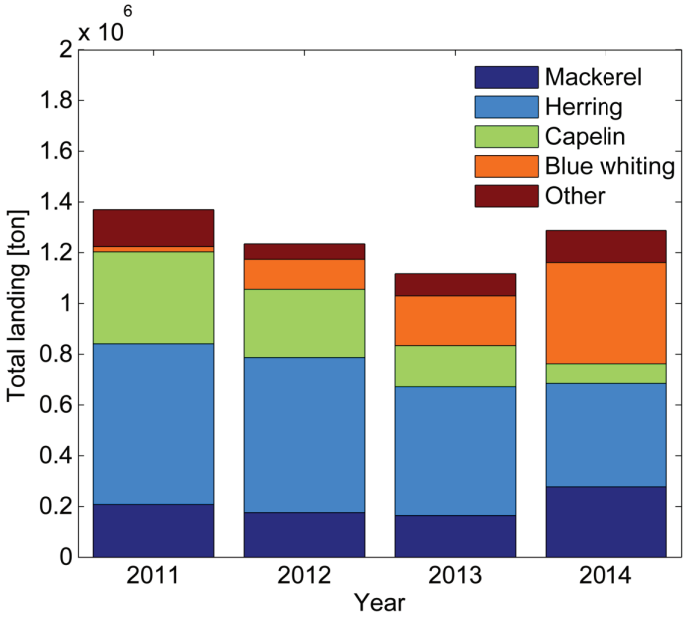

Figure 1. Illustration of the quantity of different pelagic species delivered to the Norwegian coast by Norwegian-registered fishing vessels in the years 2011, 2012, 2013 and 2014. Data from the Norwegian Directorate of Fisheries, www.fiskeridir.no.

The price of landed fish heavily depends on the species, size and quality. *Norges sildesalgslag*, a Norwegian sale organization for the pelagic fishery, states the price of herring in 2014 was 5 NOK/kg for large herring and 3.5 NOK/kg for small herring. Herring unfit for human consumption, either because it was juvenile or injured, was priced as low as 2.65 NOK/kg. This, together with the fact that every Norwegian fishing vessel has its own quota per species, is a strong motivation for selective and strategic fishing.

Ninety percent of all pelagic fish delivered by Norwegian registered fishing vessels, and 30% in a worldwide perspective, were caught by purse seiners (Watson et al., 2006; Huse & Vold, 2010; Tenningen et al., 2012). Purse seining is perhaps the most effective method for catching migrating pelagic fish (Ben-Yami, 1994; Watson et al., 2006). The vessel quickly encircles the school while shooting the seine, while carefully adapting the vessel's course to the speed and heading of the school, then the net is pursed before the hauling begins (Ben-Yami, 1994; Tenningen, 2014).

Figure 2. Photographic image showing the purse seiner F/V "Sjarmør" during the last stages of hauling a school of herring. Photo: Sindre Vatnehol.

In the last stages of the hauling (Figure 2) a representative fish sample is acquired for evaluating the species and size distribution of the catch. If this information is unsatisfactory, or if the total biomass of the school is too large, with regard to the fishing gear capability, storage capacity or quota restrictions, a common but criticized practice is to release the fish in a manner which is known as “slipping”. Although slipping is legal, the practice is not an optimal solution because of the increased fish mortality, caused by either stress, fatigue or injury due to crowding (Lockwood et al., 1983; Marçalo et al., 2010; Huse & Vold, 2010; Tenningen, 2014). To overcome this problem, early indications of the school’s species, total biomass and the mean weight of individual fish, preferably obtained by onboard instrumentation, should be available before deploying the net.

In short, this is called pre-catch information which the skipper on a purse seiner collects in the last part of the school “inspection phase”, where he must decide whether to catch the school or not. One of the key elements in this decision is to evaluate the actual biomass of the school. Many skippers have developed an indispensable expertise using sonar in a relative sense over many years, and can thus estimate the biomass fairly accurately from inspection of the sonar display. Real quantification, however, requires a more scientific approach using calibrated instruments. This is the main topic of this thesis and the main goal of one of the work packages in CRISP (Centre for Research-based Innovation in Sustainable Fishing and Pre-processing technology). CRISP is a research collaboration between research institutions and the industry, and is financed by the Research council of Norway. The aim of the project is to obtain a more sustainable fishery, with less impact on the environment, and also to enable the industry to deliver higher quality products in the future (www.imr.no/crisp).

Thesis objectives

For this thesis the industry partner, Kongsberg Simrad, has given exclusive access to the transducer element data of the Simrad SX90 multi-beam fishery sonar. This made it possible to investigate the properties and limitations of the sonar more closely. New functions could also be added.

The main objectives were:

1. Develop algorithms for estimating the location of a single target within a single acoustic beam for calibration purposes.
2. Develop calibration protocols for multi-beam fishery sonar
3. Increase the accuracy and precision of geometrical measurements of schools
4. Evaluate the suggested improvements on real catch situations

Acoustic methods

Historical survey

One of the earliest references associated with the field of underwater acoustics is the notebook written by Leonardo da Vinci, where the sentence "*If you stop your ship, put a long pipe down into the water and listen, you are able to hear the noise from distant ships*" is often quoted (MacCurdy & Linscott, 1938; Urick, 1983; Simmonds & MacLennan, 2005). Daniel Colladon (a Swiss physicist) and Charles Sturm (a French mathematician) collaborated in a scientific experiment in 1827 where an immersed bell was struck simultaneously with a flash of light on the surface. The time difference between the light and the sound was measured on the other side of Lake Geneva, Switzerland, and thus the speed of sound in fresh water was calculated to be 1450 ms^{-1} (Lasky, 1977). Two physical effects were discovered during the 19th century, essential for the development of modern acoustic devices, namely the magnetostriction and piezoelectric effects. Magnetostriction involves ferromagnetic materials which change size when affected by magnetism; James Joule explored this effect through quantitative measurements in the 1840s. Piezoelectric materials generate an electrical voltage when subjected to mechanical stress; Jacques and Pierre Curie are often credited for this discovery. Several researchers, in the late 19th century, utilized these effects when converting mechanical vibrations (such as oscillating sound waves) into electrical signals and vice versa, a phenomenon named "transduction" (Urick, 1983).

In 1914, R. A. Fessende demonstrated that active (both emitting and receiving) electromagnetic equipment could detect icebergs as far as 2 km away, just two years after the Titanic sank (Hovem, 2012). During the early years of the First World War, passive acoustic equipment (only receiving, and similar to da Vinci's underwater listening device) was used for detecting hostile submarines (Urick, 1983). In 1917, the Frenchman Paul Langevin presented a transducer made of piezoelectric material capable of emitting an acoustic signal at a frequency of 38 kHz. Mechanical steering of such transducers facilitated the detection and positioning of submerged targets.

Such acoustic equipments for detecting submarines were also developed by the secret group ASDIC in England during the First World War. According to Wood (1965), the acronym stands for "*Anti-Submarine Division-ics*". In other literature the acronym is said to stands for "*Allied Submarine Detection Investigation Committee*". Nevertheless, the term ASDIC has been used for decades to describe transducer equipment acting as an acoustical searchlight, which was mechanically steered to survey the whole water column. The world's first fishery-ASDIC (developed by the Norwegian Defence Research Institution (FFI) and later sold to Simrad in 1953) was installed on R/V G. O. Sars in 1949. After the war, in 1919, the first scientific article about sound propagation in water was published in a scientific journal, where the theory of ray-bending caused by small variations in water temperature and salinity was theoretically described (Lichte, 1919).

Kimura (1929) conducted the first successful experiment for detecting fish using acoustical methods, where the presence of fish disturbed a transmitted signal. The first echogram of fish, attributed to the Norwegian fisher R. Bokn of the vessel "Signal", was published in July 1934 (referred to in Fernandes et al. (2002)). In 1935, in advance of the annual oceanographic survey in the Lofoten area, a 16 kHz transducer was mounted on R/V Johan Hjort, where cod, *Gadus morhua*, was observed in a 10 m thick layer at a constant depth (Sund, 1935). A few years later, the distribution of the Norwegian spring spawning herring was annually evaluated using the echosounder as a standard tool (Runnstrøm, 1937, 1941; Sund, 1943). During World War II, a major effort for developing detection equipment such as radar (*Radio detection and ranging*) and sonar (*Sound navigation and ranging*) was undertaken; both acronyms are still in use. Concepts such as the sonar equation, methods of calibration, vessel noise, reverberation etc. began to be quantitatively understood (Urick, 1983). In the post-war years, the echosounder was said to be installed on hundreds of Norwegian fishing vessels (Devold, 1961) since the echosounder was now considered an essential tool for commercial fishing (Hodgson, 1951; Hodgson & Fridriksson, 1955). Finn Devold (expedition leader aboard R/V G. O. Sars in 1950) used both echosounder and ASDIC to track and study the herring migration, where

the fish location and heading was forwarded to the waiting fishing fleet (Dragesund & Midttun, 1966). In the 1950-60s, the concept of a species- and size-dependent directivity pattern of single fish was known, with these effects being highlighted through target strength measurements (Cushing, 1955; Jones & Pearce, 1958; Midttun & Hoff, 1962). Approaches using acoustics in fish stock assessment were also developed in the 1950-60s, first through counting of individual echoes (Tungate, 1958; Mitson & Wood, 1961), summing of the echo amplitudes (Richardson, 1959), and finally the echo-integration method based on the echo amplitude (Dragesund & Olsen, 1965). Integrating the echo intensity was later shown to be a more correct approach (Scherbino & Truskanov, 1966). The technique of echo-integration was attributed to Ingvar Hoff (Simmonds & MacLennan, 2005) and is still used in stock assessment.

When the transducer is designed as an array of transducer elements, a single beam can be steered towards a specified direction when a time delay is added between adjacent transducer elements (Sherman & Butler, 2007). This is the fundamental principle of the electronic sector-scanning sonar (Voglis & Cook, 1966; Forbes & Nakken, 1972) where the single beam is steered in a stepwise manner through a pre-defined sector. Such systems have been utilized to investigate fish behaviour and movements of fish schools (Harden Jones & McCartney, 1962; Welsby et al., 1963, 1964). Mitson & Cook (1971) presented a system where the transducer was mechanically steered from scanning a horizontal sector to a vertical sector. In one investigation, a vertically oriented 330 kHz scanning-sonar, the Simrad FS 3300, was used to study fish-avoidance effects when a survey vessel crossed above them (Ona & Toresen, 1988).

A collaborate project between Simrad and Norwegian research institutions began in 1968 with the intention to explore the possibility of incorporating contemporary computer technology with the new multi-beam approach (Olsen, 1972; Bodholt & Olsen, 1977). Here, a rectangular transducer array formed 10 beams simultaneously, where the beams were evenly distributed along a 60º sector. The beam width was 6º. The transducer, hence the sector, was mechanically tilted and

rotated towards any direction below the sea surface. Its successor, SM600 (Bodholdt, 1982), had a similar transducer design and functions, where the 85º sector was resolved into 17 beams, each with a beam width of 9x7º. Multi-beam sonar studies using the SIMRAD SM600 sonar (Misund & Aglen, 1992) and the RESON SeaBat 6012 (Gerlotto et al., 1994, 1999; Soria et al., 1996), when investigating vessel avoidance by schooling fish, is regarded as pioneer work (Foote et al., 2005).

Using fishery sonar for scientific purposes has been a common strategy for acquiring supplementary information about what is beneath the sea surface. Some examples of these scientific applications are noted here: The scanning sonar Simrad SU was used to track acoustically tagged fish during behaviour studies (Dalen, 1974). The omni-directional fishery sonar Simrad SP90 has been used to study the aggregation of whales around FADs (Fish Aggregating Devices) (Brehmer et al., 2012), and to develop multi-beam processing tools for identifying and tracking schools of fish (Trygonis et al., 2009). The Simrad SR240, also omni-directional, has been used for investigating the behaviour and avoidance reactions of fish schools (Misund et al., 1993; Hafsteinsson & Misund, 1995), and monitoring ecosystems in shallow water (Brehmer et al., 2003). A proposal for continuous data acquisition with automated data extraction and processing has been reported (Brehmer et al., 2006), where both the SR240 and the Furuno CSH20 sonars were to be used. The Simrad SX90, which is relevant to this thesis, has previously been used to estimate the speed of Peruvian anchovy schools (Peraltilla & Bertrand, 2014) and to measure the target strength of whales (Bernasconi et al., 2013; Geoffroy et al., 2015).

Acoustics and backscattering from fish

Fish which have a gas-filled swim bladder are grouped into two species-categories; physostomes (open swim bladder for gas release) and physoclists (closed swim bladder) (Blaxter & Batty, 1984). When ensonified by for example a downward orientated echosounder, the swim bladders are the main reflector of acoustic energy since 90-95% of the measured echo intensity, which is usually described in terms of

the target strength (TS, dB re 1 m^2), originates from this organ (Foote, 1980b). The residual energy originates from the rest of the fish body, for example the flesh, bones and the head.

Herring, being a physotome, cannot adapt its buoyancy to the pressure at depth by regulating the quantity of gas within the bladder, while the physoclisti do have this capability (Blaxter & Batty, 1984; Ona, 2003). The herring swallows gas at the sea surface, where the gas is led to the swimbladder via the stomach duct. In the clupeid swimbladder, one channel connects the bladder to the air-filled bulla system in the inner ear, and the anal duct also connects the bladder directly to the outside sea water via a sphincter muscle. During rapid descent, gas is released directly out into the sea via the anal duct, enabling a rapid escape response for herring when attacked by physoclisti predators such as cod. The swimbladder is usually not emptied in tranquil descent; therefore, the volume of the bladder shrinks with the increased pressure as a consequence of the Boyle-Mariette law. Thus the target strength of the herring is depth dependent (Ona, 1990, 2003).

Atlantic mackerel, on the other hand, belongs to a third group of species which have no swim bladder (Foote, 1980b; Gorska et al., 2005, 2007). Consequently, the target strength of a single mackerel is considerably less than that of a swimbladder bearing fish of the same size. A target strength difference between 10-13 dB between cod and mackerel has been reported (Foote, 1980b), hence the conclusion that 90-95% of the backscattered echo originates from the swim bladder.

The amplitude of the target's echo is known to be frequency dependent (e.g. Johnson, 1977; Holliday, 1978; Greenlaw & Johnson, 1983), and this frequency response can, to some degree, identify the species and the size of the fish (e.g. Horne, 1999; Kloser et al., 2002; Korneliussen & Ona, 2002, 2003; Korneliussen et al., 2009; Demer et al., 2009; Johnsen et al., 2009; Kubilius & Ona, 2012). Also, the orientation of the fish relative the acoustic axis of the transmitted beam contributes to notable changes in the target strength (Love, 1969; Cutter & Demer, 2007; Pedersen et al., 2009). For example, Love (1969) reported a target strength difference close to 10 dB

at 30 kHz when a black crappie (*Pomoxis nigromaculatus*) was ensonified in side aspect, compared to either the posterior or anterior aspect (head-tail directions).

Individual fish cannot be distinguished through standard acoustical methods if they are in too dense aggregations, which is common for species such as herring and mackerel. Nevertheless, if the aggregations are not so dense that acoustic extinction occurs (Foote, 1983, 1990), the linear relationship between the density of targets and the accumulated backscattered energy from the effective volume of the signal pulse has been proven valid (Foote, 1983; MacLennan, 1990). Consequently, if a representative mean target strength of the fish, and their length distribution, are known, the density of fish within the aggregation can be computed from the ratio of the accumulated energy and the mean backscattering cross-section (which is a linear measure equivalent to the target strength).

Still, the total backscattered energy from a school is highly dependent on the orientation of each fish inside the school (Cutter & Demer, 2007; Holmin et al., 2012). The volume backscattering coefficient, s_v, is often observed to be greatest when a polarized school is ensonified in its lateral aspect, and smallest in the posterior or anterior aspects. If the fish inside the school were more randomly orientated, the mean backscattered energy from the school is weaker although less directive. This orientation effect must therefore be considered when evaluating the school biomass, and needs to be further investigated here.

If the mean size of fish is known, and the density of fish inside the school is accurately estimated, the total biomass within a school (M) can be simply expressed as:

$$M = \bar{\rho}_v \overline{w}_i V, \tag{1}$$

where $\bar{\rho}_v$ is the mean volume density of fish, $\overline{w}_i$ is mean weight per fish, and V is the correct volume of the school.

Single-Beam echosounder systems

A typical echosounder system includes a hull-mounted, downward orientated transducer unit which emits, and receives, acoustic signals. Such equipment is commonly used for quantitative evaluation of fish abundance during scientific surveys (Simmonds & MacLennan, 2005). Multi-frequency analysis, such as for species classification, can be achieved by simultaneous operation of several transducer units, each transmitting at a different frequency (e.g. Kloser et al., 2002; Korneliussen & Ona, 2002; Gorska et al., 2005; Fässler et al., 2007). The scientific echosounder system facilitates recording of the echo amplitudes detected by each transducer unit, for each simultaneous transmission/receiving event (aka. ping), in a digital raw-data format (Korneliussen et al., 2008).

To prevent loss of acoustic energy due to scattering by air bubbles in the near-surface region (Dalen & Løvik, 1981), the transducers are mounted on the bottom of the vessel, or sometimes lowered below the hull of the vessel by means of a drop keel (Ona & Traynor, 1990). The transducer draft and the lack of useful quantitative measurements in its near-field, and ringing effects on the transmission, means that fish close to the sea surface, that is to say in the acoustical blind zone (Totland et al., 2009), are excluded from the echo-integration. Therefore, on the research vessel G. O. Sars, the echo integration starts at 10 m below the sea surface in good weather, and 12 m in bad weather conditions. Additionally, the fish may react to the presence or approach of the vessel at close range, where the school structure or its location, after noise exposure, may be distorted (Misund 1993; Soria et al. 1996; Ona et al. 2007). For these reasons, vertical echosounders are not the preferred tool when investigating a possible catch.

Multi-beam systems

A multi-beam system transmits several acoustic beams, all formed simultaneously by processing the signals from multiple elements of the same transducer unit, where each beam is directed in a specified direction (Sherman & Butler, 2007). Only multi-beam systems which can operate in the echosounder's acoustical blind zone are of relevance here and are further addressed. According to preferences, there are two categories of such multi-beam sonars; full 3D-systems and 2D-systems.

In a full 3D-system, the beams are orientated to completely ensonify a specified sector-volume. For the horizontally transmitting Simrad MS70 Scientific Multi-Beam sonar (Andersen et al., 2006; Ona et al., 2006), a sector volume is ensonified by 20 beams in a vertical fan (distributed from 0 to 45º below horizon) and 25 beams horizontally, covering a 60º sector. The 500 beam widths are all close to 3º. The system gains of each beam are accurately measured by a multi-beam calibration using split-beam target positioning (Ona et al., 2007a, 2009). The fish species is determined by evaluating the school's morphological features (e.g. Gerlotto & Paramo, 2003; Korneliussen et al., 2009); here, specifically, by evaluating the school's structure, depth distribution, and its backscattering properties. The MS70 system is not, however, installed on any commercial fishing vessel. It is installed on only a few research vessels, and hence is presently not available as a tool for the fishing industry.

The 2D-system has multiple beams orientated within a single contiguous fan, revealing a narrow cross-section of the water column, for example the Simrad SM2000 (Chu et al., 2002). Such instruments do not have the same spatial coverage as the full 3D-system, although they have been used for counting and evaluating the migration speed of whales and fish schools (Misund, 1990; Peraltilla & Bertrand, 2014; Pyc et al., 2015). Also, the 2D-system has been used to estimate school biomass through visual evaluation of the sonar display (Misund et al., 1992, 1995), and to estimate school volume and structure using various scanning modes and algorithms (Gerlotto et al., 1994; Gerlotto & Paramo, 2003; Tang et al., 2009). The

new Simrad SN90 fishery sonar is being used on an increasing number of fishing vessels. This instrument presents both a vertical and a horizontal cross-section of a school sequentially. However, the SN90 is still too recent a development for evaluation of its scientific potential.

Another 2D-system is the so-called omni-directional fishery sonar, a common equipment found onboard most fishing vessels (Brehmer et al., 2006). The term "omni-directional" in this context means the transmissions are omni-directional in the horizontal cross-section, but they cover only a narrow range of angles in the vertical section. Previously, such sonars have been used for evaluating school biomass (Misund, 1993a) through comparison of the school's cross-section area, determined using the Furuno CSH-70, and the actual catches from purse-seining. Tenningen et al. (2015) recorded screen shots from the SH80 (a high-frequency fishery sonar, 110-122 kHz) sonar display, where these images were analyzed along with observations of the pursed volume, and the size of the mackerel school within the net. Brehmer et al. (2006) proposed a scheme for storing and analysing non-digital sonar data. More recently, the echo amplitude from each sonar beam has been digitized in a new raw-data format, which allows further and more comprehensive analysis. Nishimori et al. (2009) presented a method for quantitative echo-integration when evaluating the fish-school abundance, independent of the school volume, using digital beam data from the Furuno FSV-30 (22.5 kHz). Peña et al. (2013) used the software PROFOS (Processing system for omni-directional fisheries sonar) to track herring schools after exposure to seismic activities, using raw and un-calibrated echo-amplitude data from the SH80 fishery sonar. Trygonis et al. (2009) presented an operational system for automatic identification and tracking of fish schools using raw data from the Simrad SP90 fishery sonar.

In this thesis, such multi-beam fishery sonars are further evaluated, and their key features are briefly described in the following section.

Sonar Discription

Both simulated and field data from the Simrad SX90 and the Simrad SU90, manufactured by Kongsberg Maritime AS (Simrad, 2007), were utilized in the presented work. The two sonars are almost identical, except that the SU90 transducer is a 1.5 times longer than the SX90 transducer and its vertical beam width is narrower than that of the SX90. Fishers prefer the sonar transducer to be mounted as far towards the bow as practicable. A mechanical hoisting device (Figure 3 left) is used to lower the transducer to a depth 1.2-1.6 m below the hull of the vessel, in order to reduce the adverse absorption effects from wind-induced air bubbles in bad weather conditions (Dalen & Løvik, 1981).

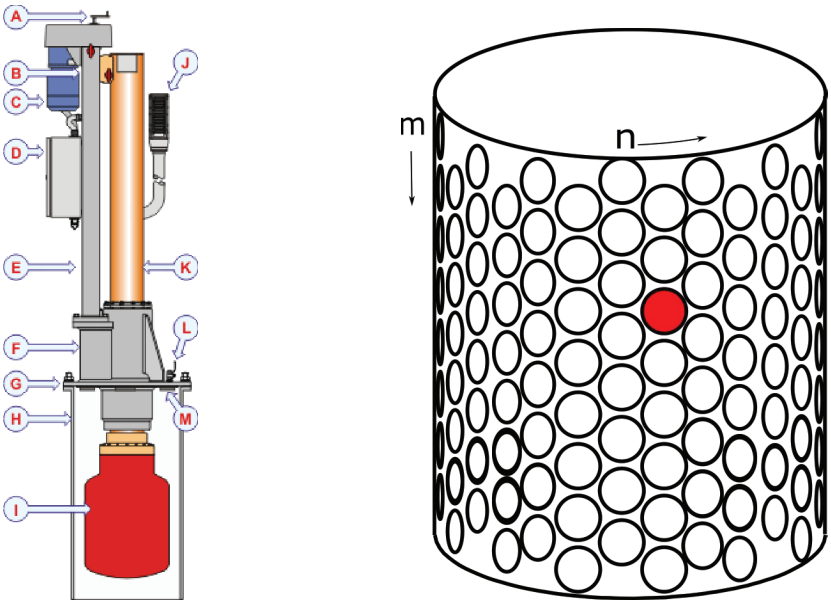

Figure 3, To the left, schematic diagram of the mechanical hoisting device used to lower the transducer. Full description of the diagram is shown in Simrad (2007). *To the right, schematic diagram of a cylindrical transducer array with 256 elements (equivalent to part I in the figure to the left). One element is coloured red. The element index along the cylindrical wall is 'n', increasing counter-clockwise. The vertical element index is m, increasing downwards.*

The transducer unit is a vertically-aligned cylindrical array composed of either 256 (SX90) or 384 (SU90) transducer elements (Figure 3 right). The exact alignment of each element was not given due to company restrictions, and only approximate figures are given here. Therefore, the cylinder radius is $a_r = 0.185\ m$, and the radius of the circular transducer elements is $a_e = 0.020\ m$. The array is preferentially partitioned into $N = 32$ evenly separated line arrays with either $M = 8$ (SX90) or $M = 12$ (SU90) transducer elements, uniformly separated by 1.5 mm physical spacing between each element. When the array pitch and roll are disregarded, the orientation of each element is $(\theta_{nm}, \phi_{nm}) = \left(\frac{\pi}{2}, \frac{2\pi(n-1)}{N}\right)$, where $n = [1, \ldots, N]$ is the index of the line array (counter-clockwise when seen from above) and $m = [1, \ldots, M]$ is the index of the element within each linear array (downward increasing) (Figure 3). Each transducer element is a *tonpilz* piezoelectric transducer, which implies the element is comprised by several tightly stacked piezoceramic rings (e.g. Yao & Bjørnø, 1997). The acoustic performance of each element was measured in a laboratory tank at Simrad in Horten as part of their QA-system (quality assurance).

Each of the active transducer elements radiates either a single frequency (CW) or a hyperbolic frequency modulated (FM) signal. The purpose of the FM signal is to minimise the degradation of matched filter processing caused by the Doppler effect (Readhead, 2010). The signal's centre frequency is selectable between 20 and 30 kHz in 1 kHz steps, and the sonar's detection range is selectable between 150 m and 8 km. For practical reasons, such as interference from bottom reverberation and ray bending (Lichte, 1919), the detection range was limited to 600 m in any investigation. The duration of the signal pulse is dictated by both the selected signal type and detection range, which in our case gave a maximum pulse duration of 4 milliseconds when using the preferred range settings and a short CW signal (Table 1).

Table 1. Duration of the transmitted signal for various target ranges and the selectable signal types. The full table includes the pulse durations up to 8 km range, as reported in (Simrad, 2007).

Range (m)	*FMshort (ms)*	*FMnormal (ms)*	*FMlong (ms)*	*FMauto (ms)*	*CWshort (ms)*	*CWnormal (ms)*	*CWlong (ms)*
150	1	4	6	4	1	2	6
300	2	8	12	8	2	3	12
450	3	12	18	12	3	6	18
600	4	16	24	16	4	8	24
900	6	24	36	24	6	12	36
1200	7	28	42	42	7	14	42
1500	8	32	48	48	8	16	48

During reception (Figure 4) the complex transducer element data are recorded after the raw acoustic signals were filtered and pulse-compressed with 4 kHz sampling frequency. The sonar software utilizes the element data to form 64 receiver beams with a nominal beams width between 7.4º (30 kHz) and 11.4º (20 kHz) vertically, and between 8.5º (30 kHz) to 10º (20 kHz) horizontally. The measured echo amplitudes received by each beam are stored as raw data in the so-called "*Scientific Data Output"*. Additional filtering and processing is required in order to display a clean and preferably noise-free image on the sonar display.

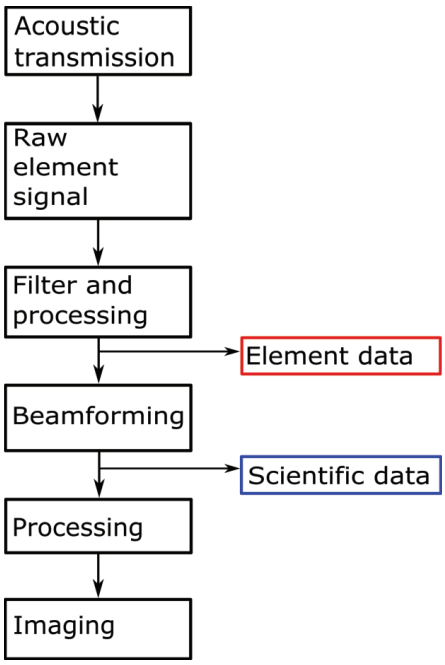

Figure 4, Sketch for sonar data flow; the acoustic reflection is recorded by the transducer elements, filtered and stored as the element data (Red). Subsequently, the element data are beam-formed, then stored as the scientific data output (Blue). The beam data are further processed with additional filters, and interpolated before displaying a smooth and preferably noise free picture on the sonar display.

The beams are orientated according to selectable transmission modes, namely the *horizontal mode* and the *vertical mode* (Figure 5;Tang et al., 2006). If both modes are activated, the two cross-sections are automatically alternated and their echograms are displayed in separate windows on the sonar screen. In the horizontal transmission mode, the sonar transmits and receives a single fan of beams evenly distributed in a cone with the transducer at the apex. Through the sonar interface, the user may electronically steer all the beams towards a common tilt angle. In the vertical transmission mode, the beams are distributed in a vertically aligned semicircle, providing a narrow cross-section of the lower hemisphere. This fan of beams can be rotated by the user with the transducer acting as a celestial pole. The direction of the beams is automatically compensated for vessel movements by the sonar software.

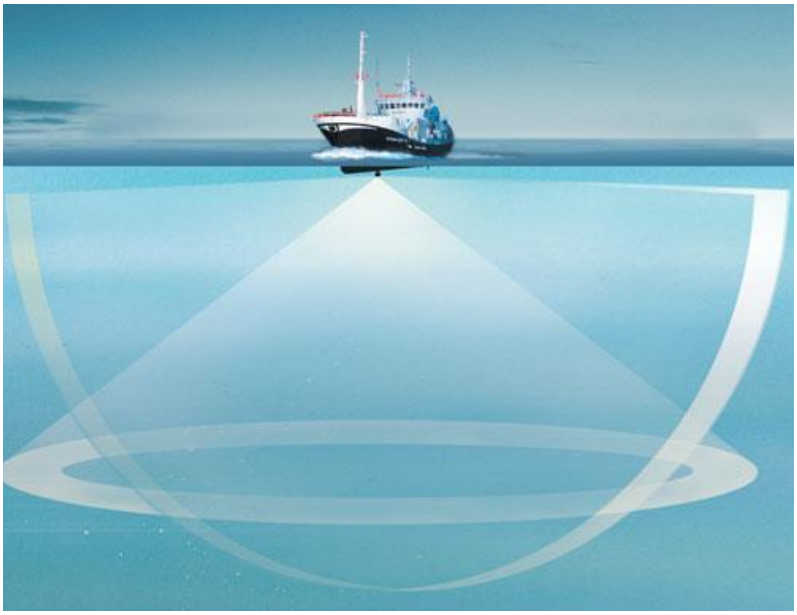

Figure 5, Picture of the two sonar fans from the SX90 sonar. The conical fan is an illustration of the beams' orientation in the horizontal mode, while the vertical aligned semicircle illustrates the orientation of the beams in the vertical mode. (SIMRAD. 322074/A 12.2011)

Discussion

Calibration of cylindrical multi-beam fishery sonar

Accurate calibration of acoustical equipment is essential for good quantitative measurements (Foote et al., 1987; MacLennan, 1990; Aglen, 1994; Simmonds & MacLennan, 2005). The mean density of targets per unit volume is computed from the measured mean volume backscattering coefficient, $\bar{s}_v$, divided by the mean backscattering cross-section of an individual target, $\bar{\sigma}_{bs}$;

$$\bar{\rho}_v = \frac{\bar{s}_v}{\bar{\sigma}_{bs}} \tag{2}$$

where the parameter to be calibrated prior to a survey is $\bar{s}_v$.

There are several methodologies for calibrating acoustic equipment, for example reciprocity calibration or using pre-calibrated hydrophones (Foote et al., 1987; Simmonds & MacLennan, 2005). However, in fishery acoustics the usual practice is to calibrate the equipment using a standard reference reflector (Foote & MacLennan, 1984). A solid spherical target is advantageous due to its relatively strong and stable ability to reflect sound, with the amplitude of the backscattered echo being independent of the transmitted wave's angle of incidence. Another advantage of using a reference target is swift mapping of the beam pattern when the position of the target can be measured directly.

Estimation of the reference target's position

The various methods which have been used to estimate the target position fall into one or other of the following two categories;

i. **Data-independent methods** – these do not utilize the acoustic data directly for estimating the target direction.
ii. **Data-dependent methods** – these do utilize the acoustic data for estimating the target direction.

Data-independent methods

The typical procedure for calibrating a single-beam echosounder was to carefully steer the calibration sphere within the acoustic beam until a maximum echo strength was observed (Foote et al., 1987; Simmonds & MacLennan, 2005). Since the sphere location relative to the transducer was unknown, moving the sphere to the centre of the beam was a tedious process. Another pitfall, although uncommon among experienced calibration personnel, is to centre on one of the side lobes and misinterpret it as the main lobe.

Another common approach is to calibrate the acoustical device either in a tank or deployed at sea, with known or controlled environmental conditions (Chu et al., 2001; Doherty et al., 2002; Jech et al., 2003; Cochrane et al., 2003; Melvin et al., 2003; Foote et al., 2005; Nishimori et al., 2009; Lanzoni & Weber, 2011). A typical protocol involves rotating the acoustic transducer while the reference target is held stationary. In practical terms, this is not a desirable procedure as it involves removing the transducer from the ship's hull. This incurs extra costs and time.

Using a reference target deployed from a second vessel for calibration comparisons between multiple beams has been suggested for cylindrical multi-beam sonar (Brehmer & Gerlotto, 2001). Such a procedure was here rejected due to its poor accuracy, and consequent bias in biomass estimates. It should be noted, however, that

the authors suggested the split-beam technique could be used to locate the calibration sphere inside each beam during field calibrations.

In this thesis, a reference target was steered with millimetre precision inside a single beam from the cylindrical transducer using a specially designed calibration rig (Paper 1). The rig was mainly utilized for developing a within-beam target-position algorithm for field calibrations (Paper 2). While this method may still be used to compute the system gain and the beam widths, in practice the rig performance was found to be too laborious in situations where external forces, such as water currents or ship movements, influenced the position of the reference target. Also, the horizontal scope of the rig was confined to only one beam at each rig mounting location (Paper 1). That design did not allow a quick and effective multi-beam calibration; however, it motivated the development of a new calibration rig which, when operated with a target-positioning algorithm, enabled faster calibrations of a larger fraction of the sonar beams.

Data-dependent methods

This category covers instruments capable of determining the target position relative to the transducer, based on acoustic measurements alone. The Dual-Beam method was one of the first developments of this kind (Ehrenberg et al., 1976). Here, two concentric beams with collinear acoustic axes are formed simultaneously. To correct echo measurements for the beam shape, the inclination angle between the target direction and the (common) acoustic axis is determined from the ration of the two measured echo amplitudes. The Dual-Beam method was later superseded by the split-beam technique which has superior performance in the presence of noise (Ehrenberg, 1983). The split-beam principle involves a transducer with four quadrants whose signals are processed separately. The target direction, defined by two angles, is determined by comparing the time delays between the four quadrant signals (Carlson & Jackson, 1980; Ehrenberg, 1983; Degnbol, 1988).

The same split beam principle was adapted for calibrating the cylindrical multi-element transducer, where the array processing applied to the transducer elements was a crucial step, improving the signal-to-noise ratio to better separate the target echo from the background noise (Paper 2). Two pairs of transducer halves, one for vertical and the other for horizontal positioning, were formed through the combination of data from selected transducer elements. Overlapping transducer halves were considered, but rejected because this approach did not improve the precision with any practical significance (Paper 3). Still, a precision between 0.2 and 0.24º is expected under typical calibration conditions (eSNR ~5dB) and using a low tilt angle (-5º) (Figure 6). During the calibration of the SU90 on F/V "Eros" on 19th October 2015, the calibration conditions were nearly ideal, with almost no sea or vessel movement, and the precision in that case was computed to be as good as 0.09º, corresponding to an element signal to noise ratio (eSNR) around 15 dB (Figure 6). The precision of the split beam approach is reduced when the beam is steered towards steeper angles below the horizon.

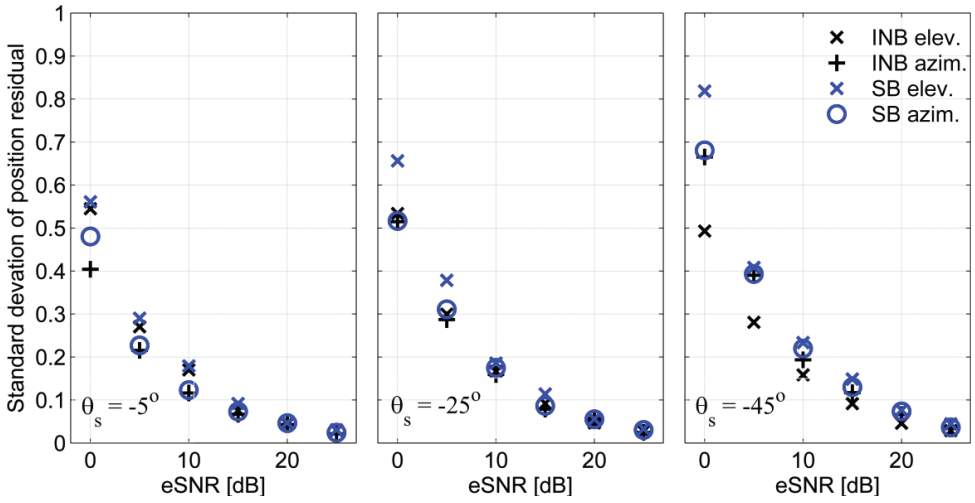

Figure 6, Figure illustrating the expected precision of the SB (blue) and INB (black) methods, along horizontal (x) and vertical (+) directions, when the target is at the centre of a beam steered towards $-5°$ (left), $-25°$ (middle) and $-45°$ (right) relative the horizon. The effect of noise is shown by changing eSNR from 25 dB to 0 dB with -5 dB steps.

The offset between the target positions determined mechanically by the calibration rig (Paper 1) and those from the split beam data (Paper 2) was believed to be caused by incorrect allocation of the rig's reference position. Still, it may also be caused by unexpected variability between the element sensitivities, as such irregularities could generate position offsets similar to those reported in Jech et al. (2003, 2005). In essence, the split beam approach was found to be sufficiently accurate for practical field calibrations. A dedicated Matlab script facilitated real time positioning of the sphere, since the computational time was less than the minimum ping interval (0.2 s). Real time detection of the sphere is highly advantageous during practical calibrations, since this will reveal any unwanted sphere movements when they occur.

A second target position algorithm was also included in Paper 2, namely the Interpolated Neighbouring Beam (INB). With this method, the target direction within the beam is estimated from the amplitude differences between the two adjacent beams. When the two amplitudes are equal the target is at the centre in the beam in between, where the method's precision equals that of the split beam approach (Figure 6). In a practical calibration where the beam pattern is measured, the accuracy of the INB is insufficient once the target is located outside the centre of the beam (Paper 2).

There are other algorithms for estimating the reference target's direction, such as Esprit, MUSIC, minimum variance, etc. (Krim & Viberg, 1996). However, several of these methods were considered unsuitable for the typical fishery sonar, due to their poor performance in situations with coherent signals, or because the sonar design did not meet the requirements of a linear array structure, such as uniformly spaced elements.

Calibration of the SX90

Initial preparation

The fishery sonar transmits nearly horizontally. Therefore, its calibration has challenges beyond what was experienced during traditional echosounder calibration. Inside fjords, sheltered from the wind and weather, fresh water inflows cause stratification of the water column, (Skarthhamar & Svendsen, 2010). As a consequence, the sound speed close to the sea surface is highly variable. This causes bending of the sound transmission (and reception) (Lichte, 1919). Near surface waters further out in the fjords may be more homogeneous, resulting in less ray bending. However, close to the open sea the vessel is much more susceptible to wind, waves and weather than inside the fjords, then positioning of the reference target is an onerous task. For this reason, it was preferred to calibrate inside the fjords, sheltered by mountains, even if the accuracy of the calibration was reduced as a consequence of the variable environmental parameters.

Three environmental parameters need to be computed prior to the calibration; the acoustic absorption coefficient, the sound speed in water, and the water density. The **absorption coefficient** (α; [dB/km]) was determined by the following expression (Ainslie, 1998)

$$\alpha = 0.106\frac{f_1 f^2}{f_1^2 + f^2}e^{(pH-8)/0.56} + 0.52\left(1+\frac{T}{43}\right)\left(\frac{S}{35}\right)\frac{f_2 f^2}{f_2^2 + f^2}e^{\frac{-D}{6}} + 0.00049\, f^2 e^{-\left(\frac{T}{27}+\frac{D}{17}\right)}, \quad (3)$$

where T is the temperature in degrees Celsius, S is the salinity in PSU (practical salinity units, [g kg^{-1}] (Millero, 1993)), D is the depth in metres, f is the central frequency of the signal (kHz), $f_1 = 0.78\sqrt{\frac{S}{35}}e^{T/26}$ is the relaxation frequency of boric acid (Francois & Garrison, 1982) and $f_2 = 42\, e^{T/17}$ is the relaxation frequency of magnesium sulphate.

The **propagating sound speed** in salt water (c [m/s]) follows from Chen & Millero (1977);

$$\begin{aligned} c_{sw} = {} & 1402.392 + a_1 T - a_2 T^2 + a_3 T^3 + a_3 S + a_4 S^2 + a_5 P \\ & + a_6 P^2 - a_7 P^3 - a_8 T S + a_9 T P + a_{10} T^2 P^2 - a_{11} T P^2 \\ & + a_{12} T P^3 - a_{13} T^3 P - a_{14} S^2 P^2 + a_{15} T^2 S \\ & + a_{16} T S^2 P - a_{17} T S P, \end{aligned} \tag{4}$$

where P is the absolute pressure, and $a_1 - a_{17}$ are the empirical coefficient detailed in Chen & Millero (1977). There are other approximations (e.g. Kinsler et al., 1999), but the model proposed by Chen & Millero (1977) is the standard adopted by the Norwegian Institute of Marine Research and was thus adopted here.

The **density** of sea water is, according to Fofonoff & Millard (1983),

$$\rho_{sw}(S,T,P) = \frac{\rho_{sw}(S,T,0)}{1 - \frac{P}{K(S,T,P)}}. \tag{5}$$

Here, the density of sea water, at the surface, is

$$\begin{aligned} \rho_{sw}(S,T,0) = {} & 999.842594 + b_1 T - b_2 T^2 + b_3 T^3 - b_4 T^4 + b_5 T^5 \\ & + S(b_6 - b_7 T + b_8 T^2 - b_9 T^3 + b_{10} T^4) \\ & + S^{1.5}(b_{11} + b_{12} T - b_{13} T^2) + b_{14} S^2, \end{aligned} \tag{6}$$

and the secant bulk modulus is:

$$\begin{aligned} K(S,T,P) = {} & 19652.21 + d_1 T - d_2 T^2 + d_3 T^3 - d_4 T^4 + S(d_5 - d_6 T \\ & + d_7 T^2 - d_8 T^3) + S^{1.5}(d_9 + d_{10} T - d_{11} T^2) + P[d_{12} + d_{13} T \\ & + d_{14} T^2 - d_{15} T^3 + S(d_{16} - d_{17} T - d_{18} T^2) + d_{19} S^{1.5}] \\ & + P^2[d_{20} - d_{21} T + d_{22} T^2 + S(d_{23} + d_{24} T + d_{25} T^2)]. \end{aligned} \tag{7}$$

The constants $b_1 - b_{14}$ and $d_1 - d_{25}$ are empirical coefficient shown in Fofonoff & Millard (1983). The Salinity (S), Temperature (T), and Depth (D) (which defines the pressure (P)) are all measureable by performing CTD (Conductivity, Temperature and Depth) casts, using for example the Seabird 911 CTD system (Seabird, 2015).

Backscattering properties of elastic sphere

A 64 mm diameter Tungsten Carbide calibration sphere with 6% cobalt binder was selected as the reference target. This sphere was initially produced for calibrating sonars at higher signal frequencies ($\sim 114\ kHz$); although, its theoretically computed frequency response showed that the sphere was also a suitable reference target for sonars with an operational frequency similar to the SX90 (Figure 7). A 63 mm copper sphere has also been used in the calibration of the SX90 sonar (Geoffroy et al., 2015; Pyc et al., 2015). The frequency response of the calibration sphere is theoretically computed using the scattering theory of elastic spheres (Faran, 1951; Hickling, 1962; MacLennan, 1981), where the steady-state signal and far-field determination of the backscattering cross-section of an elastic sphere is (here reprinted from MacLennan (1981))

$$\sigma = a^2\,|f_\infty(ka)|^2, \tag{8.a}$$

where k is the wave number, a is the sphere's radius, and

$$f_\infty(ka) = -\frac{2}{ka}\sum_{l=0}^{\infty}(-1)^l(2l+1)\sin\eta_l\, e^{i\eta_l}\,. \tag{8.b}$$

Here

$$\eta_l = \operatorname{atan}\left\{-\frac{B_2 j_l(ka) - B_1 j_l(ka)}{B_2 y_l'(ka) - B_1 y_l(ka)}\right\}, \tag{8.c}$$

where j_l is the spherical Bessel function of first kind and y_l is the spherical Bessel function of the second kind, and

$$B_1 = ka\left[A_2 ka\frac{c_{sw}}{c_{sph,l}} j_l'\left(ka\frac{c_{sw}}{c_{sph,l}}\right) - A_1 j_l\left(ka\frac{c_{sw}}{c_{sph,t}}\right)\right], \tag{8.d}$$

$$\begin{aligned} B_2 = A_2\left(ka\frac{c_{sw}}{c_{sph,t}}\right)^2\left[\beta j_l\left(ka\frac{c_{sw}}{c_{sph,l}}\right) - \gamma j''\left(ka\frac{c_{sw}}{c_{sph,l}}\right)\right] \\ - A_1\gamma\left[j_l\left(ka\frac{c_{sw}}{c_{sph,t}}\right) - ka\frac{c_{sw}}{c_{sph,t}} j_l'\left(ka\frac{c_{sw}}{c_{sph,t}}\right)\right]. \end{aligned} \tag{8.e}$$

Here $c_{sph,l}$ is the velocity of the longitudinal wave, and $c_{sph,t}$ is the speed of the transverse wave inside the sphere,

$$\gamma = 2\left(\frac{\rho_{sph}}{\rho_{sw}}\right)\left(\frac{c_{sph,t}}{c_{sw}}\right)^2, \tag{8.f}$$

$$\beta = \left(\frac{\rho_{sph}}{\rho_{sw}}\right)\left[\left(\frac{c_{sph,l}}{c_{sw}}\right)^2 - 2\left(\frac{c_{sph,t}}{c_{sw}}\right)\right], \tag{8.g}$$

$$A_1 = 2l(l+1)\left[ka\frac{c_{sw}}{c_{sph,l}}j_l'\left(ka\frac{c_{sw}}{c_{sph,l}}\right) - j_l\left(ka\frac{c_{sw}}{c_{sph,l}}\right)\right], \tag{8.h}$$

$$A_2 = (l^2+l-2)j_l\left(ka\frac{c_{sw}}{c_{sph,t}}\right) + \left(ka\frac{c_{sw}}{c_{sph,t}}\right)^2 j_l''\left(ka\frac{c_{sw}}{c_{sph,t}}\right), \tag{8.i}$$

and ρ_{sph} is the density of the sphere.

Equation 8.a can be adapted for signals of finite length, which include a band of frequencies, as shown by MacLennan (1981); however, the principle dependencies of the backscattering cross-section are the transmitted signal frequency (or its wave number, k), the material properties of the sphere ($a, \rho_{sph}, c_{sph,l}, c_{sph,t}$), and the environmental factors (ρ_{sw}, c_{sw}), where the latter are computed using equations 4 and 5. These dependencies are seen in equations 8.a to 8.i. The material properties of the sphere are provided by the manufacturer, although these may be checked for a particular sphere by measuring its frequency-response spectrum (Hobaek & Forland, 2013). In this procedure, the transverse and longitudinal sound speeds are computed from the position of nulls in the echo frequency spectrum, revealed by broad-band transmitted pulses.

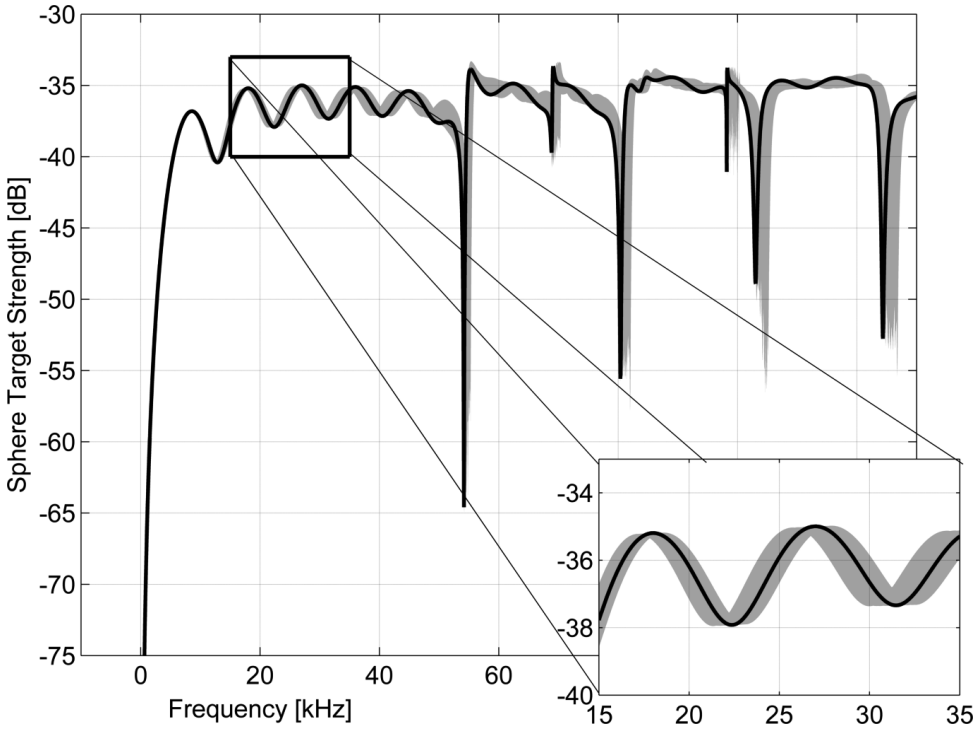

Figure 7. The computed target strength of a 64 mm diameter Tungsten Carbine sphere with 6% cobalt binder, specially designed for fishery sonars operating at 20-30 kHz and 110-120 kHz (Ona, pers. communication 2015). Typical variations in reference target response as a function of temperature (-2, 20ºC) and salinity (0 – 50 PSU) are shown as grey areas. The specific response during our measurements (T = 10ºC, PSU = 35, and reference target depth of 13 m) is shown as a black line. The frequency range is 0 to 120 kHz in the main plot, and 15 to 35 kHz in the expanded window.

Typical survey and fishing grounds in the North Sea, Norwegian Sea and the Barents Sea have relatively stable temperature and salinity features. The temperature near the sea surface changes in a seasonal manner between 2 and 15ºC. At the calibration sites inside fjords, however, both temperature and salinity in the upper 20 m may be affected by freshwater runoff into the fjords. Significant stratification may therefore occur within the ensonified volume. Repeated calibrations have shown that a vertically orientated echo sounder, despite the stratification, can be calibrated with

an accuracy better than 0.1 dB (Knudsen, 2009). For horizontally orientated transducers, stratification across the acoustic beam may cause some error.

Air bubbles attached to the knots and suspension lines that support the sphere were carefully removed by soaking both the sphere and its suspensions in a solution of water and liquid detergent (Foote et al., 1987). Even small air bubbles are a source of acoustic interference, and must be avoided. Also, the sphere was positioned well outside the near-field of the transducer. The far-field of a circular transducer array begins at a range r_{ff} which is, approximately (Medwin & Clay, 1998),

$$r_{ff} \geq \frac{d_t h_t}{\lambda} \tag{9}$$

where h_t is the height of the transducer and d_t is the diameter, where (Sherman & Butler, 2007)

$$d_t \approx \frac{1.6\lambda}{\pi \sin \frac{\phi_{BW}}{2}} \tag{10}$$

and ϕ_{BW} is the horizontal beam width. This equation (eq. 10) is not exact for our transducer array, but approximate. Still, the sphere was usually located at a distance around 10-14 meters from the transducer, corresponding to 5-6 times the near-field/far-field boundary.

Completion of calibration

When the sonar transducer on a particular vessel is to be calibrated, the sphere is first deployed to the approximate depth of the sonar transducer, as indicated from the vessel's general arrangement plans, and then it is sequentially steered through a selected number of the beams (Paper 1). The echo amplitude of the sphere, as received in each beam, was determined from the signal power (in Watt units) which was logged in the scientific data output. These data were converted into acoustical

parameters using an equation provided by the sonar manufacturer, which is similar to the one normally used for echosounders (Ona et al., 2009), where

$$TS = 10\log_{10} p_r + 40\log_{10} r + 2\alpha r - 10\log_{10}\left(\frac{p_t\lambda^2}{16\pi^2}\right) - B^T(\theta_s,\phi_S)B^R(\theta_s,\phi_s) - 40\log_{10}(\cos\theta_{tilt}) \quad (11)$$

is the equation for computing the target strength, and

$$S_v = 10\log_{10} p_r + 20\log_{10} r + 2\alpha r - 10\log_{10}\left(\frac{p_t\lambda^2 c}{32\pi^2}\right) - 2G_0 - (10\log_{10}\tau_{norm} + 2S_{a,corr}) - \Psi - 40\log_{10}(\cos\theta_{tilt}), \quad (12)$$

is the equation for the volume backscattering coefficient (Paper 3). Here p_r is the received power (W), r is the range between the transducer and target (m), p_t is the transmitted power (W), λ is the acoustic wavelength (m), $B^T(\theta_s,\phi_s)$ and $B^R(\theta_s,\phi_s)$ are the transducer gain in the target direction during transmission and reception respectively, G_0 is the on-axis system gain (dB), θ_{tilt} is the tilt angle of the beams, c is the acoustic propagation speed (ms^{-1}), τ_{norm} is the nominal pulse duration (s), $S_{a,corr}$ is the integration correction (dB), and Ψ is the equivalent beam angle (dB rel. 1 steradian). The sum of τ_{norm} and $S_{a,corr}$ equals the effective pulse duration (Ona et al., 2009). θ_s and ϕ_s where evaluated using the split-beam method (Paper 2).

Two features of the above equations differ from those presented in (Ona et al., 2009). First, the term $-40\log_{10}(\cos\theta_{tilt})$ is included to compensate for the vertical steering of the beam. Secondly, the sonar's directivity pattern during transmission and reception is not the same as it is in echosounders; hence, the factor $2B(\theta_s,\phi_s)$ (which was the original input shown in Ona et al. (2009)) was here replaced by the product of B^T and B^R. For example, when selecting the horizontal transmission mode, the transmitted wave is omni-directional when seen from above (or $B^T(\theta_s,\phi_s) = 1\ \forall\ \phi_s$), but directive in the reception mode. Therefore, when mapping the shape of the beam, in a similar manner as shown in figure 8, the two-way half-power beam-widths (θ_{BW} and ϕ_{BW} for the vertical and horizontal beams,

respectively), relate to points 3 dB below the peak echo strength along the horizontal beam cross-section, but 6 dB below for the vertical cross-section.

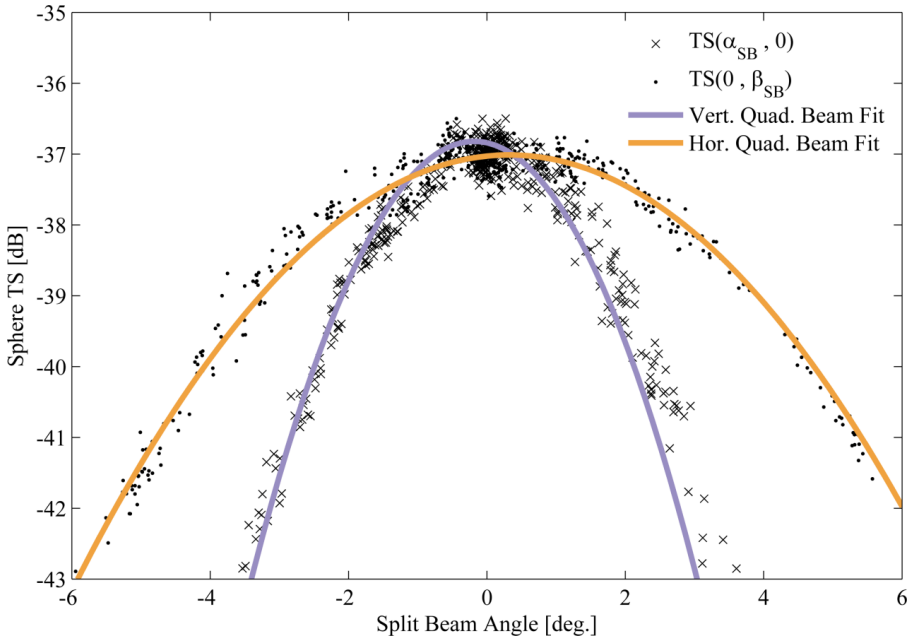

Figure 8. Mapping of a single beam on the SX90 mounted on F/V "Artus". The beam was calibrated in March 2013 while the stern of the vessel was moored to a pier in Ålesund. The sonar transmitted a 26 kHz CW signal with a detection range of 150 m and a tilt angle of -5°. The WC64 reference target was steered through the beam while a Matlab program estimated the sphere location using the split beam approach. Crosses (x) and dots (.) indicate measured sphere TS values while the sphere was steered, respectively, in depth and horizontally. The orange curve indicates the horizontal two-way beam pattern from a quadratic least-square fit, while the purple curve indicates the fitted vertical two-way beam pattern.

Several parameters in equations (11) and (12) are already known, either from the sonar's technical specification or from previously computed environmental parameters (Equation 3-4). Before sonars are delivered to the customer, the manufacturer checks that their performance matches the theoretical design, by measurements usually conducted in a calibration-tank facility. This fact simplifies our

calibration procedure, as the beam width, beam shape when steering and the equivalent beam angle may then be estimated using theory rather than measurement.

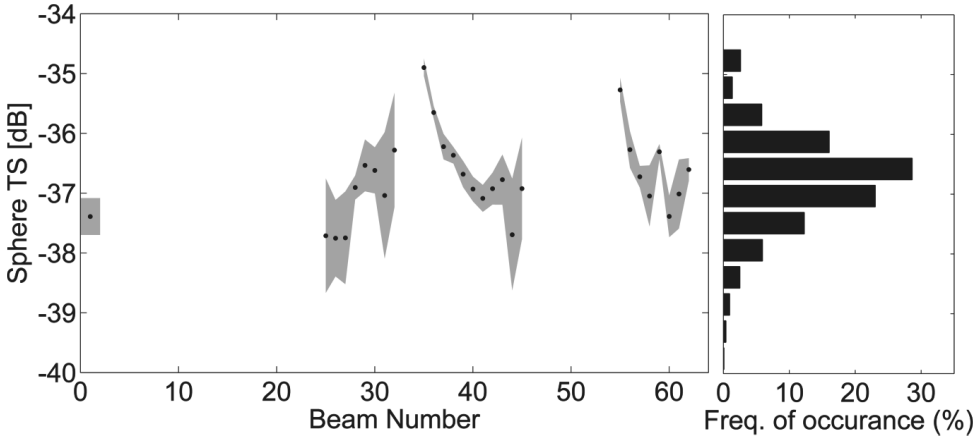

Figure 9. On-axis beam calibration of multiple beams of the SX90 installed on F/V "Artus", November 2013. The sonar was transmitting a 26 kHz CW signal with a detection range of 150 m, and the beam tilt angle was -5° relative to the horizon. A WC64 sphere was located at the centre of 28 sonar beams for a period of at least 30 s in each beam, after centring was achieved. Mean TS is shown as dots (.) and the standard deviation is shown by the grey shades. Data points with unsatisfactory split beam positions were excluded from the analysis. To the right, a histogram of all accepted TS measurements is shown in 0.5 dB bins, with the mean TS = -36.7 ± 0.8 dB.

Assuming all other parameters are correct, the system gain (G_0) is the key parameter to be measured and corrected. During the practical field calibration, the offset between the known TS of the sphere (Figure 7) and its measured value at the centre of each beam (Figure 9) was computed (Paper 1 and 3). The mean of all offsets was included in a separate calibration file. Measurements affected by occasional sphere movements were excluded by removing all those showing an unsatisfactory split beam position. When the scientific data were analysed, the calibration gain was uploaded from the relevant file, then applied to all the beams. This will increase the accuracy of the estimate of the single school biomass. The corrected sphere target

strengths for all beams on F/V Artus calibrated in 2013 (Figure 9) now gave a mean target strength of -36.7 dB with a standard deviation of 0.8 dB.

The sonar has many combinations of settings, but calibration of all possible settings would be too time consuming and is not necessary. It is better to calibrate only the particular settings that will be used during the survey. Still, if the settings need to be changed for any reason, such as acoustic interference from other vessels, an asymptotic relationship has been found between the beam gain and either the frequency or the signal's pulse duration (Paper 3).

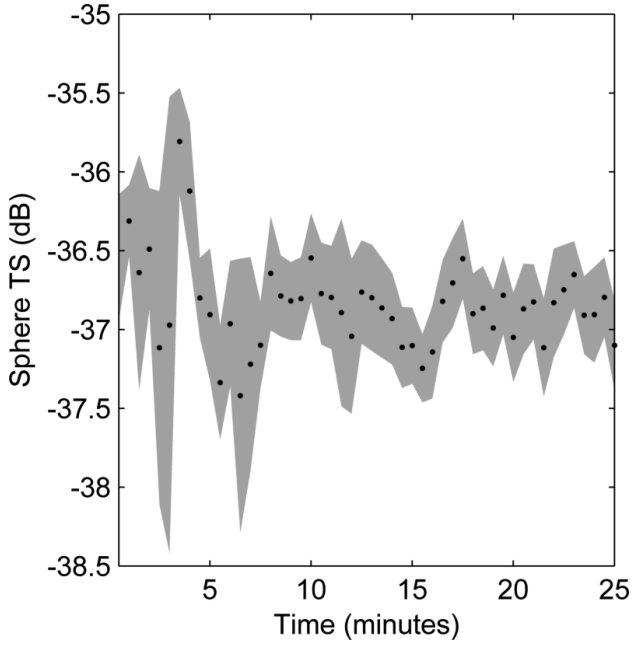

Figure 10. Temporal variation of the target strength of the WC64 sphere in the centre of one beam of the SU90 sonar mounted on R/V G.O. Sars, 19th October 2015. The sonar was transmitting a 26 kHz FM short signal with a detection range of 150 m and a tilt angle of -5º. The start time of the measurement was 09:36 UTC. Mean TS is shown as the black dots and the standard deviation is shown by the grey shades

Adjacent beams are formed using essentially the same transducer elements, and should therefore indicate the same target strength. However, the TS discrepancy between adjacent beams was observed to be as much as 0.5 dB (Figure 9). These between-beams variations may be caused by small variations in the temperature and salinity as the vessel or water movements generate mixture of the stratified water. A longer recording, ~25 min, of the TS with the sphere located at the centre of one beam supports this hypothesis (Figure 10). Here, the mean sphere TS was computed over 60 ping intervals (corresponding to the time required to calibrate one beam), and was seen to be change with time. Typical mean TS variation was within a 0.5 dB band. The standard deviation of each half-minute increment was close to ±0.25 dB, similar to the results from the calibration on F/V "Artus" (Figure 9). The larger variation of the mean indicate the TS was affected by an external source.

To further strengthen this hypothesis, a standard ES38B Simrad echosounder transducer, with known performance, was mounted at the same depth as the sonar transducer below the drop keel of the vessel G. O. Sars. A metallic support frame stabilized the transducer, which was now observing horizontally. A 60 mm copper sphere was lowered to the centre of the beam while its target strength and split beam locations were recorded (Figure 11). Simultaneously, temperature and salinity of the water close to the transducer were measured every 10 seconds using the SEABIRD SBE21 thermosaliniograph. Due to the weight of the sphere, the reels attached to the bulwark slightly discharged or stretched the support lines, hence the slow vertical movement in figure 11 (red line).

Small random variations of the sphere target strength (SD 0.1 dB) occurred throughout the first 30 minutes of the time series. From around 12:28 UTC, the variation of the target strength increased to nearly ±0.5 dB, and there was a sudden drop in the target strength of 0.8 dB around 12.35 UTC. With reference to the recorded split beam positions, these variations were not correlated with any movement of the sphere, but rather seemed to be due to rapid, but small, variations in temperature and salinity, indicating that an internal wave was passing the calibration site. This demonstrated that when calibrating horizontally in a fjord with stratified

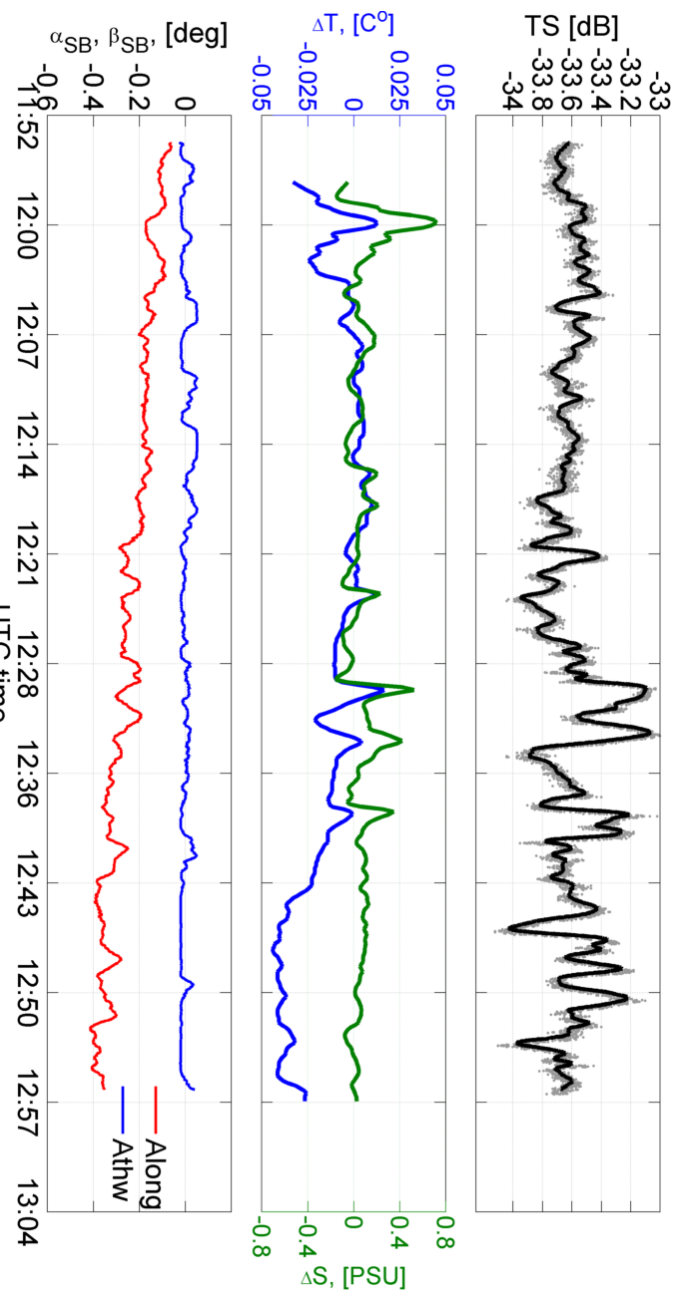

Figure 11. Temporal variation of the target strength of a 60 mm diameter copper sphere (upper), its split beam position (lower), and the changes of the water temperature and salinity levels ($\Delta T, \Delta S, middle$) relative to $T_0 = 11.92\ ^{\circ}C$ and $S_o = 29.37\ PSU$. The target strength and the positions were measured at the centre of a horizontally and starboard orientated 38 kHz split beam echosounder transducer, mounted underneath the drop-keel of the R/V G. O. Sars (~10 m). Negative vertical movements (Along, α_{SB}) indicate a descending sphere, and positive horizontal movements (Athw, β_{SB}) indicates movements towards aft. The sphere was steered using the two starboard points from the three-points calibration rig presented in (Foote et al., 1983). Water near the transducer was pumped through pipes in the keel to the thermosaliniograph inside a laboratory on the vessel, where the temperature and salinity levels was measured every 10^{th} seconds. Positive ΔT indicates colder temperatures, and positive ΔS indicates fresher water.

water, the apparent TS may be more influenced by the environmental parameters and their variation, compared to calibrations of a vertically directed transducer. This suggests that further investigations on how physical oceanography affects calibrations of horizontally observing systems should be undertaken, beyond what has been presented here.

Despite the adverse effects caused by the inhomogeneous medium, it is still not desirable to calibrate further out in the open sea, since the location of the sphere has been found to be highly susceptible to water currents and uncontrollable movements of the vessel. The locations which were selected have previously been experienced as satisfactory for calibrating keel mounted and vertically observing echosounders. They were also close to the port of survey departure. Other sheltered fjords, with more homogeneous water, could be found more suitable for sonar calibration, thus potentially improving the calibration accuracy. Still, a calibration accuracy of ±0.5 dB has been found to be achievable in the fjord locations selected for the present study.

Evaluation of the accuracy of the school biomass estimate

Estimation of the school volume

Fishermen, who have long experience of using sonar, often observe schools which appear large at long ranges often appear smaller when measured at shorter ranges. This effect has been demonstrated for simulated schools with known sizes and locations, and is attributed to a spatial smearing of the target across multiple sonar beams (Paper 4).

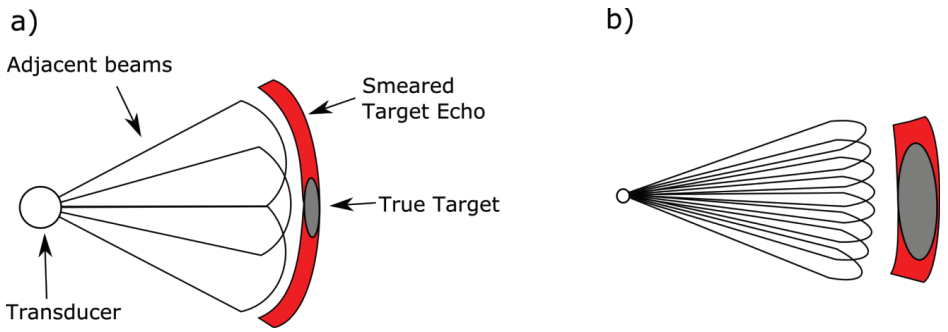

Figure 12. Illustration of the two categorized smearing effects; the long range smearing effect (a) and the short range smearing effect (b). In figure (a) the true target is partially detected within 3 adjacent beams, thus smeared over all three beams. In (b) the true target fully covers several central beams but only partially intersects the border beams. Again, the target echo is smeared over all the intersected beams.

Spatial smearing occurs when the target school partially intersects one or two beams, and due to the spatial resolution, or the lack of such, the target echo is smeared across the entire cross-section of the beam fan. This is also an issue with echosounders, where the length of the school can be overestimated due to border effects caused by the finite beam width (Diner, 2001, 2007). Two kinds of beam smearing effects have been classified; *the long range smearing effect* (LRS) and *the short range smearing effect* (SRS). The latter occurs when the school is detected within several beams but only partially within the border beams (Figure 12b). In this

case, the smearing effect is relatively small. The true extension of the school is between that represented by the whole beam fan, and that with one beam less. For example, if the school was smeared through 8 beams, its true extension is somewhere between 7 and 8 beams. As the range from the transducer increases, the extension of the school, in terms of the number of beams intersecting the school, is gradually reduced, resulted the zigzag pattern as illustrated in figure 13.

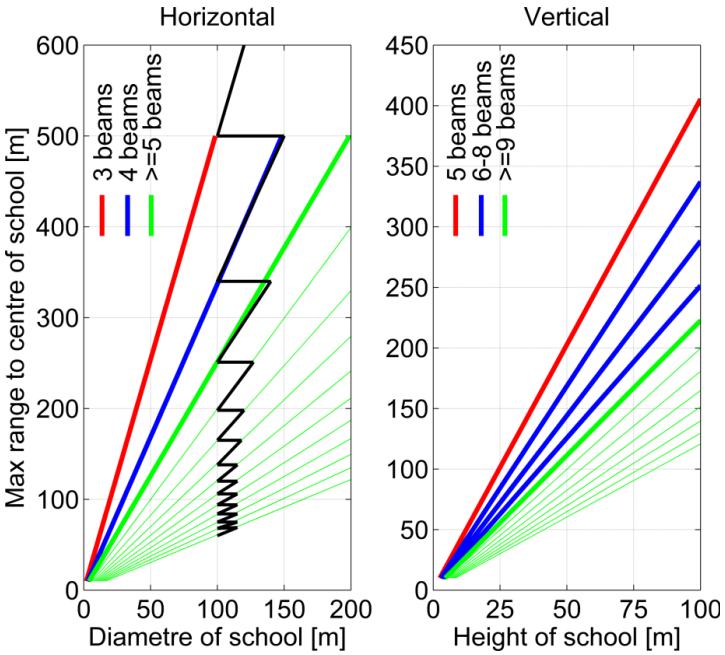

Figure 13. Simplified illustration of the measured width (left) and height (right) of a school relative to the distance (R) from the transducer. The measured width is given by $C_W = 2R\,tan\left(\frac{n\phi_{ang}}{2}\right)$*, where n is the across-beam extension in terms of number of beams and* ϕ_{ang} *is the angular separation between adjacent beams. The black line indicates a typical width measurement of a school with a true width of 100 meter. The red line indicates the region where the long range smearing effect is dominant for all sonar settings. The blue lines indicate the region where the long range smearing effect is dominant depending on the sonar setting (narrower width gives longer distances). The green lines indicate the region where only the short range smearing effect applies.*

Once the minimum of three, or sometimes four, beams intersect the school, the apparent extension is overestimated by a factor proportional to the range, until the school is either out of sonar view or is no longer visible above the background noise. This effect is attributed to the long range smearing effect, as illustrated in figure 13 with the red lines for the narrowest beams and blue lines for wider beams. Only the SRS is present in the area given with the green lines.

Two threshold criteria were adopted to prevent the LRS effect being included in the biomass estimation, where, in principle, all schools with a crosswise extension less than the nominal beam width were excluded. If the school was to be accepted, its crosswise extensions must be larger than the swath length of minimum 3 beams horizontally and 5 beams vertically for transmissions at 30 kHz, and 4 (horizontal) and 8 (vertical) when transmitting at 20 kHz (Figure 13 and Paper 4).

Two correction models have been developed for mitigating the SRS effect, one for the school's width and the other for the height. Including the correction models will increase the biomass estimation accuracy of a single fish school. A prerequisite of both models was that the two transmission fans (Figure 5) were directed towards the centre of the school. The horizontal model was a reformulation of that presented by Misund (1990), where the reformulation included the concept of overlapping and digitized beam responses. The vertical correction model was a function of both the height of the school (in terms of number of beams) and its angular direction relative to the transducer. A precision of ±6.6-8.7% for the width and ±8.6-10.5% for the height is anticipated when the models are implemented on real acoustic data. The length of the school was defined as the along-beam extension (Diner, 2001), where the corrected length is compensated for a known extension, equal to half the transmitted pulse length. For the sake of clarity, in Diner (2001) this model is referred to as the height correction since this is the along-beam extension viewed by a vertical echosounder. The model does not, however, correct for any further deviation caused by multiple scattering within the school nor acoustic extinction. The echo strength of any multiple scattering is likely to be 2-3 orders of magnitude weaker (Ona, E. Pers. communication, 2016) than that from direct scattering; hence, this effect will be

ignored if a high enough echo amplitude threshold is included in the analysis. Henceforth, uncertainty in the along-beam extension of the school is assumed to be absolute and mainly caused by the sampling frequency (4 kHz) and inadvertent changes in the sound speed, and was here assumed to be ±1m. Any other acoustic effects are at this stage ignored.

Element data for several migrating schools of herring have been collected; however, these were insufficient for a proper analysis of the school volume (e.g. Korneliussen et al., 2009; Gerlotto & Paramo, 2003), since the schools were often located in regions where they were susceptible to the LRS effect. Manual scrutiny of school, that was close enough, showed on average a 55% reduction of the mean estimated volume when the spatial smearing was corrected (Paper 4). Manual scrutiny may also introduce bias if the interpreter is using too large or too small amplitude threshold criteria, which may be the case in this example. Using an automatic procedure for extracting the school data would be a more objective approach (e.g. Balabanian et al., 2007; Holmin et al., 2012; Peña et al., 2013).

Improving the total volume accuracy through a full 3D reconstruction of the fish school is possible using the element data from the fishery sonar, if they are available. In practice, it was found that the vertical beam width of the transmission is too narrow for ensonifying the entire volume of large schools. As a consequence, parts of the school may be excluded from the volume estimate. Increasing the beam width during transmission will, however, increase the noise level in an already noisy environment (Gerlotto et al., 2000), and is therefore not an ideal solution. Still, if a 3D reconstruction of the whole school is used to obtain higher spatial resolution than what is possible with typical 2D reconstructions, the whole school must be sufficiently resolved by several beams in both the horizontal and vertical directions. This may be achievable if the whole school is within the green sectors in figure 13. For example, a small herring school which is 100 m in diameter and 50 m high needs to be within 100 m of the sonar transducer to be accurately measured. Logically, such short distances are problematical since the entire school will then not be ensonified, and such close ranges may also cause vessel avoidance behaviour by the fish.

The distance until the LRS effect becomes the dominant bias may be increased if additional, but narrower, beams are formed. This is theoretically possible if the signal frequency or the transducer size is increased (Kinsler et al., 1999; Sherman & Butler, 2007). Increasing the signal frequency could result in the formation of grating lobes, since the element spacing is then greater than half the wavelength. Having a larger cylindrical transducer involves producing a completely new sonar with additional elements, updating of the beam former software, and a stronger mechanical hoist system, resulting in a much more expensive product. Therefore, if higher spatial resolution is required, it is proposed to use other presently available equipment, such as the previously mentioned Simrad SN90 which is anticipated to provide improved volume measurement accuracy at shorter ranges.

Evaluation of the backscattering cross section

Referring back to equation 1 and 2, the next parameter which has to be evaluated is the mean lateral backscattering cross-section, $\overline{\sigma_{bs}}$. This parameter is used to convert the received acoustic energy into quantitative fish density measures. Computing $\overline{\sigma_{bs}}$ in the lateral aspect is more complicated than in the dorsal aspect because $\overline{\sigma_{bs}}$ is then not only dependent on the fish pitch and roll angles (Nakken & Olsen, 1977), the depth (Ona, 2003) and length of the fish (Foote, 1980b), but also the yaw angle (Cutter & Demer, 2007). The difficulty of selecting a $\overline{\sigma_{bs}}$, representative of typical schooling behaviour is further discussed below, along with two proposed methods for improving the precision of fish density measures. To facilitate this study, scattering data from virtual schools of herring have been simulated where, for simplicity, the length and the depths of the herring schools were assumed to be known.

Some elaboration of the backscattering cross-section is needed before continuing. $\overline{\sigma_{bs}}$ is computed using the directivity pattern of one representative fish weighted by the fish orientation distribution (Foote, 1980a). For echosounders, where the fish are ensonified from above, the tilt-angle distribution of non-reactive fish is

likely to be relatively narrow, for example a mean tilt-angle of -3.9º with a standard deviation of 11.9º has been reported for caged herring (Ona, 1984). When transmitting horizontally, however, any horizontal aspect of the fish may be ensonified, and, additionally, the yaw-angle distribution of fish in an aggregation may be anything from purely random to, for example, a normal distribution. Consequently, the mean TS of adult mackerel, with randomly distributed yaw-angles, were recently measured in the field to be 3-4 dB weaker in the lateral aspect than in the dorsal aspect (Ona, E. Pers. communication, 2015), probably because the backscattering from the posterior and anterior directions had now a higher influence on the mean backscattering cross-section. Also, the TS in lateral aspect is more depth dependent than in the dorsal aspect. The lateral TS was reported to be 2.5 dB higher then dorsal at 50 m depth, but 5 dB lower at 350 m (Pedersen et al., 2009), and was concluded to be caused by proportionately more compression of the swimbladder in the dorso-ventral aspect than the lateral.

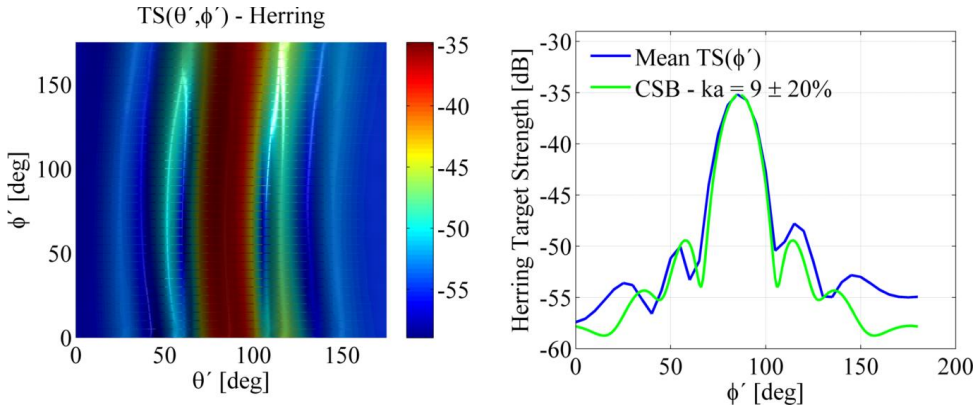

Figure 14. To the left, the computed, and interpolated, directivity pattern of a suspended herring 29.2 cm long in terms of target strength (TS, [dB re 1 m^2]) using the boundary element approach. To the right; mean lateral target strength as a function of ϕ (horizontal angle of incidence) of the 29.2 cm fish (blue). Green curve - mean TS of a straight cylinder with ka = 9 ± 20%. Coordinates of key anatomical directions are: anterior end $(\theta', \phi' = 0, 0)$*, posterior end* $(\theta', \phi' = 180, 180)$*, left lateral side* $(\theta', \phi' = 0, 90)$ *and dorsal side* $(\theta', \phi' = 90, 90)$*. Target strength was defined as TS = 10 log$_{10}$(σ_{bs}). The data from the boundary element calculations were supplemented by Hector Pena at IMR.*

First, the directivity of every fish needs to be included in the simulation. The acoustic reflectivity of the fish is mainly influenced by the swim bladder, if one is present, but also to some extent by the flesh and bones in the fish body (Nesse et al., 2009; Peña & Foote, 2008; Blaxter & Batty, 1984). Numerous methods for computing the directivity pattern of a gas-filled swim bladder have been described in the scientific literature. Here are a few examples: *Boundary Element* (Cunefare et al., 1989; Fischer et al., 2004; Śmigaj et al., 2015), *Kirchoff Ray - method* (Clay & Horne, 1994; Peña & Foote, 2008; Horne et al., 2009; Macaulay et al., 2013), *Prolate-spheroid modal – series* (Stanton & Chu, 2000; Gorska & Ona, 2003; Tang et al., 2009), and the *Straight Cylinder* (Gorska et al., 2007; Medwin & Clay, 1998). Since the simulation is done at a conceptual level, the choice of swimbladder-scattering model is not critical. Here it was assumed that the directivity pattern of a single fish was equivalent to that of a cylindrical swim bladder (CSB) with ka = 9 ± 20%, since this reasonably approximated the computed directivity pattern of a 29.2 cm herring (Figure 14).

Two kinds of fish aggregation have been observed in the field, namely shoaling fish (un-polarized with randomly distributed yaw angles) and schooling fish (polarized with normally distributed yaw angles). In the simulation exercises, the two aggregation types were consecutively located at the centre of a global coordinate system. The orientation of each fish is described by the angles $(\theta_{ori}, \phi_{ori})$; for simplicity only the effects caused by the yaw-angle distribution were evaluated. Therefore, $(\theta_{ori}, \phi_{ori}) = (0,\ N(-15°, 15°))$ for the polarized school and $(\theta_{ori}, \phi_{ori}) = (0,\ U(-180°, 180°))$ for the shoal. Here N indicates a normal distribution and U indicate uniform distribution. The beam's angle of incidence is determined by the directions $(\theta_{inc}, \phi_{inc})$, with the constraint $\theta_{inc} = 0°$. The volume backscattering strength for each aggregation, with a density of 5 fish per cubic meter, was computed when accumulating the directivity indices of all fish within the volume (Figure 15). The beam's angle of incidence relative to the anterior-posterior axis of the fish was given by $\phi' = \phi_{ori} - \phi_{inc}$, leading to the appropriate swimbladder directivity index computed from the CSB model. Ignoring any acoustic extinction (Foote, 1990), the assumed density of fish was found to have no effect on the final biomass estimate.

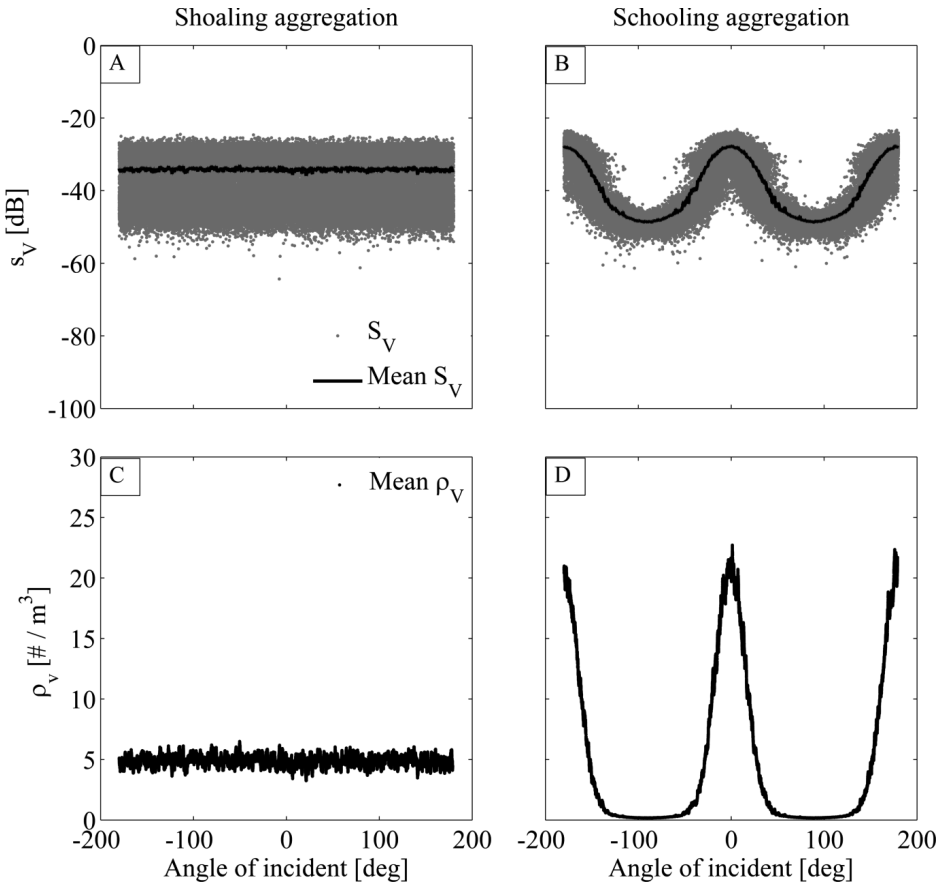

Figure 15. Volume backscattering strength (grey) and its mean (black) from circumnavigation of a simulated un-polarized school (A) and a polarized school with yaw angles normally distributed within ±15° (B), both for a true density of 5 fish per cubic metre. Computed mean volume densities for (C) the un-polarized school and (D) the polarized school. Volume backscattering strength was defined as $S_V = 10\,log_{10}\,s_V$. *Simulation parameters include the cylindrical swimbladder model, 26 kHz transmissions with ensonification only in the horizontal plane. Angle of incidence is relative to the head-on direction of the polarized school.*

The overall directivity pattern of the shoal was found to be omni-directional (Figure 15A). When the mean volume backscattering coefficient was divided by the

mean backscattering cross-section (weighted with a randomly distributed yaw-angle), the mean volume density was 5.0 fish per cubic meter with a proportional standard deviation of 8% (Figure 15C).

Circumnavigating the school, however, provided an overall directivity pattern similar to a sine function, with maximum reflectivity in the lateral aspects ($\phi_{inc} = 0$ and $\phi_{inc} = \pm 180^{o}$) and minima in both the anterior and posterior aspects (ϕ_{inc} ±90º) (Figure 15B). This particular pattern has been observed in the field, when circumnavigating migrating schools of both herring and mackerel. Schooling Atlantic mackerel was, however, found to be almost immeasurable due to the background noise when ensonified in the anterior/posterior aspects. When the same $\overline{\sigma_{bs}}$ used for computing the volume densities in the shoal was applied to the school, $\overline{\rho_V}$ was found to be overestimated by a factor of 4 at lateral aspects and grossly underestimated at posterior/anterior aspect (Figure 15D). Still, $\overline{\rho_V} = 4.94\, m^{-3}$ (RSD 138.7%) was computed when including all measurements.

For better precision, only $\bar{s_v}$ at what is regarded as favourable angles of incidence are considered, for example around the peak of the school's overall directivity pattern ($|\phi_{inc}| < 20°$). In this case

$$\bar{\rho}_V = \frac{\bar{s}_v^{max}}{\bar{\sigma}_{bs}^{max}}, \tag{14}$$

where $\bar{s}_v^{max}$ is the mean volume backscattering coefficient of the selected data, and $\bar{\sigma}_{bs}^{max}$ is then a computed mean lateral backscattering cross-section based on the ±20º incidence angle relative to the fish lateral aspect. The estimated volume density of the polarized school was $\bar{\rho}_V = 5.02\, m^{-3}$ (SD 1.4). The relative standard deviation of the estimated volume density for different constraints on ϕ_{inc} is presented in Table 2. The best precision was obtained when only the data closest to the peak of the school's overall directivity pattern were utilized, with less precise results when including more off-peak measurements.

Table 2: The Relative Standard Deviation of the mean volume density during circumnavigation of a fish school, when only data from various favorable angles (ϕ_{inc}) were selected ($\overline{\sigma_{bs}}^{max}$); and when the angle of incidence was corrected using the Dual-frequency approach ($\sigma_{bs}(\phi_{df})$). ϕ_{df} was constrained similarly to ϕ_{inc}.

Limitation	*RSD(%)*	
$\lvert\phi_{inc}\rvert$ or $\lvert\phi_{df}\rvert$	*Favorable angle of incidents,* $\overline{\sigma_{bs}}^{max}$	*Dual-frequency approach,* $\sigma_{bs}(\phi_{df})$
$< 10°$	6.2%	22.5%
$< 20°$	20.8%	27.0%
< 30	42.6%	36.7%
$< 40°$	63.2%	47.8%

In practical calculations with actual survey data, we have used recent TS measurements of adult herring and mackerel in lateral aspect, measured by other work packages within CRISP, rather than the theoretical computed values used earlier. Still, a value between the maximum and the mean TS has been used when converting the $\bar{s}_V^{max}$ of migrating schools during field exercises. Measuring $\bar{s}_V^{max}$ is difficult when circumnavigating an aggregation, and nearly impossible in a survey situation. When a circumnavigation is not possible, alternative approaches are needed to maintain the accuracy of the quantitative measure. The mean values of both volume backscattering and the lateral TS can be used, assuming that the movements of the schools are random in relation to the survey grid. In detailed tracking of a single school, its movement along with the water current must then be incorporated in the computations. Also, multi-frequency sonar, or two similar sonars observing the same school using different frequencies, may reveal information on the internal orientation. Therefore, a proposed dual-frequency analysis using two fishery sonars is described below.

Dual-frequency analysis

The main lobe of the fish-directivity pattern is known to become narrower as the frequency increases (Nakken & Olsen, 1977; Ona & Korneliussen, 2000). As a result, the backscattered echo energy decreases faster at higher than at low frequencies when the fish adopt steep diving angles. Computing the diving (or tilt) angle using the echo-energy ratios between multiple frequencies has been proposed (Ona & Korneliussen, 2000). Using this concept, the orientation of the fish inside the school may be estimated using a dual-frequency analysis. The two signal frequencies need to be well separated, which could be feasible on commercial fishing vessels if both for example the SX90 and the SH90 (high-frequency fishery sonar, ~114 kHz) sonars are available to simultaneously observe the same school.

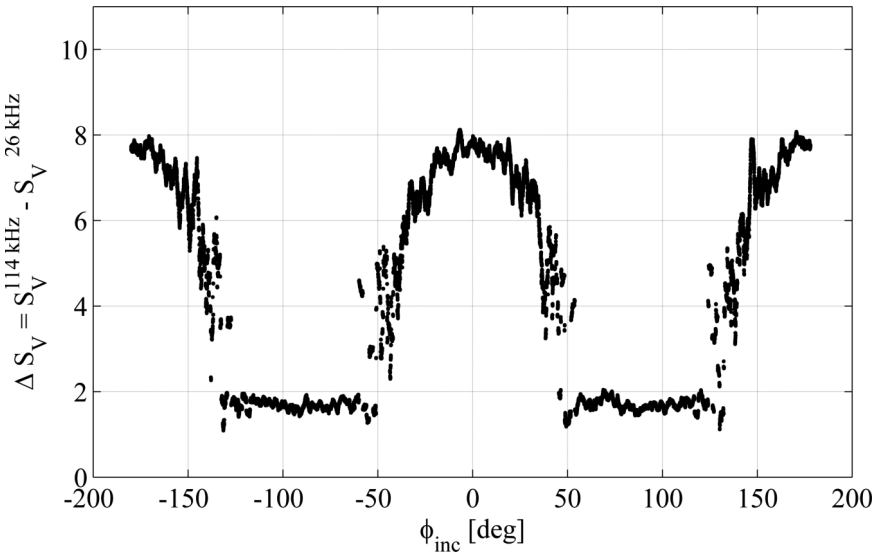

Figure 16. Difference between the simulated mean volume backscattering strengths of a polarized school of swimbladder bearing fish ensonified at 114 kHz $\left(S_V^{114kHz}\right)$ *and 26 kHz* (S_V^{26kHz}) *for the true angle of incidence,* ϕ_{inc}*. The density of fish was set to 5 m*$^{-3}$*, where the directivity pattern of each fish was determined from the scattering model of a straight cylinder with ka = 9 ± 20%. The yaw-angle was assumed normally distributed within* $\pm 15°$ *relative to* $\phi_{inc} = 90°$ *(Direction of head).*

The discrepancies between the volume backscattering strength of the polarized school at 114 kHz (S_V^{114kHz}) and at 26 kHz (S_V^{26kHz}), Δs_V, were 8 dB in the lateral aspect ($\phi_{\text{inc}} = \sim 0^{\circ}$) and close to 2 dB around the posterior/anterior directions ($\phi_{\text{inc}} = \pm 50\text{-}90$) (Figure 16). In the intervening region, Δs_v decreases as a quadratic function of the incidence angle. Such information may then be used to estimate the school orientation.

The next step is to replace equation 2 with

$$\overline{\rho_V} = \frac{\overline{s_v}}{\overline{\sigma_{bs}}(\phi_{df})}, \tag{15}$$

where $\overline{\sigma_{bs}}(\phi_{df})$ is the mean backscattering cross-section as a function of the evaluated angle of incidence, ϕ_{df}, using the dual-frequency approach. Assuming

$$\overline{\sigma_{bs}}(\phi_{df}) = \overline{\sigma_{bs}}^{min} + 20 \cos 2.25\, \phi_{df} \tag{16}$$

and

$$\phi_{df} = \operatorname{acos}\left(\frac{\Delta S_v + 12}{20}\right), \tag{17}$$

where $\overline{\sigma_{bs}}^{min}$ is the mean backscattering cross-section around both the anterior and posterior directions. The computed density at each true angle of incidence is shown in figure 17. When only $|\phi_{df}| < 20°$ is accepted, the result is $\overline{\rho_V} = 5.21\, m^{-3}$ (SD 1.41). The relative standard deviations of the volume density for different constraints on ϕ_{df} are also given in Table 2. These indicate that the dual-frequency approach gives more precise results when a larger proportion of the data below the maximum school reflectivity are used.

Further investigation of the proper $\overline{\sigma_{bs}}(\phi_{df})$ is still needed, and a comparison with real data. Variation of depth and fish size must then be included in the analysis. However, both the SH90 and the SX90 or SU90 sonar are presently not installed on any Norwegian research vessels, and so the data must be collected on commercial

vessels which usually have both sonars. Until such data are available, further investigation of this topic can only be speculative. Still, the present results provide a foundation for future research.

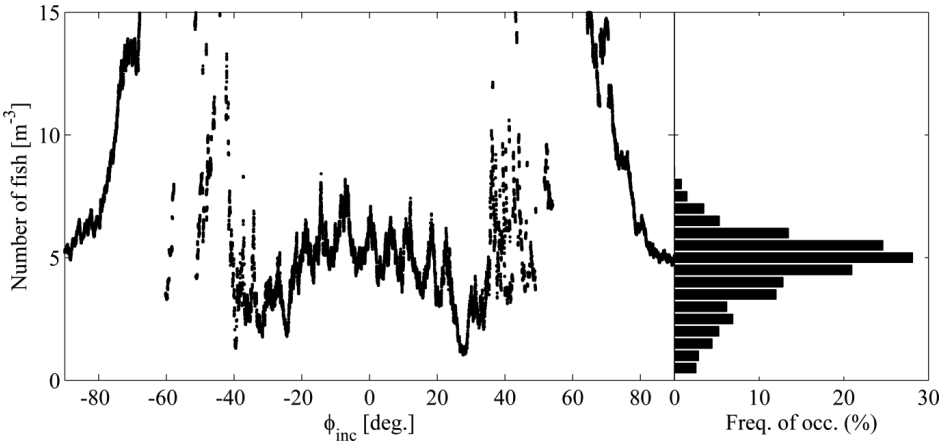

Figure 17. To the left; the corrected $\overline{\rho_V}$ using the dual frequency approach, $\overline{\sigma_{bs}}(\phi_{df})$. ϕ_{inc} indicates the true angle of incidence of the beam. The distribution of the corrected $\overline{\rho_V}$ for all measurements within $|\phi_{df}| \leq 20°$ are shown in the figure to the right.

Further analysis of the measurement uncertainty

Both the school's estimated biomass and its uncertainty are valuable information in the pre-catch scenario. Computation of the total uncertainty is presently premature as several of the key elements in Equation 1 and 2 are not yet sufficiently studied or evaluated. However, GUM software was used to give a preliminary assessment of each component's contribution to the overall uncertainty of the biomass estimate for an ellipsoidal school (Guide to the expression of Uncertainty in Measurement (Kacker et al., 2007)). This software analyses the combined uncertainty of multiple measurements, given the distribution of each measurement and the correlation between them, according to the ISO Guide to the Expression of Uncertainty in Measurement (SASO, 1995).

For simplicity, the uncertainties of each component were assumed to be normally distributed. The fish weight was assumed to be ±0.02 kg from the mean and the school's length, height and width were supposed to be fully correlated. When converting echo data to quantitative fish measures, only the variations caused by fish orientation are considered; hence, any TS variation with depth was ignored. It should be mentioned that in future work, wideband echosounder technology, such as the Simrad EK80, may facilitate sizing of individual fish in the outskirts of the school by analysis of echo strengths, pulse-stretching and frequency response (Ona, 2014). The individual fish weight may then be derived from the standard growth equation (Fulton, 1904; Froese, 2006). Since this technology is very new, such investigations were not included in the present analysis.

Table 3. Input values used with the GUM-software to compute the combined uncertainty of the biomass estimate for an ellipsoidal school. The individual components in the biomass equation are the school width, height, length, the fish weight, calibration and the acoustic/fish density conversion factors. The values and associated uncertainties are presented for three cases.

	Values and uncertainties		
Component	Case 1	Case 2	Case 3
Width: C_W	$100\ m \pm 9\%$	$100\ m \pm 9\%$	$100\ m \pm 9\%$
Height: C_H	$50\ m \pm 10\%$	$50\ m \pm 10\%$	$50\ m \pm 10\%$
Length: C_L	$100 \pm 1\ m$	$100 \pm 1\ m$	$100 \pm 1\ m$
Weigh: w_i	$0.35 \pm 0.02\ kg$	$0.35 \pm 0.02\ kg$	$0.35 \pm 0.02\ kg$
Calibration: $\overline{s_v}$	$2 \cdot 10^{-4}\ m^{-1} \pm 14\%$	$2 \cdot 10^{-4} m^{-1} \pm 14\%$	$2 \cdot 10^{-4} m^{-1} \pm 1\%$
Conversion into density : $\overline{\sigma_{bs}}$	$1 \cdot 10^{-4} m^2 \pm 138.7\%$	$1 \cdot 10^{-4} m^2 \pm 20.8\%$	$1 \cdot 10^{-4} m^2 \pm 20.8\%$

The combined biomass uncertainty for a polarized school (Figure 18), along with the individual component contributions, are presented for 3 illustrative cases, all based on the data distributions adopted elsewhere in this thesis. The results are

summarized in Table 3. In the first case, a polarized school was virtually circumnavigated, and all the generated data were used to compute the volume density. This is the same case as was illustrated in figure 15B. In the second case, only data around the maximum school reflectivity (equivalent to $|\phi_{inc}| < 20°$ in figure 15B) were selected. The third case is similar to the second one, however, a calibration accuracy of ±1% was assumed. This is a reasonable assumption since a maximum calibration error around ±2% has previously been reported for 38 kHz echo sounders (Foote, 1982; Knudsen, 2009).

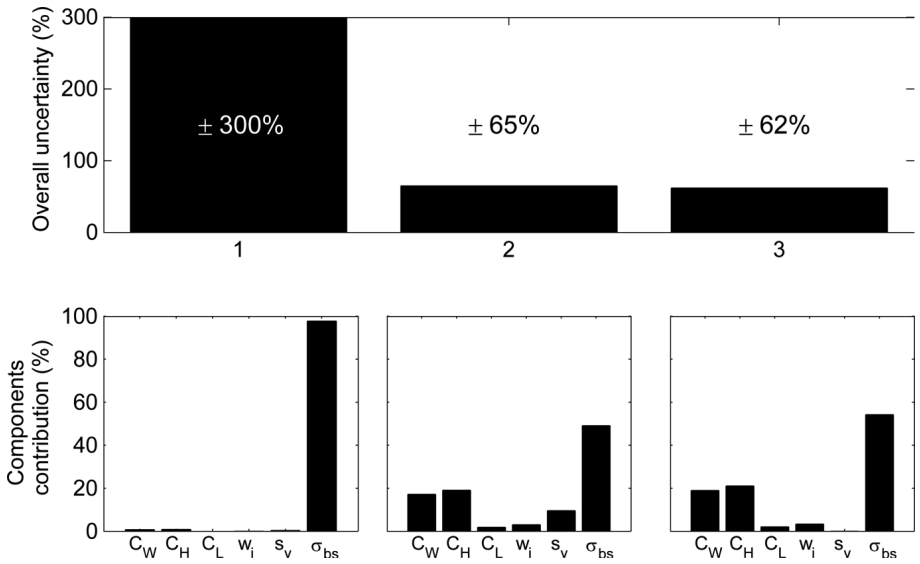

Figure 18. The combined uncertainties of the biomass of a polarized school (upper) during a full circumnavigation (1), with selection of data close to the maximum reflectivity (2), and the same data but with a calibration accuracy of ±1%. Each component's contribution to the combined uncertainty is presented for each case in the three lower histograms.

In the first case the combined uncertainty was as high as ±300%, where the conversion into quantitative fish measures contributed 97.7% of the total (Figure 18, left). In the second case (Figure 18, middle), the combined uncertainty was ±65%, with the quantification uncertainty contributing 49.1%, and the total contribution of

the school dimensions was 38.2%. With a better calibration accuracy (±1%, Figure 18 right), the combined uncertainty is only 3% less. This result shows that greater effort to improve the calibration accuracy will not provide any significant benefit as regards the total biomass uncertainty. Also, the results demonstrate that a continuing commitment to establish the correct mean backscattering cross-section representative of the species, school depth, fish size and orientation is essential for further reducing the total uncertainty, since this factor is presently the largest contribution.

Using a sonar operating at lower frequency (for example 10 kHz) will reduce the directivity of single fish. This effect may also contribute to a simple way of reducing the uncertainty caused by the quantification process, since the difference between maximum and minimum volume backscattering strength during circumnavigation (e.g. Figure 15) is then less. Hence, the density estimate may then be less dependent on the orientation and polarization of the school. Still, if the accuracy of the volume estimate must be preserved, a new and larger sonar transducer is then needed.

Using fishery sonar for abundance estimation

In acoustic surveying to quantify the abundance and distribution of fish populations, multi-frequency echosounders are now common and indispensable tools. However, this technique may not be effective for pelagic species that swim close to the sea surface, when part of the population may occur in the echosounder blind zone or be vulnerable to vessel avoidance behaviour (Misund, 1993b; Soria et al., 1996). The use of fishery sonar together with an echosounder can yield supplementary information, improving the accuracy of stock estimates since bias may be corrected by quantifying any fish in the acoustic blind zone, or evaluating the effect of fish avoidance reactions. Even when the sonar reveals no fish close to the surface, this information will strengthen the quality of the survey estimate.

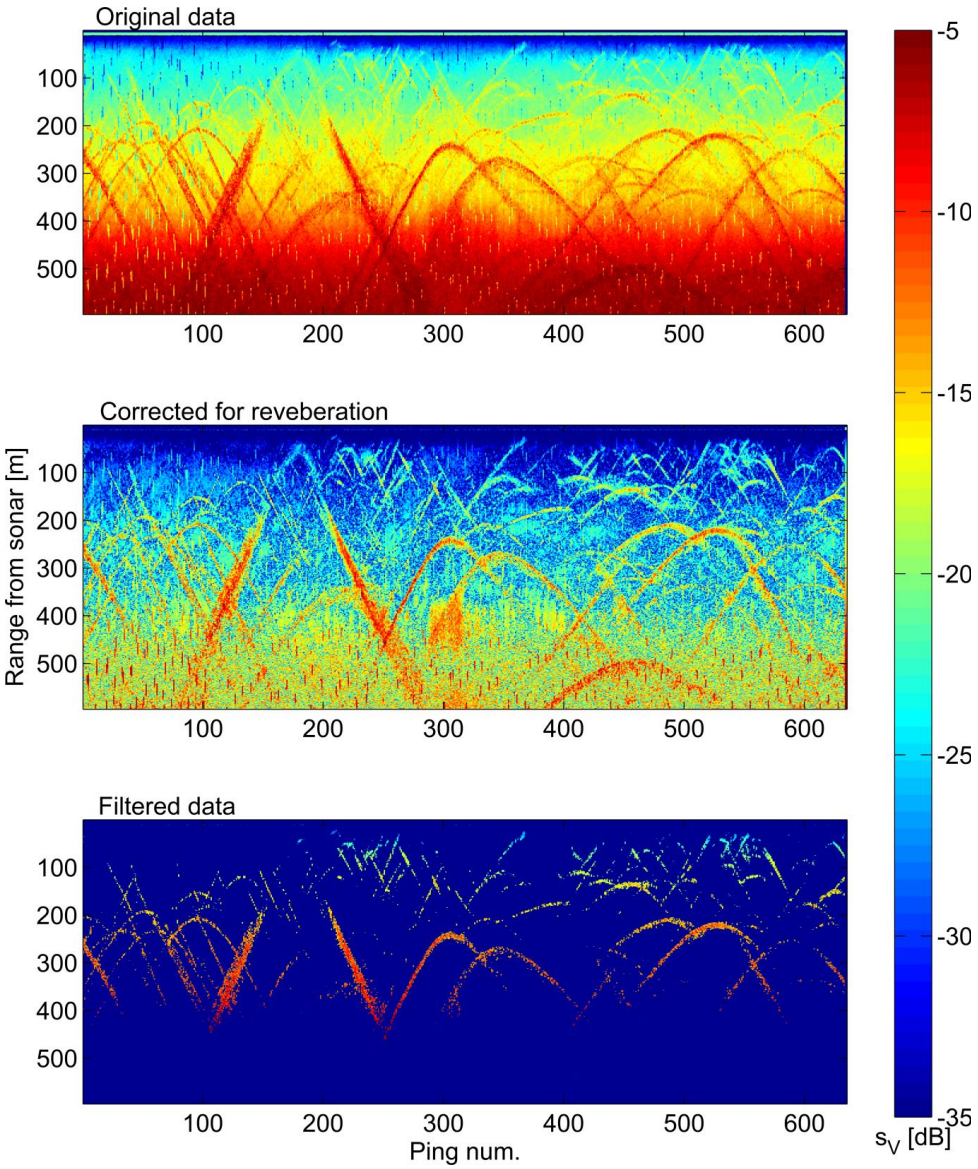

*Figure 19. The ABD over a period of 635 pings (~1.5 nm) near **Vikingbanken** in March 2013. The SU90 multi-beam fishery sonar, mounted on F/V Eros, transmitted a continuous 26 kHz CW signal, where the beams were tilted at -10 degree inclination and the observation range was up to 600 m. Upper window - the original data from the ABD; middle window - data corrected for bottom reverberation; lower window - , after the background noise has been excluded. The calibration gain was not considered in this exercise.*

Analyzing sonar data may be a tedious process when around 2.6 million pings have to be analyzed separately (assuming a ping rate of 1 per second over 30 days). In many cases over long periods, there are literally no fish in the water column and a simple system to direct the operator to which periods should be analyzed are needed. For large scale surveys, it is further proposed to sum the amplitudes of all beams within each ping, and present these data in a similar manner as a typical echosounder display (Figure 19). Such a simplified view (here named as the *accumulated beam data* (ABD)) makes it easy to detect the presence of schools within a specified time period during a survey, as illustrated by the ~1.5 nm echogram in figure 19. It can also be used to determine if the swimming speed and/or direction of the school changed while the vessel was passing. Echo-integration of the beam data, after correcting for the mean fish orientation relative to the vessel, and bottom reverberation, may still prove to be a simple, but adequate approach for improving the accuracy of survey estimates.

Two of the schools shown in figure 19 have been highlighted from the ABD, one around ping number 350 (Figure 20A) and the other one around ping number 520 (Figure 20B). Both schools have unique track patterns similar to the traces of single fish on an echosounder display, where the peak of the school-trace occurs when it is nearest to the vessel. It is then located on either the port or the starboard side. The shape of the school-track in figure 20B was found to be close to a quadratic function of the ping number (i.e. the along-ship distance), both before and after the vessel was passing the school.

The school-track in figure 20A, on the other hand, changed shape once the school was aligned with the vessel. This suggests that the fish swam more slowly when passed by the vessel; hence, their behaviour was indeed influenced by the presence of the vessel. Information on fish avoidance is important in acoustic surveying, as it may significantly bias the fish density estimate (Aglen, 1994). The suggested processing of the sonar data is a good start for such evaluation.

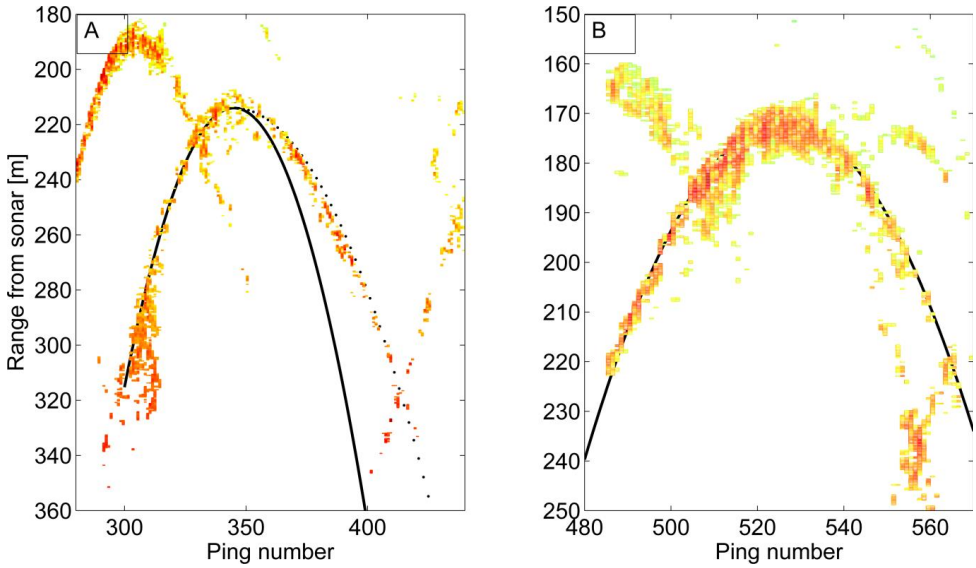

Figure 20. Two selected schools from the ABD, around ping numbers 350 (A) and 520 (B). The track-lines of both schools are plotted using parabolic fitted functions. The track-line in (A) has been fitted with two parabolic functions, the solid curve for the period before and the dotted curve for the period after the vessel passed the school. The track-line of the school in (B) is described by the same parabolic function both before and after the vessel passed.

Concluding remarks

This doctoral thesis is part of a work package within the CRISP project, where the total biomass of a fish school is to be measured with sufficient accuracy for use by the fishing industry. If successful, the plan is to incorporate new biomass-algorithms into fishery-sonar software which will help skippers in their catch decisions. The work described in this thesis was based on a specific instrument, the Simrad SX90 sonar. Only some of the key parameters of the biomass formula (Equation 1) have been evaluated so far, but solutions for the remaining parameters have been proposed.

Much effort was applied to facilitate multi-beam sonar calibration. Two calibration rigs for steering the reference target were developed along with an acoustic position-fixing algorithm for measuring its within-beam location, (Papers 1-2). Additionally, a protocol for practical field calibration of multi-beam fishery sonar has been developed (Paper 3). Variations in temperature and salinity in the stratified near-surface water layer were found to influence the measured sphere target strength when the sound beams were transmitted in a horizontal fan. Thus, the sonar calibration could not be done with the same accuracy as reported for standard vertically-transmitting echosounders (Knudsen, 2009). The calibration results were nevertheless concluded to be satisfactory when compared to the overall uncertainty in estimating the biomass of a fish school.

The fishery sonar's capability to provide accurate school-volume estimates was validated, along with an assessment of its limitations (Paper 4). To avoid adverse beam-smearing effects, the resolution of the school's cross-section, with respect to the beam coverage, must be sufficient in both the horizontal and vertical cross-sections. Further studies of the mean backscattering cross-section in the lateral aspect to provide values representative of the relevant species, signal frequency and fish-orientation distribution are essential to achieve more accurate and precise estimates of the mean fish density within schools. A dual-frequency approach has been proposed, using two well separated signal frequencies, for estimating the mean orientation of

fish inside migrating schools. If such an approach is feasible, an overall uncertainty around ±60 % is considered plausible for each measurement when estimating the school biomass during the inspection phase, before deploying the purse seine. For the sake of clarity, the mean biomass of the school, computed after completing half a circumnavigation, may be regarded as one measurement in this context. Circumnavigating the school repeatedly, until the mean biomass stabilizes, is here proposed as part of a strategic investigation. In fact, this is a procedure also used by some experienced skippers. More "variable" or difficult schools are inspected more in detail before the catch. In the CRISP projects, other researchers have estimated the correlation between the biomass in real catches, 6 mackerel schools and 2 herring schools, and the estimates using the sonar. So far, the deviations of the measurements compared with the catches fits well with a uncertainty of about ±60%. This result will be published when additional validation catches are available, and when the computation methods have been properly tested on more schools of different species.

Many of the skippers we have worked with during the project have by experience developed a fairly good but subjective judgement of how the sonar images relate to the likely catch. In many cases, this may even compete with the objective accuracy level reported above (±60%). However, using un-calibrated sonar, the skipper must be careful with the sonar settings, and preferably not change any to achieve a good comparison with previous sonar observations and the resulting catches. Large differences between catches are, however, expected if the fish density is changing or if the catch must be taken in a layer of herring or mackerel. Using calibrated sonar, the important density estimate may be determined objectively in both situations. Since the area and volume covered by the purse seine is known, realistic catch estimates may also be made when the fish are in layers. After the end of the CRISP project, the proposed methods will be part of a new biomass-algorithm incorporated within the sonar software. Such algorithm may then give reliable biomass estimates, including uncertainty, from calibrated sonars to further build the fisherman's experience.

More difficult acoustic phenomena, such as acoustic extinction (Zhao & Ona, 2003; Foote et al., 1992) or multiple scattering (Stanton, 1983) within the school, have not been properly discussed or accounted for in this thesis. For Atlantic mackerel, there are no indications of significant extinction in the schools or layers observed with echosounders and therefore none is expected in sonar images. For dense schools and large layers of herring, however, acoustic extinction is definitely a problem when they are observed with echosounders. Methods for correcting the mean volume backscattering coefficient for extinction have been developed by (Foote et al., 1992) and (Zhao & Ona, 2003). Due to the wide yaw-angle distribution compared to that of the fish tilt-angles, the mean target strength is 4-5 dB less when measured in the horizontal mode compared to the dorsal mode (Ona, 2015 personal communisation). The extinction cross–section is therefore expected to be similarly weaker, with less likelihood of significant acoustic shadowing. Investigations of this problem will be a future activity within the CRISP project, including both field measurements and simulations, but this work has not yet begun. At this stage, the collected data on single schools will reveal any large deviations between the acoustically measured biomass and pursed catch, and if the extinction effect is a significant problem. For the small and midsized schools which we have been fishing on, usually less than 500 tons, we have not seen such effects.

References

Aglen, A. (1994). Sources of error in acoustic estimation of fish abundance. *Marine fish behaviour in capture and abundance estimation*. p.pp. 107–133.

Ainslie, M.A. (1998). A simplified formula for viscous and chemical absorption in sea water. *The Journal of the Acoustical Society of America*. 103 (3) p.pp. 1671–1672.

Andersen, L.N., Berg, S., Gammelster, O.B. & Lunde, E.B. (2006). New scientific multibeam systems (ME70 and MS70) for fishery research applications. *The Journal of the Acoustical Society of America*. 120 (5). p.p. 3017.

Balabanian, J.-P., Viola, I., Ona, E., Patel, R. & Gröller, E. (2007). Sonar Explorer: A New Tool for Visualization of Fish Schools from 3D Sonar Data. In: *EuroVis*. pp. 155–162.

Ben-Yami, M. (1994). *Purse seining manual*. Fishing news books.

Bernasconi, M., Patel, R., Nøttestad, L., Pedersen, G. & Brierley, A.S. (2013). The effect of depth on the target strength of a humpback whale (Megaptera novaeangliae). *The Journal of the Acoustical Society of America*. 134 (6). p.pp. 4316–4322.

Blaxter, J.H.S. & Batty, R.S. (1984). The herring swimbladder: loss and gain of gas. *Journal of the Marine Biological Association of the United Kingdom*. 64 (2). p.pp. 441–459.

Blomberg, A.E.A., Austeng, A. & Hansen, R.E. (2012). Adaptive Beamforming Applied to a Cylindrical Sonar Array Using an Interpolated Array Transformation. *Oceanic Engineering, IEEE Journal of*. 37 (1). p.pp. 25–34.

Bodholdt, H. (1982). A multi-beam sonar for fish school observations. In: *FAO Symposium on Fisheries Acoustics, Bergen, Norway*. 1982, p. 24.

Bodholt, H. & Olsen, K. (1977). Computer-generated display of an underwater situation: applications in fish behaviour studies. *Rapp. P.-v. reun. Cons. int. Explor. Mer*. 170. p.pp. 31–35.

Brehmer, P. & Gerlotto, F. (2001). A simple standardisation of omnidirectional sonar in fisheries research through field calibration and sampling data. *Hydroacoustics*. 4. p.pp. 27–30.

Brehmer, P., Gerlotto, F., Guillard, J., Sanguinède, F., Guénnegan, Y. & Buestel, D. (2003). New applications of hydroacoustic methods for monitoring shallow water aquatic ecosystems: the case of mussel culture grounds. *Aquatic Living Resources*. 16 (3). p.pp. 333–338.

Brehmer, P., Josse, E. & Nøttestad, L. (2012). Evidence that whales (Balaenoptera borealis) visit drifting fish aggregating devices: Do their presence affect the processes underlying fish aggregation? *Marine Ecology*. 33. p.pp. 176–182.

Brehmer, P., Lafont, T., Georgakarakos, S., Josse, E., Gerlotto, F. & Collet, C. (2006). Omnidirectional multibeam sonar monitoring: applications in fisheries science. *Fish and Fisheries*. 7 (3). p.pp. 165–179.

Carlson, T.J. & Jackson, D. (1980). *Empirical evaluation of the feasibility of split beam methods for direct in situ target strength measurement of single fish*. Applied Physics Laboratory, University of Washington.

Chen, C.-T. & Millero, F.J. (1977). Speed of sound in seawater at high pressures. *The Journal of the Acoustical Society of America*. 62 (5). p.pp. 1129–1135.

Chu, D., Baldwin, K.C., Foote, K.G., Yanchao, L., Mayer, L.A. & Melvin, G.D. (2001). Multibeam sonar calibration: target localization in azimuth. In: *OCEANS, 2001*. 2001, IEEE, pp. 2506–2510.

Chu, D., Foote, K.G. & Hufnagle Jr., L.C. (2002). Measurement of multibeam sonar directivity patterns. In: *OCEANS '02*. 2002, IEEE, pp. 1411–1414.

Clay, C.S. & Horne, J.K. (1994). Acoustic models of fish: the Atlantic cod (Gadus morhua). *The Journal of the Acoustical Society of America*. 96 (3). p.pp. 1661–1668.

Cochrane, N.A., Li, Y. & Melvin, G.D. (2003). Quantification of a multibeam sonar for fisheries assessment applications. *The Journal of the Acoustical Society of America*. 114 (2). p.pp. 745–758.

Cunefare, K.A., Gary, K. & Klaus, B. (1989). A boundary element method for acoustic radiation valid for all wavenumbers. *The journal of the acoustical society of America*. 85 (1). p.pp. 39–48.

Cushing, D. (1955). Some echo-sounding experiments on fish. *Journal du Conseil: ICES Journal of Marine Science*. 20 (3). p.pp. 266–275.

Cutter, G.R. & Demer, D. a. (2007). Accounting for scattering directivity and fish behaviour in multibeam-echosounder surveys. *ICES Journal of Marine Science: Journal du Conseil*. 64 (9). p.pp. 1664–1674.

Dalen, J. (1974). Forsøk med akustiske merker i Lofoten i mars 1974. *Havforskningsinstituttet*.

Dalen, J. & Løvik, A. (1981). The influence of wind-induced bubbles on echo integration surveys. *The Journal of the Acoustical Society of America*. 69 (6). p.pp. 1653–1659.

Degnbol, P. (1988). *A calibration method for split beam echo sounders including calibration of directivity compensation and level*. Danmarks Fiskeri-og Havundersøgelser.

Demer, D.A., Cutter, G.R., Renfree, J.S. & Butler, J.L. (2009). A statistical-spectral method for echo classification. *ICES Journal of Marine Science: Journal du Conseil*. 66 (6). p.pp. 1081–1090.

Devold, F. (1961). The life history of the Atlanto-Scandian herring. In: *ICES*. 1961.

Diner, N. (2001). Correction on school geometry and density: Approach based on acoustic image simulation. *Aquatic Living Resources*. 14 (4). p.pp. 211–222.

Diner, N. (2007). Evaluating uncertainty in measurements of fish shoal aggregate backscattering cross-section caused by small shoal size relative to beam width. *Aquatic Living Resources*. 20 (2). p.pp. 117–121.

Doherty, K.W., Hammar, T.R. & Foote, K.G. (2002). Transducer mounting and rotating system for calibrating sonars in a sea well. In: *OCEANS '02*. 2002, IEEE, pp. 1407–1410.

Dragesund, O. & Midttun, L. (1966). The development of acoustic instrumentation in fisheries research and commercial fisheries in Norway. *ICES CM*.

Dragesund, O. & Olsen, S. (1965). On the possibility of estimating year-class strength by measuring echo-abundance of 0-group fish. *FiskDir. Skr. Ser. Havunders*. 13. p.pp. 47–

75.

Ehrenberg, J. (1983). A review of in situ target strength estimation techniques. *FAO Fisheries Report (FAO)*. p.pp. 85–90.

Ehrenberg, J., Green, J. & Wirtz, A. (1976). A Dual-Beam Acoustic System for Measuring the Target Strength of Individual Fish. In: *OCEANS '76*. 1976, IEEE, pp. 434–438.

Faran, J.J. (1951). Sound Scattering by Solid Cylinders and Spheres. *The Journal of the Acoustical Society of America*. 23 (4). p.p. 405.

Fernandes, P.G., Gerlotto, F., Holliday, D.V., Nakken, O. & Simmonds, E.J. (2002). Acoustic applications in fisheries science: the ICES contribution. In: *ICES Marine Science Symposia*. 2002, pp. 483–492.

Fischer, M., Gauger, U. & Gaul, L. (2004). A multipole Galerkin boundary element method for acoustics. *Engineering Analysis with Boundary Elements*. 28 (2). p.pp. 155–162.

Fofonoff, P. & Millard, R. (1983). Algorithms for computation of fundamental properties of seawater. *UNESCO Technical papers in marine science*. 44. p.p. 53.

Foote, K.G. (1990). Correcting acoustic measurements of scatterer density for extinction. *The Journal of the Acoustical Society of America*. 88 (3) p.pp. 1543–1546.

Foote, K.G. (1980a). Effect of fish behaviour on echo energy: the need for measurements of orientation distributions. *Journal du Conseil*. [Online]. 39 (2). p.pp. 193–201. Available from: http://icesjms.oxfordjournals.org/content/39/2/193.abstract.

Foote, K.G. (1980b). Importance of the swimbladder in acoustic scattering by fish: A comparison of gadoid and mackerel target strengths. *The Journal of the Acoustical Society of America*. 67 (6). p.pp. 2084–2089.

Foote, K.G. (1983). Linearity of fisheries acoustics, with addition theorems. *The Journal of the Acoustical Society of America*. 73 (6) p.p. 1932.

Foote, K.G. (1982). Optimizing copper spheres for precision calibration of hydroacoustic equipment. *The Journal of the Acoustical Society of America*. [Online]. 71 (3). p.pp. 742–747. Available from: http://dx.doi.org/10.1121/1.387497.

Foote, K.G., Chu, D., Hammar, T.R., Baldwin, K.C., Mayer, L.A., Hufnagle, J.L.C. & Jech, J.M. (2005). Protocols for calibrating multibeam sonar. *The Journal of the Acoustical Society of America*. 117 (4). p.pp. 2013–2027.

Foote, K.G., Knudsen, H.P. & Vestnes, G. (1983). Standard calibration of echo sounders and integrators with optimal copper spheres. *FiskDir. Skr. Ser. HavUnders*. 17. p.pp. 335–346.

Foote, K.G., Knudsen, H.P., Vestnes, G., Maclennan, D.N. & Simmonds, E.J. (1987). Calibration of acoustic instruments for fish density estimation: a practical guide. *International Council for the Exploration of the Sea*. (144). p.p. 69.

Foote, K.G. & MacLennan, D.N. (1984). Comparison of copper and tungsten carbide calibration spheres. *The Journal of the Acoustical Society of America*. 75 (2). p.pp. 612–616.

Foote, K.G., Ona, E. & Toresen, R. (1992). Determining the extinction cross section of aggregating fish. *The Journal of the Acoustical Society of America*. 91 (4). p.p. 1983.

Forbes, S.T. & Nakken, O. (1972). *Manual of methods for fisheries resource survey and*

appraisal. Food and Agriculture Organization of the United Nations.

Francois, R.E. & Garrison, G.R. (1982). Sound absorption based on ocean measurements. Part II: Boric acid contribution and equation for total absorption. *The Journal of the Acoustical Society of America*. 72 (6). p.p. 1879.

Froese, R. (2006). Cube law, condition factor and weight-length relationships: History, meta-analysis and recommendations. *Journal of Applied Ichthyology*. 22 (4). p.pp. 241–253.

Fulton, T.W. (1904). The rate of growth of fishes. *22nd Ann. Rep. Fish. Board of Scotland*. 3. p.pp. 141–241.

Fässler, S.M.M., Santos, R., García-Núñez, N. & Fernandes, P.G. (2007). Multifrequency backscattering properties of Atlantic herring (Clupea harengus) and Norway pout (Trisopterus esmarkii). *Canadian Journal of Fisheries and Aquatic Sciences*. 64 (2). p.pp. 362–374.

Geoffroy, M., Rousseau, S., Knudsen, F.R. & Fortier, L. (2015). Target strengths and echotraces of whales and seals in the Canadian Beaufort Sea. *ICES Journal of Marine Science: Journal du Conseil*. p.p. fsv182.

Gerlotto, F., Fréon, P., Soria, M., Cottais, P. & Ronzier, L. (1994). Exhaustive observation of 3D school structure using multibeam side scan sonar: potential use for school classification, biomass estimation and behaviour studies. *ICES CM*. 19948. p.p. 26.

Gerlotto, F., Georgakarakos, S. & Eriksen, P.K. (2000). The application of multibeam sonar technology for quantitative estimates of fish density in shallow water acoustic surveys. *Aquatic Living Resources*. 13 (5). p.pp. 385–393.

Gerlotto, F. & Paramo, J. (2003). The three-dimensional morphology and internal structure of clupeid schools as observed using vertical scanning multibeam sonar. *Aquatic Living Resources*. 16 (3). p.pp. 113–122.

Gerlotto, F., Soria, M. & Fréon, P. (1999). From two dimensions to three: the use of multibeam sonar for a new approach in fisheries acoustics. *Canadian Journal of Fisheries and Aquatic Sciences*. 56 (1) p.pp. 6–12.

Gorska, N., Korneliussen, R.J. & Ona, E. (2007). Acoustic backscatter by schools of adult Atlantic mackerel. *ICES Journal of Marine Science: Journal du Conseil*. 64 (6). p.pp. 1145–1151.

Gorska, N. & Ona, E. (2003). Modelling the acoustic effect of swimbladder compression in herring. *ICES Journal of Marine Science*. 60 (3). p.pp. 548–554.

Gorska, N., Ona, E. & Korneliussen, R. (2005). Acoustic backscattering by Atlantic mackerel as being representative of fish that lack a swimbladder. Backscattering by individual fish. *ICES Journal of Marine Science: Journal du Conseil*. 62 (5). p.pp. 984–995.

Greenlaw, C.F. & Johnson, R.K. (1983). Mulitple-frequency acoustical estimation. *Biological Oceanography*. [Online]. 2. p.pp. 227–252. Available from: papers2://publication/uuid/6076317D-2985-420C-9F1D-3E3406EE1BC4.

Hafsteinsson, M. & Misund, O. (1995). Recording the migration behaviour of fish schools by multi-beam sonar during conventional acoustic surveys. *ICES Journal of Marine Science*. 52 (6). p.pp. 915–924.

Harden Jones, F.R. & McCartney, B.S. (1962). The use of electronic sector-scanning sonar

for following the movements of fish shoals: sea trials on R.R.S. DISCOVERY II. *J. Cons. perm. int. Explor. Mer*. 27 (2). p.pp. 141–149.

Hickling, R. (1962). Analysis of Echoes from a Solid Elastic Sphere in Water. *The Journal of the Acoustical Society of America*. 34 (10). p.pp. 1582–1592.

Hjellvik, V., Handegard, N.O. & Ona, E. (2008). Correcting for vessel avoidance in acoustic-abundance estimates for herring. *ICES Journal of Marine Science*. 65 (6). p.pp. 1036–1045.

Hobaek, H. & Forland, T.N. (2013). Characterization of Target Spheres for Broad-Band Calibration of Acoustic Systems. *Acta Acustica united with Acustica*. 99 (3). p.pp. 465–476.

Hodgson, W.C. (1951). No TitleEcho-sounding and the pelagic fisheries. *Operational Research Quarterly*. p.p. 33.

Hodgson, W.C. & Fridriksson, A. (1955). *Report on echo-sounding and asdic for fishing purposes*. Conseil Permanent International pourl'Exploration dela Mer.

Holliday, D.V. (1978). *Use of acoustic frequency diversity for marine biological measurements*. Tracor.

Holmin, A.J., Handegard, N.O., Korneliussen, R. & Tjøstheim, D. (2012). Simulations of multibeam sonar echos from schooling individual fish. *The Journal of the Acoustical Society of America*. 132 (6) p.pp. 3720–3734.

Horne, J. (1999). Multi-frequency estimates of fish abundance: constraints of rather high frequencies. *ICES Journal of Marine Science*. [Online]. 56 (2). p.pp. 184–199. Available from: http://icesjms.oxfordjournals.org/content/56/2/184.short.

Horne, J.K., Sawada, K., Abe, K., Kreisberg, R.B., Barbee, D.H. & Sadayasu, K. (2009). Swimbladders under pressure: anatomical and acoustic responses by walleye pollock. *ICES Journal of Marine Science: Journal du Conseil*. 66 (6). p.pp. 1162–1168.

Hovem, J.M. (2012). *Marine Acoustics: The Physics of Sound in Underwater Environments*. Peninsula publishing.

Huse, I. & Vold, A. (2010). Mortality of mackerel (Scomber scombrus L.) after pursing and slipping from a purse seine. *Fisheries Research*. 106 (1). p.pp. 54–59.

Jech, J.M., Foote, K.G., Chu, D. & Hufnagle, L.C. (2005). Comparing two 38-kHz scientific echosounders. *ICES Journal of Marine Science*. 62 (6). p.pp. 1168–1179.

Jech, J.M., Foote, K.G., Chu, D. & Liberatore, S.P. (2003). Comparing two scientific echo sounders. In: *OCEANS 2003. Proceedings*. 2003, IEEE, pp. 1630–1632.

Johnsen, E., Pedersen, R. & Ona, E. (2009). Size-dependent frequency response of sandeel schools. *ICES Journal of Marine Science: Journal du Conseil*. 66 (6). p.pp. 1100–1105.

Johnson, R.K. (1977). Acoustic estimation of scattering-layer composition. *The Journal of the Acoustical Society of America*. [Online]. 61 (6). p.p. 1636. Available from: http://link.aip.org/link/JASMAN/v61/i6/p1636/s1&Agg=doi.

Jones, F. & Pearce, G. (1958). Acoustic reflexion experiments with Perch (Perca fluviatilis Linn.) to determine the proportion of the echo returned by the swimbladder. *J. exp. Biol*. 35. p.pp. 437–450.

Kacker, R., Sommer, K.-D. & Kessel, R. (2007). Evolution of modern approaches to express

uncertainty in measurement. *Metrologia*. 44 (6). p.pp. 513–529.

Kimura, K. (1929). On the detection of fish-groups by an acoustic method. *Journal of the Imperial Fisheries Institute, Tokyo*. 24. p.pp. 41–55.

Kinsler, L.E., Frey, A.R., Coppens, A.B. & Sanders, J. V (1999). *Fundamentals of acoustics*. John Wiley & Sons, Inc.

Kloser, R.J., Ryan, T., Sakov, P., Williams, A. & Koslow, J.A. (2002). Species identification in deep water using multiple acoustic frequencies. *Canadian Journal of Fisheries and Aquatic Sciences*. 59 (6). p.pp. 1065–1077.

Knudsen, H.P. (2009). Long-term evaluation of scientific-echosounder performance. *ICES Journal of Marine Science*. [Online]. 66 (6). p.pp. 1335–1340. Available from: http://icesjms.oxfordjournals.org/cgi/doi/10.1093/icesjms/fsp025.

Korneliussen, R. & Ona, E. (2002). An operational system for processing and visualizing multi-frequency acoustic data. *ICES Journal of Marine Science*. 59 (2). p.pp. 293–313.

Korneliussen, R. & Ona, E. (2003). Synthetic echograms generated from the relative frequency response. *ICES Journal of Marine Science*. 60 (3). p.pp. 636–640.

Korneliussen, R.J., Diner, N., Ona, E., Berger, L. & Fernandes, P.G. (2008). Proposals for the collection of multifrequency acoustic data. *ICES Journal of Marine Science*. 65 (6) p.pp. 982–994.

Korneliussen, R.J., Heggelund, Y., Eliassen, I.K. & Johansen, G.O. (2009). Acoustic species identification of schooling fish. *ICES Journal of Marine Science: Journal du Conseil*. 66 (6). p.pp. 1111–1118.

Krim, H. & Viberg, M. (1996). Two Decades of Array Signal Processing Research. *IEEE Signal Processing Magazine*. 13 (4). p.pp. 67–94.

Kubilius, R. & Ona, E. (2012). Target strength and tilt-angle distribution of the lesser sandeel (Ammodytes marinus). *ICES Journal of Marine Science*. 69 (6). p.pp. 1099–1107.

Lanzoni, J. & Weber, T. (2011). A method for field calibration of a multibeam echo sounder. In: *OCEANS 2011*. 2011, IEEE, pp. 1–7.

Lasky, M. (1977). Review of undersea acoustics to 1950. *The Journal of the Acoustical Society of America*. 61 (2). p.pp. 283–297.

Lichte, H. (1919). On the influence of horizontal temperature layers in seawater on the range of underwater sound signals. *Physikalische Zeitschrift*. 17 ((translated by A.F. Wittenborn)). p.pp. 385–389.

Lockwood, S.J., Pawson, M.G. & Eaton, D.R. (1983). The effects of crowding on mackerel (Scomber scombrus L.) — Physical condition and mortality. *Fisheries Research*. 2 (2). p.pp. 129–147.

Love, R.H. (1969). Maximum Side-Aspect Target Strength of an Individual Fish. *The Journal of the Acoustical Society of America*. 46 (3B) p.pp. 746–752.

Macaulay, G.J., Peña, H., Fässler, S.M.M., Pedersen, G. & Ona, E. (2013). Accuracy of the Kirchhoff-approximation and Kirchhoff-ray-mode fish swimbladder acoustic scattering models. *PloS one*. 8 (5). p.p. e64055.

MacCurdy, E. & Linscott, R.N. (1938). *The notebooks of Leonardo da Vinci*. Jonathan Cape

London.

MacLennan, D.N. (1990). Acoustical measurement of fish abundance. *The Journal of the Acoustical Society of America*. 87 (1) p.pp. 1–15.

MacLennan, D.N. (1981). *The Theory of Solid Spheres as Sonar Calibration Targets*. Department of Agriculture and Fisheries for Scotland.

Marçalo, A., Marques, T.A., Araújo, J., Pousão-Ferreira, P., Erzini, K. & Stratoudakis, Y. (2010). Fishing simulation experiments for predicting the effects of purse-seine capture on sardine (Sardina pilchardus). *ICES Journal of Marine Science: Journal du Conseil*. 67 (2). p.pp. 334–344.

Medwin, H. & Clay, C.S. (1998). *Fundamentals of Acoustical Oceanography*. Boston: Academic Press.

Melvin, G., Cochrane, N.A. & Li, Y. (2003). Extraction and comparison of acoustic backscatter from a calibrated multi- and single-beam sonar. *ICES Journal of Marine Science*. 60 (3). p.pp. 669–677.

Midttun, L. & Hoff, I. (1962). Measurements of the reflection of sound by fish. *Fiskeridirektoratets skrifter*. 13. p.pp. 1–18.

Millero (1993). What is PSU? *Oceanography*. 6 (3). p.p. 67.

Misund, O., Aglen, A., Beltestad, A.K. & Dalen, J. (1992). Relationships between the geometric dimensions and biomass of schools. *ICES Journal of Marine Science*. 49 (3). p.pp. 305–315.

Misund, O.A. (1993a). Abundance estimation of fish schools based on a relationship between school area and school biomass. *Aquatic Living Resources*. 6 (03). p.pp. 235–241.

Misund, O.A. (1993b). Avoidance behaviour of herring (Clupea harengus) and mackerel (Scomber scombrus) in purse seine capture situations. *Fisheries Research*. 16 (2) p.pp. 179–194.

Misund, O.A. (1990). Sonar observations of schooling herring: school dimensions, swimming behaviour, and avoidance of vessel and purse seine. *ICES council for the exploration for the sea*. 189. p.pp. 135–149.

Misund, O.A. & Aglen, A. (1992). Swimming behaviour of fish schools in the North Sea during acoustic surveying and pelagic trawl sampling. *ICES Journal of Marine Science*. 49 (3). p.pp. 325–334.

Misund, O.A., Aglen, A. & Fronaes, E. (1995). Mapping the shape, size, and density of fish schools by echo integration and a high-resolution sonar. *ICES Journal of Marine Science*. 52 (1) p.pp. 11–20.

Misund, O.A., Aglen, A., Johanessen, S., Skagen, D. & Totland, B. (1993). Assessing the reliability of fish density estimates by monitoring the swimming behaviour of fish schools during acoustic surveys. In: *ICES mar. sci. symp*. 1993, pp. 202–206.

Mitson, R. & Wood, R. (1961). An automatic method of counting fish echoes. *Journal du Conseil*. 26 (3). p.pp. 281–291.

Mitson, R.B. & Cook, G.J. (1971). Shipboard installation and trials of an electronic sector scanning sonar. *J. Br. Institn Radio Engrs*. 41.

Nakken, O. & Olsen, K. (1977). Target strength measurements of fish. *ICES*.

Nesse, T.L., Hobæk, H. & Korneliussen, R.J. (2009). Measurements of acoustic-scattering spectra from the whole and parts of Atlantic mackerel. *ICES Journal of Marine Science*. 66 (6). p.pp. 1169–1175.

Nishimori, Y., Iida, K., Furusawa, M., Tang, Y., Tokuyama, K., Nagai, S. & Nishiyama, Y. (2009). The development and evaluation of a three-dimensional, echo-integration method for estimating fish-school abundance. *ICES Journal of Marine Science: Journal du Conseil*. 66 (6). p.pp. 1037–1042.

Olsen, K. (1972). *Rapport om evaluering av Simrad sonar dataskjerm på operativt snurpefartøy*.

Ona, E. (2003). An expanded target-strength relationship for herring. *ICES Journal of Marine Science*. 60 (3). p.pp. 493–499.

Ona, E. (2014). Måling av fiskestørrelse i stim med bredbånds ekkolodd. *Havforskningsinstituttet*.

Ona, E. (1990). Physiological factors causing natural variations in acoustic target strength of fish. *Journal of the Marine Biological Association of the United Kingdom*. 70 (01). p.pp. 107–127.

Ona, E. (1984). Tilt angle measurements on herring. *ICES CM B*. 19.

Ona, E., Andersen, L.N., Knudsen, H.P. & Berg, S. (2007a). Calibrating multibeam, wideband sonar with reference targets. In: *OCEANS 2007 - Europe*. 2007, IEEE, pp. 1–5.

Ona, E., Dalen, J., Knudsen, H.P., Patel, R., Andersen, L.N. & Berg, S. (2006). First data from sea trials with the new MS70 multibeam sonar. *The Journal of the Acoustical Society of America*. 120 (5). p.p. 3017.

Ona, E., Godo, O.R., Handegard, N.O., Hjellvik, V., Patel, R. & Pedersen, G. (2007b). Silent research vessels are not quiet. *The Journal of the Acoustical Society of America*. 121 (4). p.pp. EL145–EL150.

Ona, E. & Korneliussen, R.J. (2000). Herring vessel avoidance; diving or density draining. In: *Proceedings of the Fifth European Conference on Underwater Acoustics, ECUA*. 2000, pp. 1515–1520.

Ona, E., Mazauric, V. & Andersen, L.N. (2009). Calibration methods for two scientific multibeam systems. *ICES Journal of Marine Science: Journal du Conseil*. 66 (6). p.pp. 1326–1334.

Ona, E. & Toresen, R. (1988). Avoidance reactions of herring to survey vessels, studied by scanning sonar. *ICES*.

Ona, E. & Traynor, J.J. (1990). Hull mounted, protruding transducer for improving echo integration in bad weather. *ICES CM*. B:31.

Pedersen, G., Handegard, N.O. & Ona, E. (2009). Lateral-aspect, target-strength measurements of in situ herring (Clupea harengus). *ICES Journal of Marine Science: Journal du Conseil*. 66 (6). p.pp. 1191–1196.

Peña, H. & Foote, K.G. (2008). Modelling the target strength of Trachurus symmetricus murphyi based on high-resolution swimbladder morphometry using an MRI scanner.

ICES Journal of Marine Science. 65 (9). p.pp. 1751–1761.

Peña, H., Handegard, N.O. & Ona, E. (2013). Feeding herring schools do not react to seismic air gun surveys. *ICES Journal of Marine Science: Journal du Conseil*. p.p. fst079.

Peraltilla, S. & Bertrand, S. (2014). In situ measurements of the speed of Peruvian anchovy schools. *Fisheries Research*. 149. p.pp. 92–94.

Pyc, C.D., Geoffroy, M. & Knudsen, F.R. (2015). An evaluation of active acoustic methods for detection of marine mammals in the Canadian Beaufort Sea. *Marine Mammal Science*.

Readhead, M. (2010). *Calculations of the Sound Scattering of Hyperbolic Frequency Modulated Chirped Pulses from Fluid-filled Spherical Shell Sonar Targets*.

Richardson, I.D. (1959). *Echo sounding experiments in the Barents Sea*. HM Stationery Office.

Runnstrøm, S. (1937). A review of the Norwegian herring investigations in recent years. *Journal du Conseil*. 12 (2). p.pp. 123–143.

Runnstrøm, S. (1941). *Quantitative investigations on herring spawning and its yearly fluctuations at the west coast of Norway*. J. Griegs boktr.

SASO (1995). Guide to the Expression of Uncertainty in Measurement. *Saudi Arabian Standards Organization*.

Scherbino, M. & Truskanov, M. (1966). Determination of fish concentration by means of acoustic apparatus. *ICES CM1*. 3 (6).

Seabird (2015). *Seabird 911+ CTD spesification*. [Online]. 2015. Available from: http://www.seabird.com/sbe911plus-ctd.

Sherman, C.H. & Butler, J.L. (2007). *Transducers and arrays for underwater sound*. Springer.

Simmonds, J. & MacLennan, D. (2005). *Fisheries Acoustics*. 1st Ed. 1 (ed.). London: Chapman & Hall.

Simrad (2007). *Operator Manual SX90, Fish finder sonar* S. AS (ed.).

Skarthhamar, J. & Svendsen, H. (2010). Short-term hydrographic variability in a stratified Arctic fjord. *Geological Society, London, Special Publications*. 344 p.pp. 51–60.

Śmigaj, W., Betcke, T., Arridge, S., Phillips, J. & Schweiger, M. (2015). Solving Boundary Integral Problems with {BEM++}. *ACM Transactions on Mathematical Software*. 41 (2). p.pp. 6:1 –6:40.

Soria, M., Fréon, P. & Gerlotto, F. (1996). Analysis of vessel influence on spatial behaviour of fish schools using a multi-beam sonar and consequences for biomass estimates by echo-sounder. *ICES Journal of Marine Science*. 53 (2). p.pp. 453–458.

Stanton, T.K. (1983). Multiple scattering with applications to fish-echo processing. *The Journal of the Acoustical Society of America*. 73 (4). p.p. 1164.

Stanton, T.K. & Chu, D. (2000). Review and recommendations for the modelling of acoustic scattering by fluid-like elongated zooplankton: euphausiids and copepods. *ICES Journal of Marine Science*. 57 (4). p.pp. 793–807.

Sund, O. (1935). Echo sounding in fishery research. *Nature*. 135. p.p. 953.

Sund, O. (1943). The fat and small herring on the coast of Norway in 1940. *Ann. Biol. Cons. Int. Explor. Mer*. 1. p.pp. 58–79.

Tang, Y., Iida, K., Mukai, T. & Nishimori, Y. (2006). Estimation of fish school volume using omnidirectional multi-beam sonar: scanning modes and algorithms. *Japanese journal of applied physics*. 45 (5S). p.p. 4868.

Tang, Y., Nishimori, Y. & Furusawa, M. (2009). The average three-dimensional target strength of fish by spheroid model for sonar surveys. *ICES Journal of Marine Science: Journal du Conseil*. 66 (6). p.pp. 1176–1183.

Tenningen, M., Peña, H. & Macaulay, G.J. (2015). Estimates of net volume available for fish shoals during commercial mackerel (Scomber scombrus) purse seining. *Fisheries Research*. 161. p.pp. 244–251.

Tenningen, M., Vold, A. & Olsen, R.E. (2012). The response of herring to high crowding densities in purse-seines: survival and stress reaction. *ICES Journal of Marine Science: Journal du Conseil*. 69 (8). p.pp. 1523–1531.

Tenningen, M.M. (2014). *Unaccounted mortality in purse seine fisheries. Quantification and mitigation of slipping mortality*. University of Bergen.

Totland, A., Johansen, G.O., Godø, O.R., Ona, E. & Torkelsen, T. (2009). Quantifying and reducing the surface blind zone and the seabed dead zone using new technology. *ICES Journal of Marine Science*. 66 (6). p.pp. 1370–1376.

Trygonis, V., Georgakarakos, S. & Simmonds, E.J. (2009). An operational system for automatic school identification on multibeam sonar echoes. *ICES Journal of Marine Science: Journal du Conseil*. 66 (5). p.pp. 935–949.

Tungate, D. (1958). *Echo-sounder surveys in the autumn of 1956*. HM Stationery Office.

Urick, R.J. (1983). *Principles of underwater sound*. New York: McGraw-Hill Book Company.

Voglis, G. & Cook, J. (1966). Underwater applications of an advanced acoustic scanning equipment. *Ultrasonics*. 4 (1). p.pp. 1–9.

Watson, R., Revenga, C. & Kura, Y. (2006). Fishing gear associated with global marine catches: I. Database development. *Fisheries Research*. 79 (1). p.pp. 97–102.

Welsby, V.G., Blaxter, J.H.S. & Chapman, C.J. (1963). Electronically scanned sonar in the investigation of fish. *Natur, Lond.* 199 (4897). p.pp. 980–981.

Welsby, V.G., Dunn, J.R., Chapman, C.J., Sharman, D.P. & Priestley, R. (1964). Further uses of electronically scanned sonar in the investigation of behaviour of fish. *Natur, Lond.* 203 (4945). p.pp. 588–589.

Wood, A. (1965). From the board of invention and research to the royal naval scientific servic. *Journal of the Royal Naval Scientific Service*. 20 (4). p.pp. 1–100.

Yao, Q. & Bjørnø, L. (1997). Broadband tonpilz underwater acoustic transducers based on multimode optimization. *IEEE Transactions on Ultrasonics, Ferroelectrics, and Frequency Control*. 44 (5). p.pp. 1060–1066.

Zhao, X. & Ona, E. (2003). Estimation and compensation models for the shadowing effect in dense fish aggregations. *ICES Journal of Marine Science*. 60 (1). p.pp. 155–163.

Appendix

I

A. PAPER 1

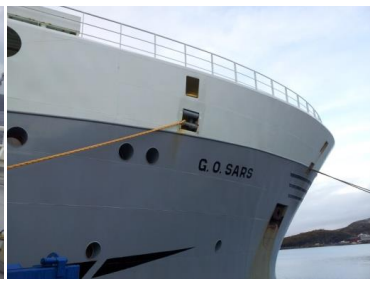

Status of paper: Manuscript accepted at Method of Oceanography.

Status author: 1st

Contribution of work;

Authorship: 80%

Data collection and analysis: 70%

Two mechanical rigs for field calibration of multi-beam fishery sonars

Sindre Vatnehol*, Atle Totland and Egil Ona

Institute of Marine Research, P.O. Box 1870 Nordnes, N-5817 Bergen, Norway

*corresponding author

E-mail address: sindre.vatnehol@imr.no

Telephone: +47 900 79 376

Keywords: Multi-beam sonar, calibration, calibration rig

Abstract

Two calibration rigs for controlling the movement of a reference target during a field calibration of multi-beam fishery sonars are described. The first rig was designed to be firmly mounted on the vessel hull and position the reference target inside a single beam, or a few selected sonar beams, with a specified spatial precision. This rig was also used for developing within-beam positioning algorithms, based upon the split-

beam principle, using data from individual transducer elements. The size and weight of this rig limited its capacity to calibrate multiple sonar beams. A second rig was therefore designed for swifter movement of the target through multiple beams from each rig-mounting location. The position of the reference target inside each beam was now directly computed from the measured target echo. The rig designs, operation and the experiences of using them, along with comparative performance tests are presented along with some examples of field calibrations.

1. Introduction

Accurately calibrated acoustical equipment is essential if quantitative estimations of fish populations are to be determined by acoustical methods (Aglen, 1994; Foote et al., 1987; Simmonds and MacLennan, 2005). For scientific investigations of fish stocks, the vertical echosounder is a vital tool that provides accurate backscattering data with a high sampling rate (Løland et al., 2007; Simmonds and MacLennan, 2005). However, for migrating pelagic fish schools which often swim near the sea surface, such as the Atlantic mackerel (*Scomber scombrus*) and the Norwegian Spring Spawning herring (*Clupea harengus L.*), the vertical echosounder may perform poorly if much of the population is within the near-surface blind zone, or if the fish move to avoid the vessel (Hjellvik et al., 2008; Misund, 1993; Ona et al., 2007b; Totland et al., 2009). Then, calibrated, horizontally-observing tools are needed if this portion of the population is to be quantified acoustically.

Scientific multi-beam systems, such as the Simrad MS70 (Andersen et al., 2006; Ona et al., 2006), are horizontally-observing and a standard calibration protocol has been established (Ona et al., 2009). These are, however, only available on a few research vessels, limiting the prospects for more comprehensive results from acoustic survey. On the other hand, commercial fishery sonars are far more available and could, if sufficiently accurate, contribute useful data for stock estimates.

Multi-beam sonar systems with a cylindrical transducer arrangement, such as the omni-directional fishery sonar (Simrad, 2007), are commonly used in purse-seine fisheries for observing fish schools (Misund, 1990; Tang et al., 2009, 2006). Such sonars typically transmit and receive a single fan of beams (Misund, 1990; Tang et al., 2006), evenly distributed in a near-horizontal cone providing observations all around the vessel (Fig. 1). Electronic steering of the beams permits observation of volumes as the user selects different tilt angles from the surface (Sherman and Butler, 2007; Van Trees, 2002), revealing cross-sections of ensonified schools or other targets. Alternatively, a vertical fan of beams can be configured, presenting a vertical cross-section through the water column at a user-selected angle relative to the heading of the vessel (Fig. 1). When both these transmission modes are activated, the two modes are automatically alternated and the relevant echoes are displayed in separate windows (Fig. 1).

The fans include 64 evenly separated acoustic beams, and the echo-amplitude data from each beam must have sufficient accuracy and range resolution for scientific purposes. Such data output, or the *scientific data output,* is now available in the

Simrad SX90 fishery sonar, and its successor the SU90 (Simrad, 2007). For the SX90, the nominal beams widths are between 7.4º (30 kHz) and 11.4º (20 kHz) in the vertical cross-section and between 8.5º (30 kHz) to 10º (20 kHz) in the horizontal. The range is sampled with 4 kHz time resolution. The amplitude data of each transducer element (256 elements on the SX90, and 384 on the SU90) were recorded in a separate data output. In addition to such facilities for primary data collection, a practical and standardised procedure for calibrating the sonar beams is essential to support research surveys on schooling pelagic fish.

Protocols for calibrating multi-beam sonars have been established (Foote et al., 2005), however, these calibrations have been conducted either in large-tank facilities or by using a free-floating buoy (Brehmer and Gerlotto, 2001; Cochrane et al., 2003; Foote et al., 2005; Lanzoni and Weber, 2011; Nishimori et al., 2009). The calibration procedure proposed in this paper is based on the methods used with scientific echosounders for decades (Foote et al., 1987); a reference target with known acoustic backscattering properties is moved through multiple beams in a practical field calibration which can be done on any fishing vessel. This procedure incorporates features of that described by (Ona et al., 2009), where a split-beam positioning algorithm was available for each sonar beam.

The software of the commercial multi-beam sonar does not include any target-positioning data (Foote et al., 1987; Ona et al., 2007a). A precise calibration rig was therefore designed to move the target with adequate control to verify its position in the beam. The results led to a target-positioning algorithm based on acoustic

measurements from these sonars, which was shown to perform accurately for cylindrical transducer arrays. A second rig was then designed which allowed faster and more efficient calibration of multiple beams. Fishermen prefer to have the transducers mounted as far towards the bow of the vessel as possible, and a mechanical device is used to lower the transducer array 1.2-1.6 m below the hull; adverse absorption effects from wind-induced air bubbles are then reduced (Dalen and Løvik, 1981), which is especially important on modern, relatively flat-bottomed vessel designs. This forward location of the transducer, directly below the forecastle of the ship, is beneficial for calibrations since it is easier to locate the standard target within the beams in that area.

The design and operational procedure of the two calibration rigs, and initial tests of accuracy and performance are described and discussed in this paper.

2. Rig Descriptions

2.1 Precision rig

2.1.1 Purpose

The purpose of the precision rig (Fig. 2) is to move the reference target in a precise geometry relative to the sonar transducer which is below the bow of the fishing vessel. During the calibration the rig data and the corresponding target positions are logged at 50 ms intervals. Given sufficient accuracy, the geometric data from the rig can be used to test new position-fixing algorithms based only on the received echo

data. Knowledge of the sphere position relative to the transducer is needed to compute the calibration parameters for individual beams.

System accuracy and limitations

In optimal conditions, with no sea current, no wind and no ship movement, the sphere can be moved with millimetre precision laterally and in depth, referenced to fixed points on the rig and the sea surface respectively. The overall spatial-location accuracy of the sphere relative to the sonar transducer is influenced by the following factors:

- Rig geometry
- Sonar range measurement (transducer – sphere distance)
- Rig orientation to the vessel
- Water movement
- Wind
- Ship movement in the x, y and z planes

Clearly favourable weather and sea conditions are a prerequisite to obtaining the best results. Sheltered calibration sites, within fjords, were therefore selected for these experiments.

2.1.2 The rig calibration system

The calibration system includes the following three components:

1) The rig

The calibration rig (Fig. 2) has two 4-m long poles which keep a 5-m long rail at that distance from the ship's side, in a region where the reference target is well outside the near-field of the transducer. On the rail, a cart can be moved back and forth along a toothed strap which avoids any slippage problems. This lateral movement is performed by a stepper motor with position feedback, enabling movement with millimetre accuracy along the rail.

To prevent the cart from running off the rail, end switches cut the motor power if the cart moves too far to either side of the rail. A lateral endpoint at the leftmost position of the rail is specified by the user during the start-up operation. An electronic sensor measured the tilt angle of the rail off the horizontal.

On the cart, a second and similar stepper motor is attached to a reel. The reel is used to lower the calibration sphere to the desired depth. Thus the motions of the two stepper motors determine the lateral and vertical location of the sphere. At the start of the operation, the sphere is lowered so that its centre is aligned with the sea surface. Here a second endpoint is defined in the software, indicating that the sphere has reached the surface during retrieval. The diameter of the reel was rather wide, around 7 cm, suggesting only 9 reel rotations are needed to lower the sphere 2 meters. The length of the discharged line, around the expected sphere depth, was measured prior to the calibration. Correct winding provides negligible changes in the drum diameter between each rotation. At the end of the operation, the sphere was hoisted back to the

second endpoint. If the sphere's centre is still aligned with the sea surface, the winding of the line may be assumed to be adequate.

During calibration of a single beam, the sphere is steered towards the centre of one selected acoustic beam. At the acoustic axis, the lateral and vertical reference position is set in the software, and the rig data output will now refer to the spatial location of the sphere relative to this position. Nominal angles relative to the transducer may then be computed.

The line used to lower the sphere is coated spectra™ rope (Cortland, 2015), where a line with a thickness of 1 mm and a tensile strength of 120 kg was commissioned. The purpose of the coating is to minimize trapped air inside the rope and consequent effects on the received echoes. It is important that the netting around the sphere and its guiding line are more or less acoustically transparent, or 40 dB weaker than the reference-target echo. To reduce arbitrary movement of the sphere, a heavy weight, around 15 kg, was sometimes attached 10 m below the sphere. The reference target and its line were soaked in a mixture of detergent soap and water before submerging.

2) Electronic control unit

An electronic control unit is an interface between the control software on a PC and the sensors and motors on the rig, operating via an Ethernet connection. Since the control unit is inside a splash-proof case with waterproof connectors, it can be located on deck in any weather conditions. The control unit is powered by 220 V_{AC} and

contains the various converters needed for motor operation, sensor logging and data distribution.

3) System software

A Labview application running on the PC is used to control, display and store relevant rig data. Prior to data collection, the clocks on the rig-control PC and the sonar-PC must be synchronized. Time-tagged motor-feedback and tilt-sensor data are stored to a file at up to 20 records per second. The reference target can be moved automatically through vertical and horizontal distance increments relative to the transducer, or manually using the arrow keys on the keyboard. A "home" button moves the sphere back to the earlier described reference position. Start-up and default values for the storage interval, IP addresses, motor speed etc., may be edited by the user in a parameter file prior to program execution.

2.2 Multi-beam calibration rig

2.2.1 Purpose

The precision rig was found to be too large and impractical for the calibration of multi-beam sonars, as it must be physically moved around the bow of the vessel to check all the beams. We therefore developed a new multi-beam rig which was more manoeuvrable (Fig. 3). This rig cannot provide high-precision data on the sphere's

spatial position, but it can swiftly move the sphere between multiple beams from one location on the bow deck. Alternative sphere-positioning procedures were then needed.

The rig calibration system

This calibration system comprises the following components:

The rig

The base of the rig (Fig. 3) is a tripod placed on the steel deck and held in position by two magnets with an attachment force of 200 kg. A motor driven rotary table on top of the tripod provides azimuthal movement of a 5 – 8 meter long glass fibre rod. The line from a motorized reel runs to the tip of the rod then down to the attached calibration sphere. A mast with supporting ropes, attached to the tip of the fibre rod, stabilizes and limits unwanted movement of the rod.

Electronic control unit

The same electronic control unit as described earlier for the precision rig forms the interface between the software running on a PC and the motors on the rig.

System software

A dedicated Labview application running on a PC is used to control, display and store the rig data. As long as the rig can position the reference target on the acoustic axis of the sonar beam, these data are not required in the calibration process, as the target positioning is now determined solely by the acoustic-echo data.

3. Testing and experiences

3.1 Test of the precision rig

A horizontally-orientated Simrad 200kHz split-beam echosounder was used for initial testing. The transducer two-way directivity pattern was measured according to standard calibration protocols (Ona, 1999). The echosounder was mounted behind the precision rig, replacing the SX90 in the sketch in Fig. 2, and the whole assembly was deployed from a pier in Bergen harbour, Norway. The rig was used to steer the calibration sphere (38.1 mm diameter tungsten carbide), within the entire beam. The spatial locations of the sphere were recorded to two separate files. The first file recorded the rig output with a reference position at the acoustic axis of the echosounder beam. The second was the split-beam target location generated directly from the echosounder system software (Simrad EK60). The computers for controlling the rig and the echosounder, along with their position records were synchronized to show corresponding time.

The cart and reel data were converted into nominal angular directions, for comparison with the split-beam measurements. A linear relationship between the two datasets was clearly demonstrated (Fig. 4). This was computed, in both the horizontal (β) and vertical (α) directions, with a mean position discrepancy close to $0.1°$. The standard deviations of the angular residuals were found to be close to $0.45°$ for both directions. Visual observations at the test site revealed that the harbour water was a stratified mixture of fresh and salt water; this is probably the main cause of the

variability shown by the standard deviations. A plausible explanation of the discrepancies is that the assumed local reference position was not exactly located at the centre of the beam; however, the discrepancies might be an artefact caused by the transducer itself, as suggested by Jech et al. (2005). Still, the initial test proved that the rig performed as intended, without any slipping or spinning problems.

3.2 Precision rig – field experiences on fishery vessels

The first attempt at an *in situ* calibration was conducted in a fjord outside Bodø, Norway, in 2012. The rig was attached to the bulwark in front of the research vessel "R/V G. O. SARS" and the calibration sphere, a 64 mm diameter tungsten carbide (WC) sphere, was lowered in the sea until it was visible on the SX90 sonar-display. Assembling the rig was particularly laborious due to the equipment being new and rather complex, hence only one beam was calibrated during this exercise (Table 1).

Apparently, the rig design was too sensitive to both the vessel movement and sea current, which made the calibration rather onerous. A stabilization weight attached to the sphere reduced the adverse effects caused by the sea current.

In spite of the large size of the precision rig, it was evident that the rig's ability to calibrate, given a particular attachment position, was confined to covering only one full sonar beam, or perhaps two partly-overlapping beams. Calibration of additional beams involved physical re-location of the rig. This involved 3 or 4 persons in the

lifting operation. If the vessel front crane could be used, 2 persons were still needed to guide the rig along the rail of the vessel forecastle.

However, three sonar beams on three selected vessels have been successfully calibrated using the precision rig, (Table 1). Both “F/V ARTUS” and “R/V G. O. SARS” sonars were calibrated in the spring of 2013 in the harbour of Ålesund, Norway. In these experiments, the vessel sterns were firmly tied to the pier, minimising most of the unwanted vessel movement. “F/V EROS” was calibrated later in 2013 while anchored in a fjord adjacent to Bergen, in a calm location favourable for calibration conditions irrespective of the wind direction.

The assembling, disassembling and re-location of the rig still proved to be both time-consuming and cumbersome, and it was only possible to calibrate three different beams within the designated time, a full working day per vessel. As a compromise, each calibration was assumed to be representative of all the beams within a defined sector. This compromise was based upon earlier calibration experience, taking account of the fact that adjacent beams are formed using mostly the same transducer elements both in transmit and receiving modes. Four sectors were defined to include a quarter of the beams; covering the port side, front, starboard side, and stern sectors. The system gain was computed for each representative beam and added to all beams within the designated sector. The vessel’s propellers generate turbulence and air bubbles giving echoes visible in most of the stern beams during normal surveying operations. Consequently, data from these beams are not included in the performance analysis.

3.3 Precision rig - general protocol

While running the sonar in search mode, a single beam steered towards -5º tilt angle was selected for the calibration. The rig was mounted on the bulwark in a manner where the railway was close to perpendicular to beam. To locate the acoustic axis inside the selected beam, the sphere, 64mm WC, was carefully moved until maximum echo strength was observed in the sonar data. This is similar to the traditional procedure for calibrating single-beam echosounders (Foote et al., 1987). The reference position was to be set at this location which was assigned the coordinates (x, z) = (0, 0) cm. The coordinate x indicates the lateral position along the railway, with negative values indicating points to the left of the reference position. The z-coordinate is the depth of the sphere, with negative values indicating points below the reference position. A third coordinate, y, is the distance from the transducer to the target, measured directly from the sonar data; this was needed to compute the angular directions of the target through trigonometry. Next, the sphere was moved in a cross-wise fashion by steering it to the following coordinates in succession: laterally (-100, 0) cm, (100, 0) cm, (0, 0) cm, and vertically (0, 100) cm, (0, -100) cm and (0, 0) cm. Combining the rig positions with the corresponding time-tagged acoustic data (target range and echo strength) will give the two-way directivity pattern of one beam, similar to the one shown in Fig. 5.

3.4 Precision rig – developing the split beam

Until a within-beam target-tracking system is available on fishery sonars, an access to the transducer element data is a necessity for computing the target's direction. The process for computing this direction is here only briefly described, but a full description of the theory will be submitted elsewhere. The elements nearest the direction of the beam was filtered and then divided into 4 quadrants. This is equivalent to the split-beam function on the echosounder (Carlson and Jackson, 1980; Ehrenberg, 1983). Here, the direction, both horizontal and vertical, of the target is computed when the signal-phase difference between quadrants are divided with an angle sensitivity coefficient. An accurate target direction is found when the correct angle sensitivity coefficients are used. In our case, these coefficients were found when a 1:1 relationship between the split-beam directions and the mechanical angles computed from the rig data output was achieved, similar to the result from Fig. 4. Assuming the elements performance are the same both between beams and between different sonars of the same model, these two sensitivity coefficients are the same for any beam. On suspicion of an inadequate accuracy of the target's direction, the angle sensitivity coefficients may be corrected by following this presented protocol. Still, the two-way directivity pattern of a selected beam may now be sufficiently measured using the split-beam position (e.g. Fig. 5).

3.5 Multi-beam rig - protocol

Since the precision rig had been used to verify adequate performance of the split-beam algorithm, through measurements on one beam of cylindrical multi-beam sonar, this calibration rig was replaced by the new multi-beam rig which was designed to allow a swifter procedure for calibrating several selected beams in one experiment.

In order to cover a suitably large number of beams, the rig was moved between three locations around the bow of the vessel. These were on the bow itself, and on the port and starboard sides. Beams pointing aft were not examined. The sphere was steered to the acoustic axis of the first selected beam, aided by the split-beam algorithm, and 100 target-strength measurements in the far-field of the transducer were made while the sphere was held at this location. These measurements were sufficient to estimate the mean and variance of the selected beam's transducer gain, thus completing its calibration. The same procedure was repeated in sequence for all beams within reach of the sphere at each rig location. The full beam pattern of several beams, each similar to figure 5, may be measured in an alternative and more detailed calibration protocol. However, this approach has not been prioritized due to the time constraints.

3.6 Multi-beam rig - experiences

In November 2013, the multi-beam sonars on "R/V G. O. SARS" and "F/V ARTUS" were calibrated in a calm fjord outside Bodø, using the multi-beam rig and the split-beam algorithm. As the vessel had to be anchored, a few beams on the

starboard side could not be measured due to interference from the anchor-chain echo (Fig. 6). Nevertheless, 26 beams on "R/V G. O. SARS" and 38 beams on "F/V ARTUS" were calibrated (Table 1) out of the 64 beams generated by each sonar. Due to time constraints, and the need to calibrate a larger fraction of the beams, only on-axis calibration was conducted. The access to the split-beam direction helped us to move the sphere swiftly to the centre of each beam.

Re-locating the rig was still fairly tedious; but the simpler mechanical design permitted more time for calibrations. There needs to be sufficient clear working area on the bow deck to facilitate rig operations. Some fishing vessels may have a rather small bow-deck area, or physical obstacles there such as cranes and anchors, which will restrict the calibration possibilities. On such vessels some of the sonar beams may be completely inaccessible.

The multi-beam rig was, like the precision rig, sensitive to water current and vessel movement. In one instance, a passing vessel caused the sphere to swing like a pendulum. This effect was only noticed through the results obtained with the split-beam algorithm. Additional echo-strength measurements were then made in order to ensure the collection of adequate good-quality data.

More comprehensive documentation of the calibration results will be published elsewhere. Nevertheless, the results presented here are considered as typical. After several calibrations covering most of the beams were completed, the results showed only small differences in the system gain between adjacent beams. 10 beams within a

single sector on “R/V G. O. Sars” were calibrated in November 2013, where the mean gain was computed to be 33.36 dB (SD 0.15 dB), (Fig. 7). Beam number 1 and 3 were here ignored as these had a larger deviation, where the deviation was believed to be caused by small changes in the temperature and salinity mixture in the stratified surface layers immediately after deploying the sphere. The small difference between the adjacent beams was to be expected, as these are formed using many of the same transducer elements. Therefore, only 2 or 3 beams need to be measured at each well-separated rig location during a swift calibration. This procedure was adopted when calibrating the sonars on “F/V KINGS BAY” and “R/V G. O. SARS”, during 2014 in Bergen (Table 1).

Calibration of horizontally-observing acoustic equipment may occasionally be a difficult task, since small variation in the inhomogeneous medium causes the path of the beam to bend differently between pings. Inside fjords, the freshwater runoff may cause a significant stratification in the near surface region, where internal movements of these layers causes variation of the beam gain. Such variation was seen in the first beams in figure 7. Still, calibrations inside fjords have been preferred due to a comfortable working environment as well as being adequate for standard echosounder calibration. In addition, when the vessel lies still, any changes in the beam’s characteristics during automatic tilt compensation is prevented.

4. Conclusion

The design and initial trials of two calibration rigs for use with multi-beam fishery sonars have been described, along with examples of calibration results. The results from the large and heavier, but more precise rig were used to develop a novel and elegant within-beam positioning algorithm, based solely on the acoustic data. To investigate the variability of the system gain over the full 64-beam fan, a second calibration rig was constructed and tested; it could measure many more beams within a reasonable time. Both rigs are large and somewhat cumbersome, but they enabled calibration of multi-beam fishery sonars nearly to the same accuracy as is commonly achieved for standard scientific echosounders. The larger spread in the calibration results for the sonar beams, compared to similar echo-sounder data is likely to be associated with greater variability in environmental factors. Hydrographical features such as thermoclines, often seen in fjords, could distort the transmission of near-horizontal sonar beams, to a greater extent than occurs with vertical beams, with consequent effects on the calibration accuracy. This problem should be investigated further, in order to understand and mitigate the consequences for near-horizontal sonar calibrations.

5. Acknowledgement

Thanks to Harald Fitje at Institute of Marine research for constructing of both calibration rigs; and the Norwegian Research council for financial support through NCR grant number 216460 (WHOFISH – Whale counting and fish school biomass

appraisal by two new Omni-directional fishery sonars) and 203477 (CRISP - Centre of Research-based Innovation in Sustainable fish capture and Processing technology). Thanks to editor Alex De Robertis and three anonymous reviewers.

References

Aglen, A., 1994. Sources of error in acoustic estimation of fish abundance. Mar. fish Behav. capture abundance Estim. 107–133.

Andersen, L.N., Berg, S., Gammelster, O.B., Lunde, E.B., 2006. New scientific multibeam systems (ME70 and MS70) for fishery research applications. J. Acoust. Soc. Am. 120, 3017.

Brehmer, P., Gerlotto, F., 2001. A simple standardisation of omnidirectional sonar in fisheries research through field calibration and sampling data. Hydroacoustics 4, 27–30.

Carlson, T.J., Jackson, D., 1980. Empirical evaluation of the feasibility of split beam methods for direct in situ target strength measurement of single fish, Applied Physics Laboratory, University of Washington. Applied Physics Laboratory, University of Washington.

Cochrane, N.A., Li, Y., Melvin, G.D., 2003. Quantification of a multibeam sonar for fisheries assessment applications. J. Acoust. Soc. Am. 114, 745–758.

Cortland, 2015. Spectra 12 Strand & 12x12 [WWW Document]. URL http://www.cortlandcompany.com/sites/default/files/downloads/media/product-data-sheets-spectra-12-strand_1.pdf

Dalen, J., Løvik, A., 1981. The influence of wind-induced bubbles on echo integration surveys. J. Acoust. Soc. Am. 69, 1653–1659.

Ehrenberg, J., 1983. A review of in situ target strength estimation techniques. FAO Fish. Rep. 85–90.

Foote, K.G., Chu, D., Hammar, T.R., Baldwin, K.C., Mayer, L.A., Hufnagle, J.L.C., Jech, J.M., 2005. Protocols for calibrating multibeam sonar. J. Acoust. Soc. Am. 117, 2013–2027.

Foote, K.G., Knudsen, H.P., Vestnes, G., Maclennan, D.N., Simmonds, E.J., 1987. Calibration of acoustic instruments for fish density estimation: a practical guide. Int. Counc. Explor. Sea 69.

Hjellvik, V., Handegard, N.O., Ona, E., 2008. Correcting for vessel avoidance in acoustic-abundance estimates for herring. ICES J. Mar. Sci. 65, 1036–1045. doi:10.1093/icesjms/fsn082

Jech, J.M., Foote, K.G., Chu, D., Hufnagle, L.C., 2005. Comparing two 38-kHz scientific echosounders. ICES J. Mar. Sci. 62, 1168–1179. doi:10.1016/j.icesjms.2005.02.014

Lanzoni, J., Weber, T., 2011. A method for field calibration of a multibeam echo sounder, in: OCEANS 2011. IEEE, pp. 1–7.

Løland, A., Aldrin, M., Ona, E., Hjellvik, V., Holst, J.C., 2007. Estimating and decomposing total uncertainty for survey-based abundance estimates of Norwegian spring-spawning herring. ICES J. Mar. Sci. 64, 1302–1312. doi:10.1093/icesjms/fsm116

Misund, O.A., 1993. Avoidance behaviour of herring (Clupea harengus) and mackerel (Scomber scombrus) in purse seine capture situations. Fish. Res. doi:10.1016/0165-7836(93)90051-8

Misund, O.A., 1990. Sonar observations of schooling herring: school dimensions, swimming behaviour, and avoidance of vessel and purse seine. ICES Counc. Explor. sea 189, 135–149.

Nishimori, Y., Iida, K., Furusawa, M., Tang, Y., Tokuyama, K., Nagai, S., Nishiyama, Y., 2009. The development and evaluation of a three-dimensional, echo-integration method for estimating fish-school abundance. ICES J. Mar. Sci. J. du Cons. 66, 1037–1042.

Ona, E., 1999. Methodology for Target Strength Measurements (with special reference to in situ techniques for fish and mikro-nekton). ICES Counc. Explor. sea.

Ona, E., Andersen, L.N., Knudsen, H.P., Berg, S., 2007a. Calibrating multibeam, wideband sonar with reference targets, in: OCEANS 2007 - Europe. IEEE, pp. 1–5. doi:10.1109/OCEANSE.2007.4302473

Ona, E., Dalen, J., Knudsen, H.P., Patel, R., Andersen, L.N., Berg, S., 2006. First data from sea trials with the new MS70 multibeam sonar. J. Acoust. Soc. Am. 120, 3017.

Ona, E., Godo, O.R., Handegard, N.O., Hjellvik, V., Patel, R., Pedersen, G., 2007b. Silent research vessels are not quiet. J. Acoust. Soc. Am. 121, EL145–EL150.

Ona, E., Mazauric, V., Andersen, L.N., 2009. Calibration methods for two scientific multibeam systems. ICES J. Mar. Sci. J. du Cons. 66, 1326–1334. doi:10.1093/icesjms/fsp125

Sherman, C.H., Butler, J.L., 2007. Transducers and arrays for underwater sound, Transducers and Arrays for Underwater Sound. Springer. doi:10.1007/978-0-387-33139-3

Simmonds, J., MacLennan, D., 2005. Fisheries Acoustics, 1st ed, Fish and Fisheries. Chapman & Hall, London.

Simrad, 2007. Operator Manual SX90, Fish finder sonar.

Tang, Y., Iida, K., Mukai, T., Nishimori, Y., 2006. Estimation of fish school volume using omnidirectional multi-beam sonar: scanning modes and algorithms. Jpn. J. Appl. Phys. 45, 4868.

Tang, Y., Nishimori, Y., Furusawa, M., 2009. The average three-dimensional target strength of fish by spheroid model for sonar surveys. ICES J. Mar. Sci. J. du Cons. 66, 1176–1183.

Totland, A., Johansen, G.O., Godø, O.R., Ona, E., Torkelsen, T., 2009. Quantifying and reducing the surface blind zone and the seabed dead zone using new technology. ICES J. Mar. Sci. 66, 1370–1376. doi:10.1093/icesjms/fsp037

Van Trees, H.L., 2002. Optimum Array Processing - Part IV, Detection, Estimation, and Modulation Theory.

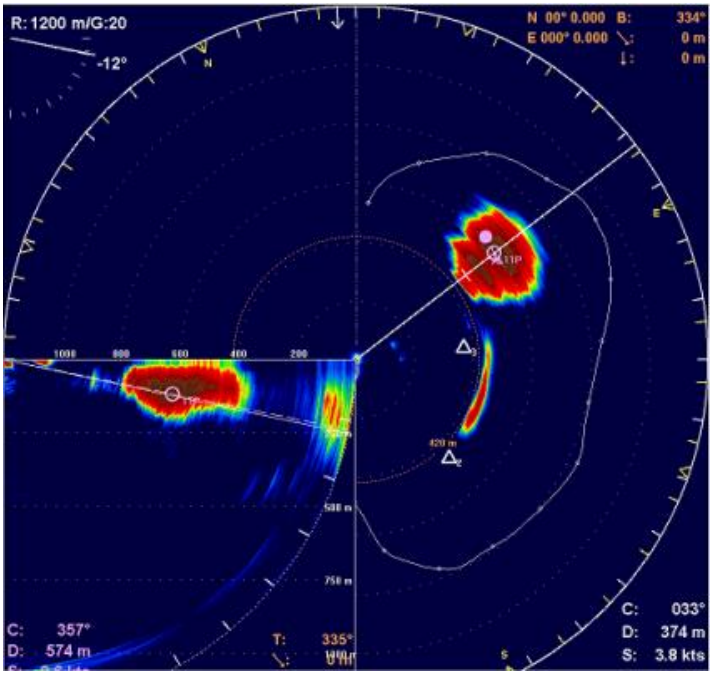

Figure 3: Screen dump from the Simrad SX90 fishery sonar, while the vessel was encircling a large herring school (Norwegian Sea, Nov. 2013). The horizontal view is displayed in the larger window and the vertical view is shown in the lower left window. The herring schools are recognised by the strong red marks on the sonar image.

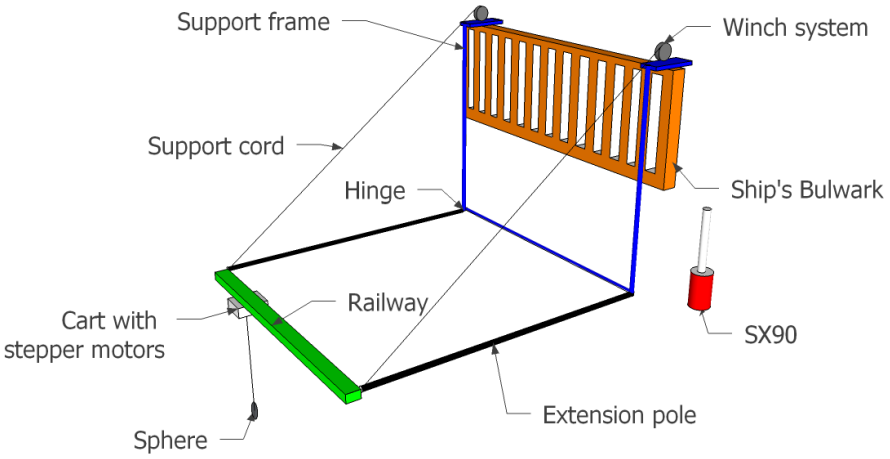

Figure 2: Main components of the precision rig used for positioning the calibration sphere with specified spatial precision, inside one selected acoustic beam. The rig includes a supporting frame (Blue) resting on the ship's hull while its upper ends are securely fastened to the bulwark (Orange). Two extension rods (Black) are attached with hinges to the respective lower corners of the supporting frame. The 5 meter long railway (Green) is attached between the ends of the extension rod. A cart (White) with two stepper motors, one for lateral movement along railway and one for lowering the sphere, is attached to the railway. The railway with extension rods are at the tip connected to winches (Grey), allowing vertical positioning and adjustment of the entire railway.

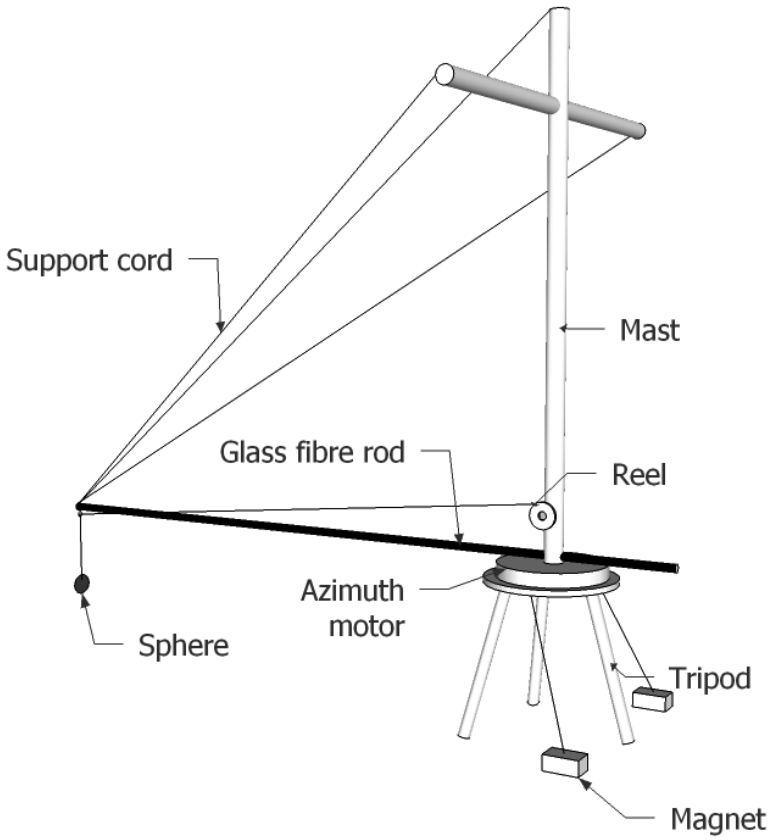

Figure 3: Sketch of the multi-beam rig used to reach multiple beams from one rig location. An azimuthally rotating table is mounted on top of the tripod, moving the sphere in a circle centred on the rotating table. A glass fibre rod attached to the motor and the sphere support ensures a sufficiently long range between the sonar transducer and the calibration target. A motorized reel controls the vertical movement of the sphere. The end of the rod is attached to a mast mounted on top of the rotary table for stability. The tripod is attached to the deck using two industrial magnets to ensure rig stability and to prevent accidents.

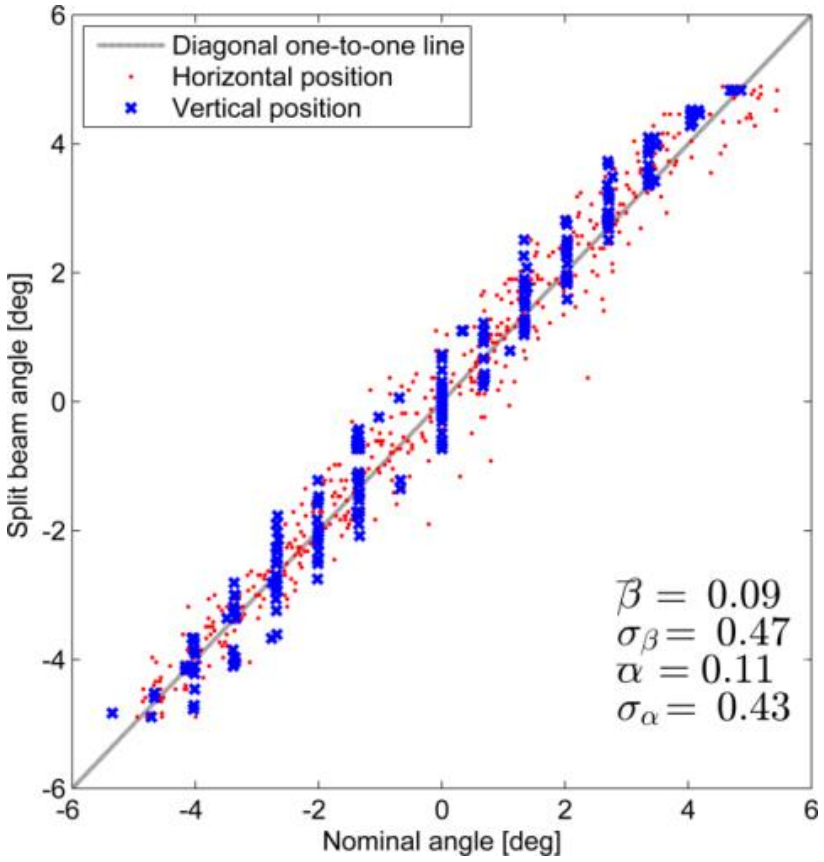

Figure 4: Comparison of the mechanical angles and the measured split-beam angles (horizontal and vertical), for the calibration sphere. The split-beam angles are derived from a horizontally-directed 200 kHz Simrad split-beam echosounder. The nominal directions are computed from the precision-rig data and the acoustic range of the target. The computed mean angles and their standard deviations, for the horizontal ($\boldsymbol{\beta}$) *and vertical* ($\boldsymbol{\alpha}$)*, angles are indicated in the figure.*

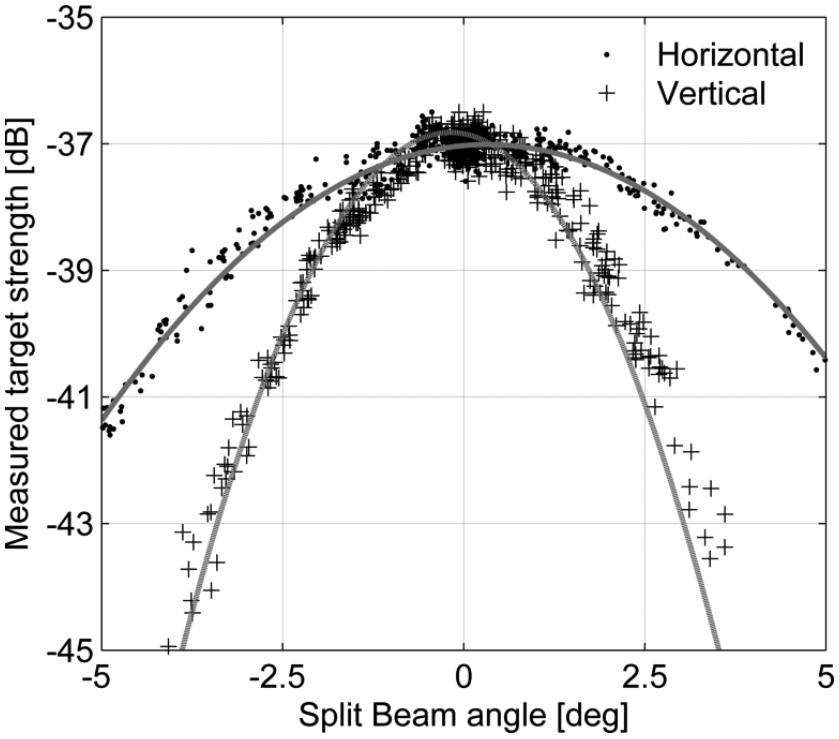

Figure 5: Horizontal (dotted) and vertical (crossed) cross-sections of the two-way directivity pattern of an acoustic beam towards the port side of the SX90 mounted on "F/V Artus", measured in March 2013. Quadratic regression curves are presented for the two cross-sections.

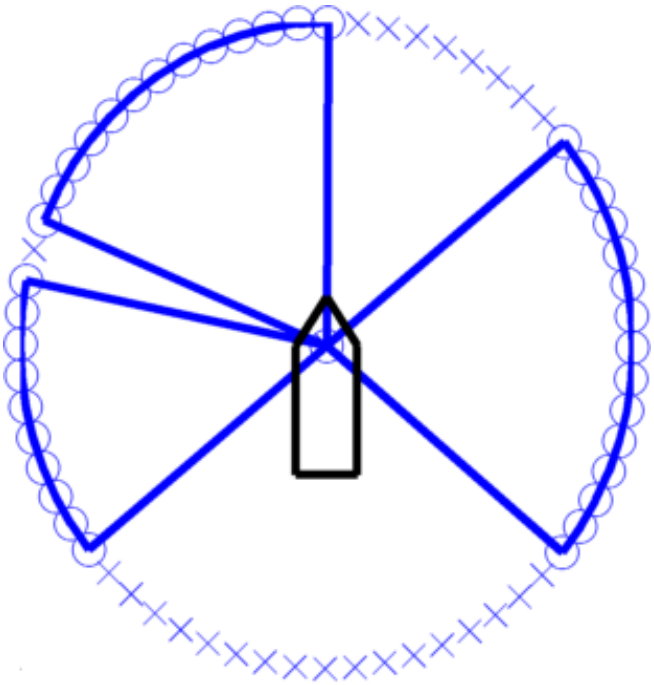

Figure 6: Illustration showing all the calibrated ("O") beams measured on "F/V Artus" using the multi-beam rig. The un-calibrated beams ("X") could not be reached due to working space limitations or anchor-chain interference. Beams pointing towards the stern were not included in the calibrations.

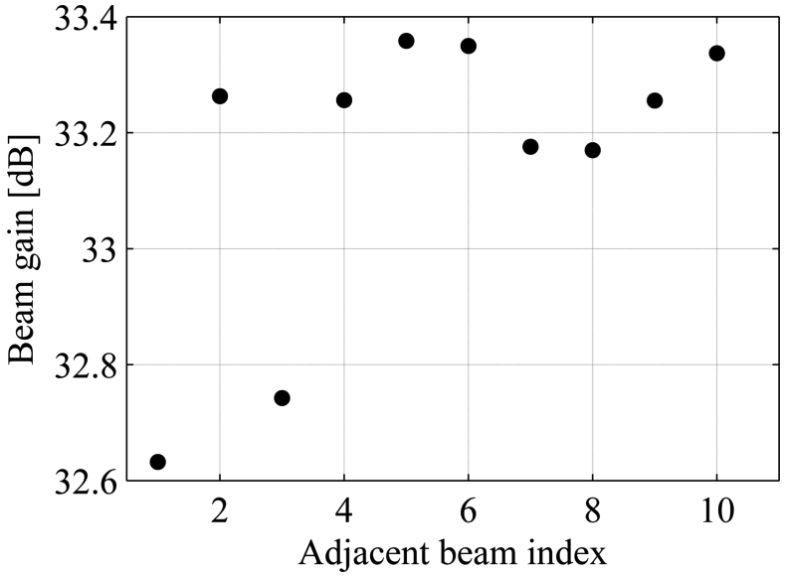

Figure 7: On-axis gain estimates of selected adjacent beams on the SX90 sonar of "R/V G. O. Sars" in November 2013.

Table 1: The total number of beams calibrated on various vessels, along with time and location of the calibration, and the rig used to steer the sphere.

Vessel	**Time/Location**	**Rig Used**	**# of beams**
R/V G.O. Sars	Fall 2012/Bodø	Precision	1
R/V G.O. Sars	Spring 2013/Ålesund	Precision	3
F/V Artus	Spring 2013/Ålesund	Precision	3
F/V Eros	Spring 2013/Bergen	Precision	3
R/V G.O. Sars	Fall 2013/Bodø	Multi-beam	26
F/V Artus	Fall 2013/ Bodø	Multi-beam	38
R/V G.O. Sars	Fall 2014/Bergen	Multi-beam	6
F/V Kings Bay	Fall 2014/ Bergen	Multi-beam	9

C.PAPER 3

III

Status of paper: Manuscript, to be submitted to Journal of acoustic society of America

Status authorship: co-author

Contribution of work;

Authorship: 20%

Data collection and analysis: 30%

Reprinted with the permission of main author, Gavin Macaulay

Title: Practical calibration of ship-mounted fisheries sonars

Authors: Gavin Macaulay, Sindre Vatnehol, Egil Ona

Institute of Marine Research, P.O. Box 1870 Nordnes, N-5817 Bergen, Norway

Abstract

Conventional ship-mounted vertically-oriented echosounders are poor at detecting organisms that are close to the sea surface. In contrast, fisheries sonars can ensonify near-surface waters and are a useful tool to cover the volumes that are unavailable to echosounders. When calibrated, sonars can be used to provide quantitative biomass estimates of pelagic aggregations. However, for sonar systems that have not been designed as scientific and research instruments, the quantification and verification of the stability of the system performance is of heightened importance, and should include how parameters such as the shape and gain of the beams vary with system and operational configurations. We present a practical methodology for absolute calibration of fisheries sonars when mounted on a ship, illustrate the achievable calibration accuracies and precision, and document their stability over time and for a range of operating parameters. This work forms an essential prerequisite to the routine use of such sonars for quantitative echo-integration surveys.

1. Introduction

Downward-looking, narrow-beam echosounders are the most commonly used tool for quantitative acoustic surveys of fish populations, being relatively simple to operate with well-developed analysis procedures for producing fish biomass estimates

(Simmonds and MacLennan, 2005). However, such ship-mounted echosounders are poor at detecting organisms that are close to the sea surface because most installations have the transducers mounted some metres below the surface to avoid the deleterious effects of air bubbles (Dalen and Løvik, 1981). In conjunction with the transducer near-field and ringing there is typically a distance of several metres below the sea surface for which no echoes can be quantitatively measured. Also, at typical survey speeds of about 5 m/s, the probability of detecting small aggregations that are close to the surface is much lower than at longer ranges, due to the small width of the acoustic beam.

Modern fisheries sonars are typically used to search for pelagic fish schools, where they aid in finding and assessing the fish as well as monitoring the catch process (Ben-Yami, 1994). Such sonars form acoustic beams from an array of transducer elements in a range of directions (Sherman and Butler, 2007). The most common arrangement is to form many narrow beams with oval cross-section that are emitted radially in all directions from the transducer, with a configurable tilt angle relative to horizontal. In effect, a surface analogous to a downwards-pointing cone with the apex at the transducer is formed. This is commonly called the horizontal mode. Additionally, some fisheries sonars can also form a vertical fans of beams with an arbitrary azimuth direction, commonly called the vertical mode.

While fisheries sonars offer improved sampling of near-surface waters and have the potential to provide quantitative estimates of pelagic biomass (Brehmer et al., 2006), they introduce other complexities. Ensonifying organisms at variable side-

aspect causes increased variation in acoustic reflectivity due to the more variable fish orientation relative to the acoustic beam (Cutter and Demer, 2007; Tang *et al.*, 2009; Holmin *et al.*, 2012), a more complicated echo-integration method (Nishimori *et al.*, 2009), and acoustic ray bending due to stratified water masses (Lichte, 1919).

Fisheries sonars provide information on schools metrics (Misund, 1990), speed (Peraltilla and Bertrand, 2014) and behaviour (e.g., Misund et al., 1996), but in most instances the amplitude information from each sonar beam has not been used in a quantitative manner that is analogous to the echo-integration method commonly used with narrow-beam echosounders. Lack of access to some form of raw signal data has restricted most work to analysis of the sonar's presentation display (Brehmer and Gerlotto, 2001; Brehmer *et al.*, 2006; Trygonis *et al.*, 2009), with associated compromises related to dynamic range, linearity, and calibration accuracy.

To make quantitative and effective use of amplitude data from sonar data requires that there be a known, consistent, and stable relationship between acoustic echo amplitude and recorded amplitude over the range of sonar operation modes that are used in a study or survey – that is, the sonar should be capable of being calibrated. In particular, for sonar systems that have not been designed as scientific and research instruments, the quantification and verification of the stability of the system performance is of heightened importance, and should include knowledge on how parameters such as the shape and gain of the beams vary with system and operational configurations. Most fisheries sonars provide the ability to set the acoustic frequency, pulse length, pulse type, beam width, and declination angle. For the sonars considered

in this paper the total number of unique combinations of these settings exceeds 98 000. When combined with the 64 beams in these sonars, there are more than six million potential calibration values. It is overwhelmingly impractical to calibrate all of these. It is instead essential to understand the independent effect of each setting, so that relative adjustments can be applied to a small number of representative beam calibrations. Variation in beam characteristics and the associated calibration can be predicted via theoretical considerations of the underlying sonar transmit and receive operations (Cochrane *et al.*, 2003), but the actual performance of individual sonars can vary significantly from the theoretical (Cochrane *et al.*, 2003).

Calibration of echosounder systems can be achieved via a number of methods, such as reciprocity or a calibrated hydrophone (Foote et al., 1987), but the most practical and commonly used method is to use metallic spheres of known acoustic reflectivity (Foote and MacLennan, 1984). Sphere-based calibration has been demonstrated for multi-beam sonars, which produce a linear fan of beams, in controlled environments such as tanks or enclosed environments (Cochrane *et al.*, 2003; Melvin *et al.*, 2003; Foote *et al.*, 2005; Lanzoni and Weber, 2011; Perrot *et al.*, 2014) and for fisheries sonars, but without full quantification of the beam parameters (Bernasconi, 2012; Geoffroy *et al.*, 2015). The routine calibration of fishery sonars in uncontrolled environments is however now practical via the availability of a calibration apparatus for ship-mounted sonars (Vatnehol *et al.*, accepted), which can be used to measure system gain and the beam parameters required for echo-integration. Coupled with an implementation of the split-beam method to locate the sphere within the beam

(Vatnehol, submitted), this removes the need for more complicated sphere positioning systems. Together, these developments facilitate the complete calibration of ship-mounted fisheries sonars in environments such as sheltered bays and fiords, rather than in tanks or enclosed environments. For the sonar calibrations presented here, the third and necessary development was the ability to record and post-process both beam-formed and transducer element sample data.

This paper presents a practical methodology for absolute calibration of ship-mounted fisheries sonars. This methodology is applied to the Simrad SX90 and SU90 fisheries sonars, illustrates the achievable calibration accuracies and precision, and quantifies their stability over time and for a range of operating parameters. This work forms an essential prerequisite to the routine use of such sonars for quantitative echo-integration surveys.

3 Methods

3.1 Theory

The Simrad SX90 fisheries sonar operates at a user-configurable frequency between 20 and 30 kHz inclusive. In horizontal mode utilises its 256 element vertically-oriented cylindrical transducer to form 64 receive beams with selectable declination relative to horizontal. The Simrad SU90 fisheries is functionally the same as the SX90 except that the cylindrical transducer array is taller, comprising 384 elements and produces vertically narrower beams than the SX90 sonar. Both systems can transmit at a single frequency (labelled here as CW) or with a hyperbolic frequency modulated (FM) signal covering a 500 Hz bandwidth, at various pulse

lengths. The vertical beamwidth can also be set to one of three options (narrow, normal, or wide). Echoes are processed with a matched filter derived from the transmitted signal. The sonar records beamformed data in the form of complex demodulated, pulse-compressed estimates of the power received by each beam at a decimated sample rate determined by the sonar configuration (typically 4 kHz). For the horizontal beam mode, this is converted into backscattered target strength (TS) via an equation provided by the manufacturer:

$$TS = 10\log_{10}(P_r) + 40\log_{10}(r) + 2\alpha r - 10\log_{10}\left(\frac{P_t\lambda^2}{16\pi^2}\right) - G(\theta,\phi) - 40\log_{10}(\cos\gamma), \quad (1)$$

where P_r is the received power (W), r the range between the transducer and target (m), α the absorption coefficient of sound in water (dB/m), P_t the transmit power (W), λ the acoustic wavelength (m), $G(\theta,\phi)$ the transducer gain in the direction of the target (dB), and γ the beam tilt angle (degrees below horizontal). The volume backscatter strength (S_v) is derived from a similar equation:

$$S_v = 10\log_{10}(P_r) + 20\log_{10}(r) + 2\alpha r - 10\log_{10}\left(\frac{P_t\lambda^2 c\tau}{32\pi^2}\right) - 2G_0 - 40\log_{10}(\cos\gamma) - 2S_{a,corr} - 10\log_{10}(\psi), \quad (2)$$

where c is the acoustic sound speed (m/s), τ the pulse duration (s), $S_{a,corr}$ the Sa correction (dB) which accounts for the energy difference between the ideal square

transmit pulse and the actual transmitted pulse, G_0 the on-axis transducer gain (dB), and ψ the equivalent beam angle (sr).

Two methods of estimating the location of the calibration sphere in the acoustic beam were used. The 'precision' calibration rig gave the precise three-dimensional location of the sphere relative to a reference point, while the 'multi-beam' calibration rig gave precise estimates only in the vertical direction (Vatnehol *et al.*, accepted). To facilitate the calibration process and to enable the use of the simpler and more flexible 'multi-beam' calibration rig, the arrival angle of calibration echoes within each beam was estimated by the split-beam method (Burdic, 1991; Demer et al., 1999) applied to the sample data from the transducer's individual elements. The use of the split-beam technique to estimate the angle of arrival of echoes requires an estimate of the 'angle factor', the conversion between the electrical phase difference of the arriving echoes at the transducer parts and the true arrival angle (Ehrenberg, 1979). This was estimated by experiments carried out using the 'precision' calibration rig (Vatnehol *et al.*, accepted).

Assuming that most of the transmitted energy from each beam is in the main lobe, the equivalent beam angle (ψ) was estimated from the integral of the beam pattern function fitted to the rig-derived sphere echo data:

$$\psi = \int_{4\pi} b, \qquad (3)$$

where b is the two-way beam pattern obtained from the sphere echo magnitude measurements.

The echo range in the sonar files is not given directly, but must be derived from estimates sound speed in water, the time since sampling began, and any processing delays. Not all of the processing delays are necessarily compensated for by the sonar processing and the conversion between sample and range was assumed to be:

$$r = \frac{c \cdot dt}{2} i - r_o, \qquad (4)$$

where dt is the time interval between samples (s), i the sample number (from zero to one less than the number of samples) and r_o an empirically derived offset that is independent of the sonar operating parameters. This offset is caused by an approximate 4 ms delay in the signal processing operations of the sonar system that is not compensated for in the recorded echo amplitude data (pers. comm., O. B. Gammelsæter, Kongsberg Maritime). To verify that estimate, the true distance between the sonar transducer and the sphere was measured. The locations of the various pivot points of the 'multi-beam' calibration rig boom (Vatnehol *et al.*, accepted) were measured relative to a common reference point on the vessel foredeck. The position of the pivot point relative to the sonar transducer was then calculated using dimensioned ship drawings. Given the azimuth angle of a particular sonar beam, the length of the boom, and the beam tilt angle, the distance between the sonar transducer and the sphere was calculated. The rig was adjusted so that the boom was horizontal and it was assumed that the sphere hung directly below the boom end and

that any motion of the sphere due to vessel or water movements was small. The true sphere range was estimated for multiple sphere ranges, sonar beams, and three pivot points. The mean difference between the true and sonar ranges was used as an estimate of r_0 in equation (4).

3.2 Calibration procedure

Calibrations were carried out using SX90 sonars on three ships (RV G.O. Sars, FV Artus, and FV Brennholm) and using SU90 sonars on two ships (FV Kings Bay and FV Eros) when moored or anchored in fiords on Norway's west coast. The water depth below the vessels was always greater than 30 m.

The sonar calibration rig (Vatnehol *et al.*, accepted) was affixed to the ship deck in the vicinity of the sonar transducer and the rig's boom extended out over the side of the ship. A sphere was suspended from the end of the boom and lowered until it was visible in the sonar display. The position of the sphere in the beam was estimated either by 'precision' calibration rig, or by split-beam processing of the raw element sample data and the amplitude of the sphere echo estimated from the beam-formed data via equation (1).

Five aspects of the sonar performance were then measured from five ships (Table 2):

- *On-axis gain* was estimated for multiple beams by centring the sphere in the selected beam and recording backscatter amplitude from at least 100 pings. The sphere was then moved to an adjacent beam and the procedure repeated. This

process continued for as many beams as possible, with changes to the rig's location as required. This was performed on RV G.O. Sars and FV Artus.

- The *beam shape* was estimated for selected beams by moving the sphere horizontally until it had left the selected beam, whereupon it was moved in the opposite direction until it had left the same beam from the other side. The sphere was then returned to the beam centre. The process was then repeated vertically. Several beams were mapped while systematically varying the acoustic frequency, formed beam width, and beam tilt angle. This was performed on FV Kings Bay.
- The *effect of pulse parameters* on transducer gain was measured by keeping the sphere stationary in one beam while the frequency, pulse length and pulse type were systematically varied. This was performed on FV Brennholm.
- The *range from the transducer* to the sphere was physically measured with the sphere at nine different distances. The range calibration was performed on FV Eros.
- The *medium-term variability* of gain estimates was estimated by placing the sphere in the centre of one beam and echo backscatter amplitude over a period of approximately 25 minutes. This was performed on RV G.O. Sars.

At least one conductivity-temperature-depth (CTD) cast was carried out during each calibration and used to estimate acoustic absorption (Francois and Garrison, 1982), sound speed (Chen and Millero, 1977), and density (Fofonoff and Millard,

1983). No CTD was taken for the FV Brennholm calibration and nominal values were instead used (a temperature of 10°C and salinity of 35 PSU).

Two tungsten carbide spheres (with 6% cobalt binder) were used for the calibrations. The diameter was 75 mm for the FV Brennholm calibration and 64 mm for the other calibrations. These spheres were chosen for their relatively strong, smooth, and slowly varying reflectivity in the sonar's operating range (20 to 30 kHz). They are also heavy (3.3 and 2 kg) and are less affected by water movements than the more commonly used smaller and lighter spheres. The expected backscatter strength was estimated using the theory for scattering by an elastic sphere (Hickling, 1962; MacLennan, 1981) in the environmental conditions experienced during the calibrations.

The sonar calibrations on RV G.O. Sars, FV Artus, FV Kings Bay, and FV Eros used a 4 kW CW transmit pulse of 2 ms duration. The acoustic frequency was varied as required. The calibration on FV Brennholm used pulse durations of 1, 2, and 6 ms with a CW signal and pulse duration of 2, 4, and 6 ms with an FM signal. All six settings were used at operating frequencies of 20, 23, 26, and 28 kHz.

The distance between the sonar transducer and calibration sphere was always greater than twice the estimated near-field range of the sonar beams. The near-field range was conservatively estimated using the equation for the near-field range of a rectangular planar transducer (Medwin and Clay, 1998):

$$r_{nf} = \frac{A}{\lambda}, \qquad (5)$$

where r_{nf} is the near field range (m), A the projected area of the sonar transducer (height multiplied by diameter, m^2), and λ the acoustic wavelength (m).

3.3 Analysis

The on-axis transducer gain (G_0) for each beam was estimated using custom-written software that read the recorded sonar data files and produced a sonar image where a beam of interest could be selected and range and time period limits applied. The maximum amplitude of the sphere echo was then estimated for the selected beam, range, and time periods. The maximum echo amplitude was obtained from the peak of a quadratic interpolation to the three sample values that defined the peak (that is, the peak and one sample either side). The transducer gain was then estimated using equation (1).

The beam mapping data were processed in a similar way, but with the addition of the sphere position obtained from the split-beam or the relative three-dimensional sphere positions (Vatnehol, submitted). An empirical beam pattern was defined as:

$$b = 6.026(\alpha^2 + \beta^2 - 0.18\alpha^2\beta^2),$$

$$\alpha = \frac{2(\theta + \theta_o)}{\theta_{BW}}, \qquad (6)$$

$$\beta = \frac{2(\varphi + \varphi_o)}{\varphi_{BW}},$$

where b is the two-way beam pattern, θ the vertical beam coordinate (°), θ_o the vertical beam offset (°), and θ_{BW} the vertical half-power beamwidth (°). Similar variables for the horizontal beam are given by the φ variables. Equation (6) was fitted to the sphere TS and position data by non-linear least squares minimisation and the vertical and horizontal beamwidths obtained.

4. Results

The mean difference between the sonar estimated sphere range and the measured range was 2.99 m (Figure 2), closely agreeing with the manufacturer's 4 ms estimate of uncorrected processing delay (equivalent to 2.9898 m using the prevailing 1494.8 m/s sound speed during the measurements).

The estimated on-axis gain for individual beams in an individual sonar had a typical variation of ±0.5 dB, with some exceeding ±1.0 dB (Figure 3a,c). Overall, the mean gain variation was ±0.7 dB for RV G.O. Sars and ±0.8 dB for FV Artus (Figure 3b,d). The variability in gain for a single beam over an extended period was approximately ±1 dB (Figure 4).

The gain increased with longer pulse durations and higher frequencies with an asymptotic form (Figure 5). The relative change in gain with pulse duration was independent of change in frequency, and vice versa. The changes in gain were not affected by the pulse type (CW or FM). These systematic changes in beam gain were fitted, using least-squares minimisation, to yield a correction function:

$$G = \frac{3690}{f} - \frac{53900}{f^2} - \frac{6.49}{\tau} - 43.2, \qquad (7)$$

where G is the transducer gain relative to that obtained for a transmitted pulse of length 1 ms and frequency 20 kHz, f is frequency (20-30 kHz) and τ pulse length (1-8 ms).

The empirical beam shape was a good representation of the measured beam shape (Figure 6) and the resulting estimates of beam width have a high confidence, albeit with some consistent variations close to on-axis that were vessel dependent.

The trends in beamwidth with changing frequency, requested beamwidth, and beam tilt were as expected (beamwidth decreases as frequency increases, beamwidth increases with increasing requested beamwidth, and constant beamwidth with beam tilt, Figure 7). The trends in transducer gain were also as expected (gain increases as frequency increases, gain decreases as beamwidth increases, and gain remains constant with beam tilt, Figure 7).

5. Discussion

The use of fisheries sonars in a quantitative acoustic survey requires adequate calibrations over the range of sonar settings that might be used during the survey, or an understanding of the effect of the sonar settings on the calibration. Our experience in

such surveys is that there are five main settings that are varied (Table 3), but with sufficient planning these can be reduced to just one, the horizontal beam tilt angle. However, for echo-integration surveys there is also the requirement to maintain a constant sampling volume with respect to the expected fish depth distribution (this also has the benefit of constraining the fish ensonification angles and reducing the need for three-dimensional fish target strength estimates). Under this constraint the tilt angle should remain constant, thereby requiring the fixing of all sonar settings and ideally reducing the calibration exercise to using just the survey setting. However, it is not always practical to conduct a calibration at the same settings as would be used during a survey. For example, the best beam tilt angle for the calibration is determined by the local bathymetry, proximity of underwater structures, and the transducer to sphere range. This may not coincide with the desired survey tilt angle. Additionally, the transmitted pulse length used by the SX90 and SU90 sonars is determined by the maximum display range (longer display ranges automatically give longer transmit pulse lengths). Furthermore, a fast ping rate is desirable during calibration as it reduces the calibration duration and hence the operating range is best kept short, but for surveys the optimal display range is typically larger. Hence, even when using just one sonar setup for a survey it is still necessary to quantify how the sonar performance varies with some of the sonar settings. This is in contrast to conventional single-beam scientific echosounders, where it is feasible and normal to calibrate the system using the same settings as used during the survey.

An echosounder or sonar calibration has two purposes: to provide the conversion factor between the system response and physically realisable measurements, and to ensure that the system is working correctly. Ideally, one would calibrate all beams of a sonar to achieve both of these purposes, but this is a time-consuming exercise and is difficult for the aft beams. However, for the SX90 sonar, a single beam is formed from a 12 by 8 array of transducer elements (Blomberg *et al.*, 2012), being 37.5% of elements in the transducer. Calibration of three beams spaced 90 degrees apart from each other will utilise 87.5% of the elements and serve to check the correct functioning of that percentage of the transducer and transceiver elements and processing channels. Similarly, since adjacent sonar beams in the SX90 are formed from an almost identical set of transducer elements we hypothesise that the calibrated gain of an individual beam is strongly correlated with the gains of its' adjacent beams. This implies that it is not necessary to calibrate adjacent beams because they will have substantially the same performance. However, the results obtained from RV G.O. Sars and FV Artus show a beam-to-beam gain variability of up to 2 dB (Figure 3), which we attribute mainly to variability in the calibration process and environmental variability, and not beam performance. Hence, to ensure a more robust and representative estimate of the gain of adjacent beams we recommend measuring the gain from three adjacent beams, and then repeating this for several well-separated directions with the aim of exercising completely different sets of transducer elements.

The SX90 and SU90 sonars could be considered to be calibrated when all of the parameters in equations (1), (2), and (4) have been estimated for the set of operating modes that will be used during quantitative surveys. Variations in transducer gain were observed due to changes in frequency and pulse length, despite these terms being in equations (1) and (4). This indicates that these equations are not fully compensating for the effect of frequency and pulse length and emphasises the need to independently verify the calibration and effect of system parameters. This has been done for the SX90 and SU90 sonars and permits the calculation of a calibration for any frequency and pulse length combination via equation (7).

The range provided by the sonar is not an accurate estimate of the true range, being some 3 m in error. Correcting for range is particularly important when calibrating at short ranges as a large error in the time-varied-gain can occur, leading to an incorrect gain estimate. In addition, since the calibration rigs that we used do not maintain a constant range between transducer and calibration sphere, the sphere TS can vary while moving the sphere around in the beam (in addition to changes due to location in the beam). This would lead to a greater variability in intra-beam gain estimates as well as a potential bias in gain.

The work presented here does not account for any changes in beam characteristics (shape and gain) due to the automatic beam tilt stabilisation performed by the sonar. The beam forming should have minimal effect on the beam characteristics and equations (1) and (4) include a term that compensates for changes in gain due to beam tilt, but the efficacy of this has not been confirmed. This could be

tested by conducting a beam calibration while the attitude of the ship (or more simply, the motion-reference unit input to the sonar) was systematically changed.

The estimated gain had a rather high variation, where the magnitude of the variability is seen to be different between vessel, between beams, and between times of calibration. Compared with the ±0.1 dB variability that is routinely achieved in the calibration of conventional echosounders (Knudsen, 2009), the sonar performs worse. The typical sonar gain variation within a single beam was around ±0.5 dB, however when a longer time interval was used, or several adjacent beams were measured, the variability was higher. A longer-term calibration from a single sonar beam (Figure 4) indicates that this variability is dominated by either changing propagation conditions or variation in sonar performance. We postulate two reasons for this – the sonar was not designed for stable quantitative scientific use and may not have high measurement stability, or variation in the propagation conditions between the sonar and the sphere may cause ray bending and associated changes in the acoustic wave incident upon the sphere. In addition, there is the potential for acoustic interference caused by multipath propagation, either via the sea surface, the seabed, or the ship's hull. It is noted that all calibrations were conducted within sheltered fiords, where fresh water runoff and calm winds can result in significant stratification with the potential for short-term variations (Skarthhamar and Svendsen, 2010). All sound speed profiles taken during the calibrations showed some degree of stratification between the sonar transducer and sphere depths and we postulate that stratification, and short-term variation of, is the

dominant cause of the observed calibration variability. Consequently the use of calibration locations with well-mixed near-surface waters is recommended.

Physical objects close to the vessel prevented calibration of some beams due to echo interference, while the ship superstructure and hull prevented us from placing the sphere into some beams, particularly to the aft of the sonar transducer. For example, the anchor chain caused a strong interfering echo in up to four beams at a similar range to the calibration sphere. When moored, wharf piles caused a similar problem.

This paper has focussed on the horizontal mode beams. Calibration of the vertical mode beams would proceed in a similar manner and similar conclusions would be expected.

For the calibration and characterisation of fisheries sonar performance we recommend the following activities be part of the calibration activities:

1. Verify the range accuracy and apply a correction if necessary, particularly for the short ranges used during sphere calibrations,
2. Measure the on-axis gain in three adjacent beams. Repeat this for three well-separated directions,
3. Calibrate with sonar settings that are as close as possible to the survey settings, or derive relationships to compensate for differences between calibration and survey settings,
4. Measure the vertical and horizontal beamwidth to enable estimation of the equivalent beam angle.

This work addresses the fundamental requirement for quantitative echo-integration of marine organisms using fisheries sonars – calibration. Confidence in the quantitative output from an fisheries sonar then provides a firm basis for addressing the other challenges associated with non-vertical ensonification of marine organisms (such as the increased variability with fish orientation (Cutter and Demer, 2007), acoustic extinction (Foote *et al.*, 1992; Zhao and Ona, 2003) and multiple scattering between single targets (Stanton, 1983)).

6. Acknowledgements

The authors acknowledge the valuable contributions of Atle Totland, Héctor Peña, and Ole Bernt Gammelsæter in the development of the calibration procedures and enhancing our understanding of the operational characteristics of the sonars. This work was funded by the CRISP Centre for Research-based Innovation.

7. References

Ben-Yami, M. 1994. Purse seining manual, Fishing News Books, Oxford. 416 pp.

Bernasconi, M. 2012. The use of active sonar to study cetaceans. Ph.D. thesis, University of St Andrews.

Blomberg, A. E. A., Austeng, A., and Hansen, R. E. 2012. Adaptive beamforming applied to a cylindrical sonar array using an interpolated array transformation. IEEE Journal of Oceanic Engineering, 37: 25–34.

Brehmer, P., and Gerlotto, F. 2001. A simple standardisation of omnidirectional sonar in fisheries research through field calibration and sampling data. Hydroacoustics, 4: 27–30.

Brehmer, P., Lafont, T., Georgakarakos, S., Josse, E., Gerlotto, F., and Collet, C. 2006. Omnidirectional multibeam sonar monitoring: applications in fisheries science. Fish and Fisheries, 7: 165–179.

Burdic, W. S. 1991. Underwater acoustic system analysis, Prentice Hall 488 pp.

Chen, C.-T., and Millero, F. J. 1977. Speed of sound in seawater at high pressures. Journal of the Acoustical Society of America, 62: 1129–1135.

Cochrane, N. A., Li, Y., and Melvin, G. D. 2003. Quantification of a multibeam sonar for fisheries assessment applications. Journal of the Acoustical Society of America, 114: 745–758.

Cutter, G. R., and Demer, D. A. 2007. Accounting for scattering directivity and fish behaviour in multibeam-echosounder surveys. ICES Journal of Marine Science, 64: 1664–1674.

Dalen, J., and Løvik, A. 1981. The influence of wind–induced bubbles on echo integration surveys. Journal of the Acoustical Society of America, 69: 1653–1659.

Demer, D. A., Soule, M. A., and Hewitt, R. P. 1999. A multiple–frequency method for potentially improving the accuracy and precision of *in situ* target strength measurements. Journal of the Acoustical Society of America, 105: 2359–2376.

Ehrenberg, J. E. 1979. A comparative analysis of *in situ* methods for directly measuring the acoustic target strength of individual fish. IEEE Journal of Oceanic Engineering, OE–4: 141–152.

Fofonoff, P., and Millard, R. 1983. Algorithms for computation of fundamental properties of seawater. UNESCO Technical papers in marine science, 44: 53.

Foote, K. G., Chu, D., Hammar, T. R., Baldwin, K. C., Mayer, L. A., and Hufnagle Jr, L. C. 2005. Protocols for calibrating multibeam sonar. Journal of the Acoustical Society of America, 117: 2013–2027.

Foote, K. G., Knudsen, H. P., Vestnes, G., Maclennan, D. N., and Simmonds, E. J. 1987. Calibration of acoustic instruments for fish density estimation: a practical guide. International Council for the Exploration of the Sea: 69.

Foote, K. G., and MacLennan, D. N. 1984. Comparison of copper and tungsten carbide calibration spheres. Journal of the Acoustical Society of America, 75: 612–616.

Foote, K. G., Ona, E., and Toresen, R. 1992. Determining the extinction cross section of aggregating fish. Journal of the Acoustical Society of America, 91: 1983–1989.

Francois, R. E., and Garrison, G. R. 1982. Sound absorption based on ocean measurements. Part II: Boric acid contribution and equation for total absorption. Journal of the Acoustical Society of America, 72: 1879–1890.

Geoffroy, M., Rousseau, S., Knudsen, F. R., and Fortier, L. 2015. Target strengths and echotraces of whales and seals in the Canadian Beaufort Sea. ICES Journal of Marine Science: fsv182.

Hickling, R. 1962. Analysis of echoes from a solid elastic sphere in water. Journal of the Acoustical Society of America, 34: 1582–1592.

Holmin, A. J., Handegard, N. O., Korneliussen, R. J., and Tjostheim, D. 2012. Simulations of multi-beam sonar echos from schooling individual fish in a quiet environment. Journal of the Acoustical Society of America, 132: 3720–3734.

Knudsen, H. P. 2009. Long-term evaluation of scientific-echosounder performance. ICES Journal of Marine Science, 66: 1335–1340.

Lanzoni, J. C., and Weber, T. C. 2011. A method for field calibration of a multibeam echo sounder. - In: OCEANS 2011. pp. 1–7.

Lichte, H. 1919. Über den Einfluß horizontaler Temperaturschichtung des Seewassers auf die Reichweite von Unterwasserschallsignalen (On the influence of horizontal temperature layers in sea water on the range of underwater sound signals). Physikalische Zeitschrift, 17: 385–389.

MacLennan, D. N. 1981. The Theory of Solid Spheres as Sonar Calibration Targets. Scottish Fisheries Research Report Number 22.

Medwin, H., and Clay, C. S. 1998. Fundamentals of Acoustical Oceanography, Academic Press, Boston. 712 pp.

Melvin, G., Cochrane, N. A., and Li, Y. 2003. Extraction and comparison of acoustic backscatter from a calibrated multi- and single-beam sonar. ICES Journal of Marine Science, 60: 669–677.

Misund, O. A. 1990. Sonar observations of schooling herring: school dimensions, swimming behaviour, and avoidance of vessel and purse seine. Rapp. P.-v Réun. Cons. int. Explor. Mer., 189: 135–146.

Misund, O. A., Øvredal, J. T., and Hafsteinsson, M. T. 1996. Reactions of herring schools to the sound field of a survey vessel. Aquatic Living Resources, 9: 5–11.

Nishimori, Y., Iida, K., Furusawa, M., Tang, Y., Tokuyama, K., Nagai, S., and Nishiyama, Y. 2009. The development and evaluation of a three-dimensional, echo-integration method for estimating fish-school abundance. ICES Journal of Marine Science, 66: 1037–1042.

Peraltilla, S., and Bertrand, S. 2014. In situ measurements of the speed of Peruvian anchovy schools. Fisheries Research, 149: 92–94.

Perrot, Y., Brehmer, P., Roudaut, G., Gerstoft, P., and Josse, Erwan 2014. Efficient multibeam sonar calibration and performance evaluation. International Journal of Engineering Science and Innovative Technology, 3: 808–820.

Sherman, C. H., and Butler, J. L. 2007. Transducers and arrays for underwater sound, Springer 612 pp.

Simmonds, J., and MacLennan, D. 2005. Fisheries Acoustics. Theory and Practice, Blackwell Science, Oxford. 437 pp.

Skarthhamar, J., and Svendsen, H. 2010. Short-term hydrographic variability in a stratified Arctic fjord. Geological Society, London, Special Publications, 344: 51–60.

Stanton, T. K. 1983. Multiple scattering with applications to fish–echo processing. Journal of the Acoustical Society of America, 73: 1164–1169.

Tang, Y., Nishimori, Y., and Furusawa, M. 2009. The average three-dimensional target strength of fish by spheroid model for sonar surveys. ICES Journal of Marine Science, 66: 1176–1183.

Trygonis, V., Georgakarakos, S., and Simmonds, E. J. 2009. An operational system for automatic school identification on multibeam sonar echoes. ICES Journal of Marine Science, 66: 935–949.

Vatnehol, S. submitted. Evaluation of target position algorithms for multibeam fisheries sonars. Journal of the Acoustical Society of America.

Vatnehol, S., Totland, A., and Ona, E. accepted. Two mechanical rigs for field calibration of multi-beam fishery sonars. Methods in Oceanography.

Zhao, X., and Ona, E. 2003. Estimation and compensation models for the shadowing effect in dense fish aggregations. ICES Journal of Marine Science, 60: 155–163.

Table 2. The vessels and sonars used for the various calibration objectives.

Calibration objective	Vessel	Date	Sonar
On-axis gain for multiple beams	RV G.O. Sars FV Artus	November 2013	SX90
Beamwidth	FV Artus	March 2013	SX90
Effect of frequency, requested beamwidth and tilt on gain and beamwidth	FV Eros	October 2015	SU90
Effect of frequency and pulse length on gain	FV Brennholm	October 2012	SX90
Range calibration	FV Kings Bay	October 2014	SU90
Medium-term variation in gain	RV G.O. Sars	October 2015	SU90

Table 3. The effect of commonly varied SX90 and SU90 sonar settings on performance.

Sonar setting	Affects
Frequency	Beam shape (G, ψ)
Beamwidth	Beam shape (G, ψ)
Beam tilt	Beam shape (G, ψ)
Display range	Pulse length (G)
Pulse type	Pulse length (G)

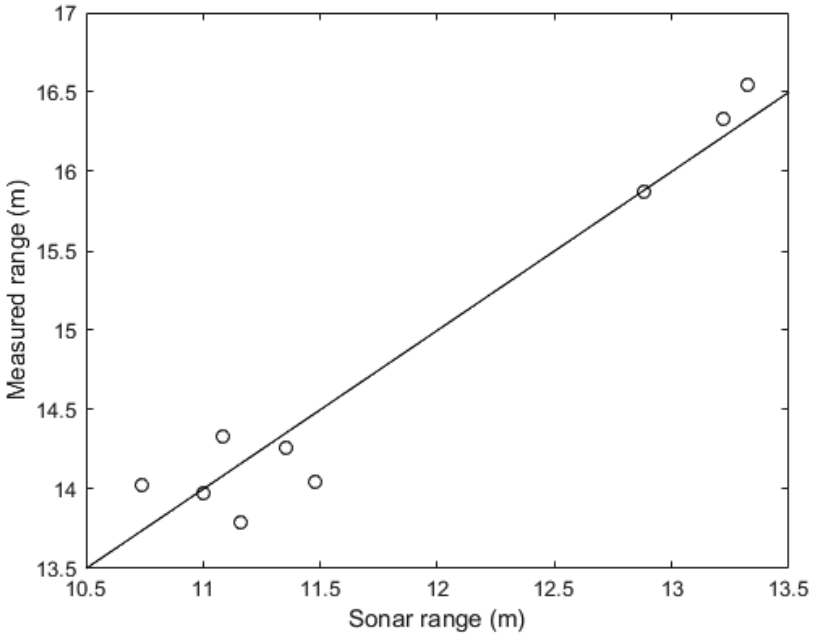

Figure 2. Comparison of sphere range estimated by the sonar and physically measured sphere range. The solid line is the sonar range correction model fitted to these data. The mean difference in range estimates is 2.99 m.

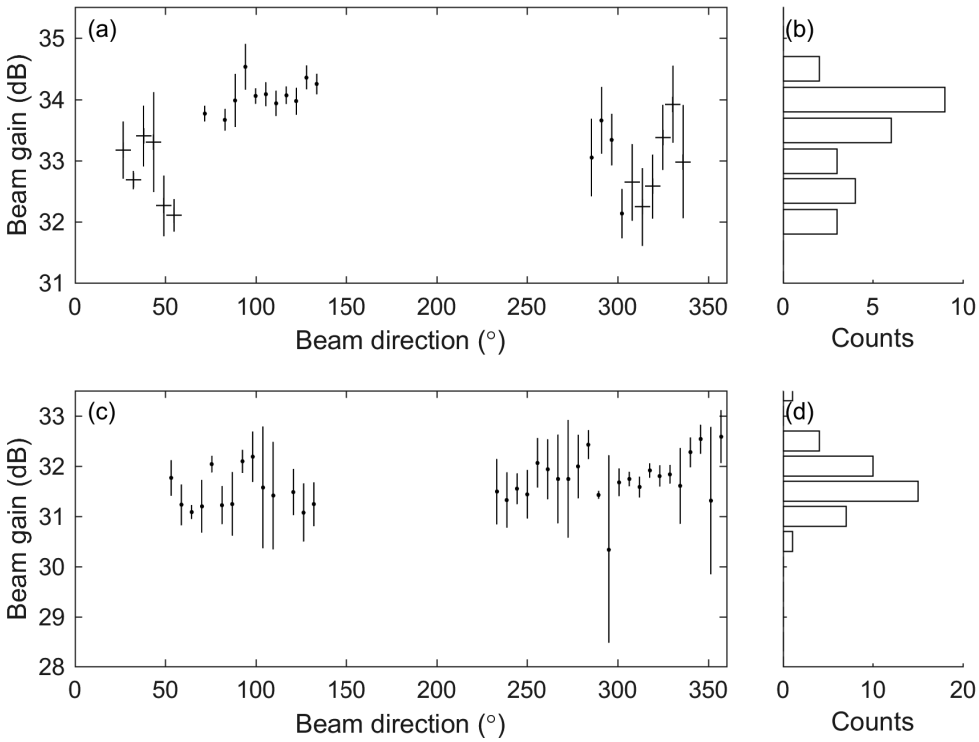

Figure 3. On-axis gain estimates and distribution for the November 2013 calibrations of selected beams on the SX90 sonars of G.O. Sars (a, b) and Artus (c, d). The G.O. Sars estimates are for a beam tilt of –10° (·) and –25° (+), a transmit frequency of 26 kHz, using a CW pulse 2 ms in duration. The Artus estimates are for a beam tilt of –3°, transmit frequency of 30 kHz using a CW pulse 2 ms in duration. The vertical lines show the root-mean-square (RMS) of the gain estimates about the mean (±RMS). A beam direction of 0° indicates the bow increasing clockwise.

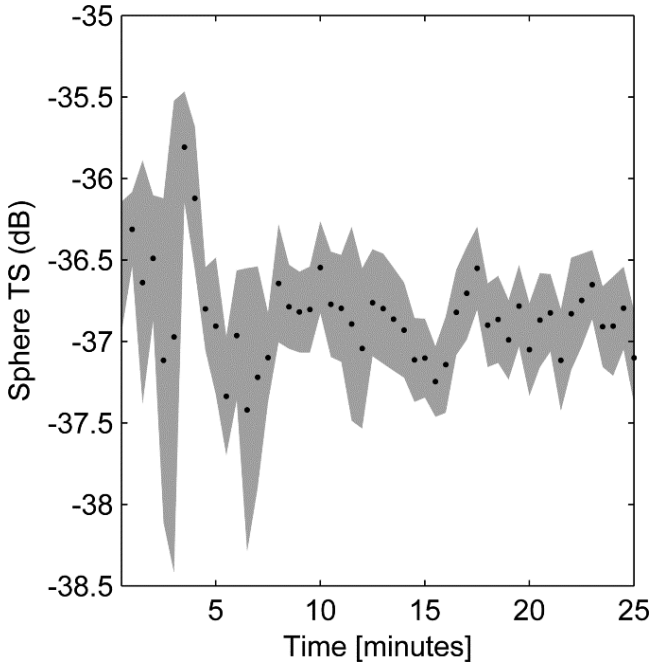

Figure 4. Variation in sphere target strength with time. The shaded region shows the variability over the preceding 60 pings (approximately 30 seconds) and the solid dots the mean.

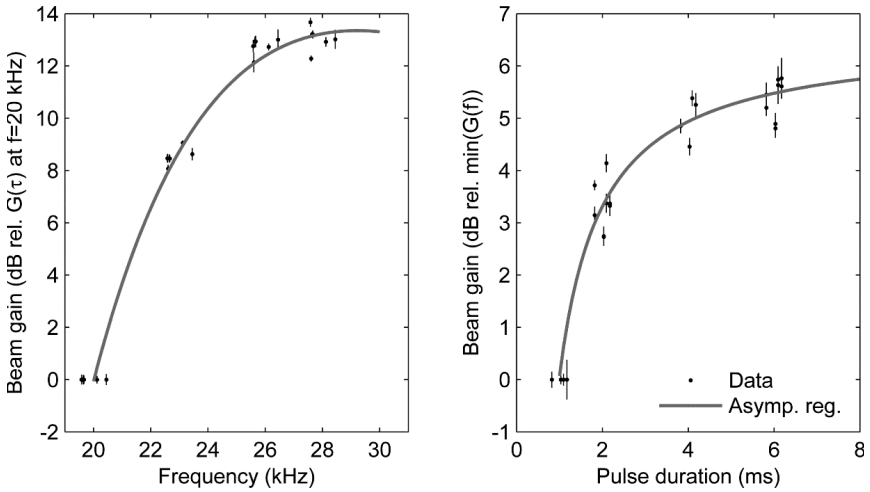

Figure 5. Relative changes of the beam gain with the changes in the pulse frequency (left panel) and with changes in the pulse duration (right panel). Dots indicate measured beam gain from the SX90 on FV Brennholm, and the line indicates the asymptotic regression. Jitter has been added to the x-axis values to more clearly separate the data points, and the root-mean-square (RMS) of the sphere echoes about the mean value is indicated by the vertical lines (of length 2RMS).

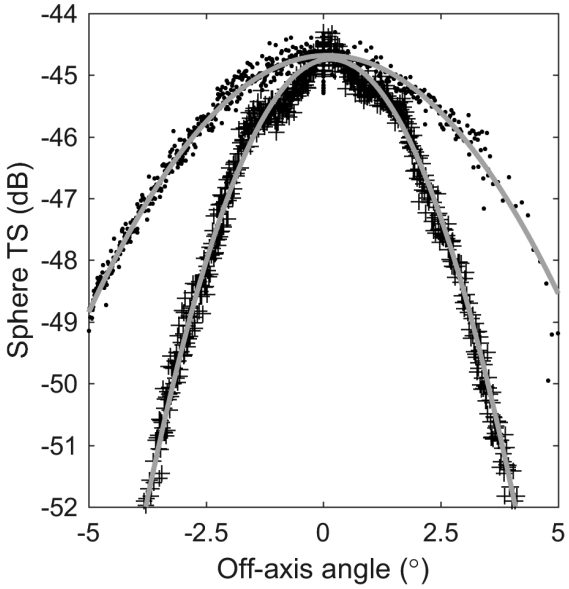

Figure 6. An example of the horizontal (dot symbol) and vertical (plus symbol) beam width data and the fitted quadratic beam shapes on FV Artus for one beam. (March 2013 calibration, beam 49, –5° beam tilt, 30 kHz transmit frequency with a CW pulse 1 ms in duration).

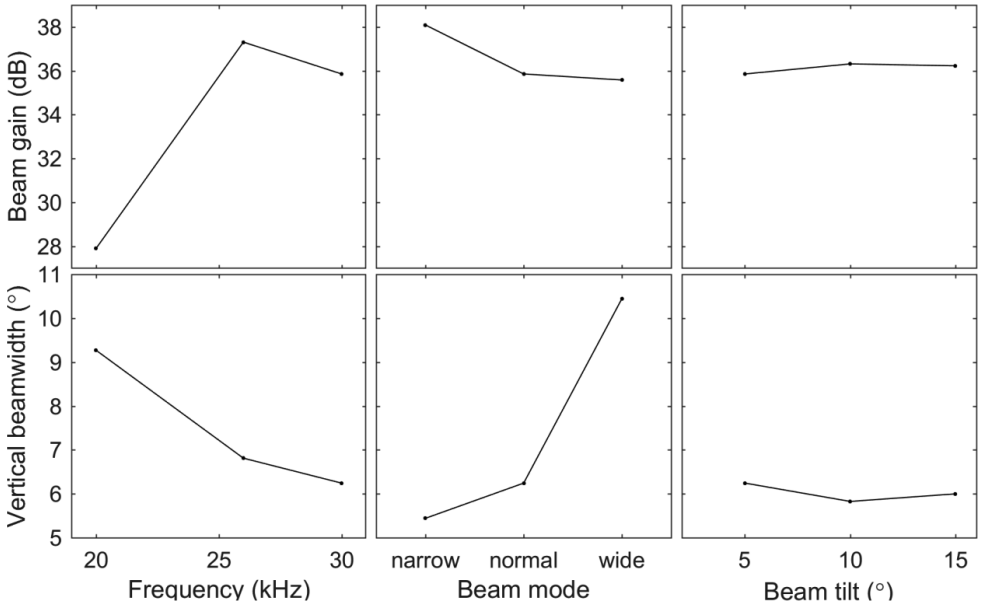

Figure 7. Changes in beam gain and vertical beamwidth as a result of changes in sonar parameters for the SU90 sonar on FV Eros.